https://theses.gla.ac.uk/

Theses Digitisation:

https://www.gla.ac.uk/myglasgow/research/enlighten/theses/digitisation/

This is a digitised version of the original print thesis.

Copyright and moral rights for this work are retained by the author

A copy can be downloaded for personal non-commercial research or study, without prior permission or charge

This work cannot be reproduced or quoted extensively from without first obtaining permission in writing from the author

The content must not be changed in any way or sold commercially in any format or medium without the formal permission of the author

When referring to this work, full bibliographic details including the author, title, awarding institution and date of the thesis must be given

Enlighten: Theses
https://theses.gla.ac.uk/
research-enlighten@glasgow.ac.uk

INTERNAL FRICTION CHARACTERISTICS AND AGEING OF IRON-VANADIUM-NITROGEN ALLOYS.

by

R. M. Jamieson

A comprehensive survey of the literature on internal friction due to stress induced diffusion of interstitial atoms in iron is made. The theory associated with this type of internal friction is reviewed. By expressing the equation of the damping peak in the form

$$\frac{Q^{-1}_{max}}{Q^{-1}} = \cosh \frac{\Delta H}{R}\left(\frac{1}{T} - \frac{1}{T_{peak}}\right)$$

several computer programmes were utilised to analyse experimental curves obtained using a torsional pendulum technique.

Pure iron and iron-vanadium alloys containing up to 0.7% V were cast under vacuum, carbon being used as a deoxidant. These alloys were worked by cold rolling and cold drawing to produce wire 0.031" diameter and subsequently treated with pure dry hydrogen at 700°C to decarburise. Nitrogen was introduced into the wires by nitriding in NH_3- H_2 mixtures at 590°C.

Solubility measurements performed on pure iron wires yielded results which were in good agreement with published values. The activation energy for the diffusion of nitrogen in iron was also confirmed. The solubility of nitrogen in

ProQuest Number: 10647354

All rights reserved

INFORMATION TO ALL USERS
The quality of this reproduction is dependent upon the quality of the copy submitted.

In the unlikely event that the author did not send a complete manuscript
and there are missing pages, these will be noted. Also, if material had to be removed,
a note will indicate the deletion.

ProQuest 10647354

Published by ProQuest LLC (2017). Copyright of the Dissertation is held by the Author.

All rights reserved.
This work is protected against unauthorized copying under Title 17, United States Code
Microform Edition © ProQuest LLC.

ProQuest LLC.
789 East Eisenhower Parkway
P.O. Box 1346
Ann Arbor, MI 48106 – 1346

the presence of vanadium, at temperatures below 590°C, was so small that it could not be measured even by the relatively sensitive technique of internal friction.

Abnormal peaks were produced in iron-vanadium-nitrogen alloys, containing more than approximately 0.3% V, when quenched from 950°C. The normal peaks obtained were broadened and this was shown to be due to the presence of carbon in solution, arising from the decomposition of vanadium carbide. It was concluded that dry hydrogen treatment was ineffective in removing carbon, present as vanadium carbide, from iron.

A high temperature abnormal peak due to carbon was found in wires containing 0.62% V, carburised at 800°C in hydrogen-toluene mixtures for short times.

The abnormal peak occurring in the range 81°C to 91°C in the Fe-V-N system was studied. Results showed that this peak could not be described by a single relaxation time curve. It is postulated that two main mechanisms give rise to the abnormal peak. The lower temperature component peak is considered to be due to nitrogen atom jumps associated with Fe-V sites, while the higher temperature component peak is thought to be due to nitrogen atom jumps associated with distorted sites surrounding coherent precipipitates of vanadium nitride. The activation energy of the diffusion of nitrogen associated with Fe-V sites has been assessed as 30 to 40 K cals./mole.

The increased rate of ageing observed in iron-vanadium-nitrogen alloys, compared with iron-nitrogen alloys, is ascribed to the presence of VN nuclei at the quenching temperatures used.

INTERNAL FRICTION CHARACTERISTICS AND AGEING OF IRON-VANADIUM-NITROGEN ALLOYS

by

R. M. Jamieson A.R.C.S.T., Grad.I.M.

Thesis submitted to

the University of Glasgow

for the degree of

Doctor of Philosophy

Department of Metallurgy,
Royal College of Science and Technology,
George Street,
GLASGOW, C.1.

February 1964

CONTENTS

C O N T E N T S

CHAPTER I

INTRODUCTION

I. INTRODUCTION

For many years strip and sheet steel, for deep drawing purposes, has been made from rimming steel. This type of steel has a very good "skin" due to the carbon-oxygen reaction occurring during solidification, and consequently, little dressing of the virgin ingot is required. Rejection of the finished product because of surface defects is usually low. However, a characteristic of such steel is that it tends to age, becoming harder, less drawable and likely to show stretcher strain bands in the finished product.

Strain-ageing is known to stem from the presence, in solid solution, of nitrogen and/or carbon which diffuses to the distorted areas surrounding dislocations, where the atoms can be accommodated at a lower energy than in the lattice. This stabilises the dislocations causing discontinuous and massive slip, appearing as stretcher strain in the surface of the finished article, when the material is pressed. Strain-ageing can be suppressed either by having no nitrogen in solid solution or by causing such nitrogen to precipitate. The latter objective can be achieved by the addition of an element with a high chemical affinity for nitrogen to the steel prior to casting.

Common practice now favours the addition of aluminium which deoxidises the melt before combining with the nitrogen,

thus producing a killed-steel. Unfortunately, this non-ageing killed steel has other less desirable features which must be tolerated. The product of the deoxidation reaction, alumina, does not separate readily from the steel. Much of the alumina finds its way to the surface layers of the ingot where it may be exposed by oxidation of the ingot during hot rolling, so that on subsequent cold working, the surface quality is inferior to that obtained from rimming steel. Further, when large quantities of alumina are present, these inclusions are flattened out into bands during rolling which, in some cases, may lead to fracture in drawing and pressing operations. Apart from the advantage of the pure skin, rimming steel contains very little pipe since the normal shrinkage is compensated by part of the gas evolved during the rimming action. Killed steel normally has a pipe which must be cropped, with the result that the ingot yield may be much less than that obtained from rimming steel.

Theoretically there is no reason why vanadium cannot be used to precipitate nitrogen from solution. It readily forms a stable nitride thereby rendering the steel non-ageing, whilst being a much less powerful deoxidising agent than aluminium, it exerts little influence on the rimming action. It is thus possible to combine the beneficial attributes of killed steel (non-ageing) and rimmed steel (good surface) in one product. From this point of view, vanadium treated

rimming steel should be of potential practical interest to the steelmaker, and has in fact been produced commercially.[1]

Fundamental investigations of the behaviour of the interstitial solutes carbon and nitrogen, in specially prepared alloys and commercial steels, have done much to elucidate the mechanisms by which steels age. The majority of such investigations have studied the influence of various heat treatments and/or degrees of cold work on the position and shape of the stress-strain curve in the neighbourhood of the yield point. Although much valuable work has been done in this field, it has been mainly concerned with the measurement of the effects produced by carbon and nitrogen rather than direct study of the behaviour of these atoms. It has been well established that ageing is caused by the migration of interstitial carbon and nitrogen in solid solution either to precipitates or dislocations. Thus, experiments which permit the study of the concentration of solute atoms in solution and of the rate at which they leave solution under varying experimental conditions are most desirable.

Internal friction offers a convenient and experimentally simple method of studying the behaviour of nitrogen or carbon in solid solution. The iron-carbon and iron-nitrogen systems have been thoroughly investigated by internal friction techniques, and very reliable data has been obtained. The next logical step is to apply the technique to the study

of ternary systems. In the present investigation, the iron-vanadium-nitrogen system has been examined by this technique in view of its practical and theoretical interest.

CHAPTER II.

THEORY

II. THEORY

1. Introduction.

It has been known for many years that solids do not behave in a perfectly elastic manner and that Hooke's Law is only applicable when forces are applied very slowly. Students of the classical theory of elasticity knew that their fundamental assumptions did not apply to real solids. However, the value of classical theory lay not in its precise description of the behaviour of solids under applied forces but in its description of this behaviour with sufficient accuracy for most practical purposes. Such phenomena as internal friction, the magneto-elastic effect and the thermo-elastic effect are contrary to the theory of elasticity in that stress and strain are not uniquely related. This property of solids by which "stress and strain are not single valued functions of one another in that low stress range in which no permanent set occurs[2] " is called "anelasticity."

A number of anelastic effects are known and have been studied in detail, viz:-

(i) Thermo-elastic effect.

(ii) Magneto-mechanical effect.

(iii) Mechanical behaviour of crystal boundaries.

(iv) Orientation of pairs of atoms in substitutional solid solutions.

(v) Stress-induced preferential distribution of interstitial solute atoms.

Each of these effects can be studied separately by making a suitable choice of the experimental conditions. In the present case, the study of stress induced preferential distribution of interstitial solute atoms can be achieved by measuring the internal friction of the specimen, in the form of a thin polycrystalline wire of random orientation, tested in torsion at low frequency.

2. Internal Friction in b.c.c. Iron.

By considering the iron atoms in the elementary body-centred cubic lattice as touching rigid spheres, it becomes apparent that two types of interstices exist. Firstly, there are positions of the type $(0, 0, \frac{1}{2})$, which correspond to the centre of the edges of the unit cell, (and of the faces, the two positions being crystallographically equivalent), having a co-ordination number of 2 and being known as the octahedral interstices. Secondly, there are tetrahedral positions of the type $(\frac{1}{2}, \frac{1}{4}, 0)$, which correspond to the centre of an irregular tetrahedron, having a co-ordination number of 4. The former type of interstice has a radius of $0.19A^{\circ}$ and the latter a radius of $0.36A^{\circ}$ (3). Because the octahedral position is smaller and has the lower co-ordination number, the tetragonality produced by the introduction of a solute atom into such an interstice is much greater than for a tetrahedral interstice.

In 1941, Snoek (4) propounded the role played by interstitials in causing internal friction. This theory assumed

that the solute atoms occupied the octahedral interstitial positions. X-ray evidence[5] has proved this hypothesis to be correct. It is, however, inconsistent with the view that interstitial atoms must be located at the largest interstitial "holes." Nevertheless, when the critereon of minimum strain energy is employed to decide the location of the interstitial solute atoms, it is found that the $(0, 0, \frac{1}{2})$ type position is indeed the most favourable. Although the iron lattice is cubic, the local symmetry of the octahedral interstices is tetragonal. Thus the interstitial position $(0, 0, \frac{1}{2})$ is closer to the two neighbouring iron atoms along the [100] axis than to the four other neighbouring iron atoms. The [100] direction may therefore be regarded as the tetragonal axis of the $(0, 0, \frac{1}{2})$ interstitial position. Similarly, every interstitial position has associated with it a tetragonal axis which is parallel to one of the three principal $\langle 100 \rangle$ axes. When an iron crystal is free from stress, all the interstitial positions are equivalent, and the interstitial solute atoms are randomly distributed. If a stress is applied, it is energetically more favourable for interstitial atoms to occupy sites with their tetragonal extension also in the direction of stress. Therefore, the equilibrium distribution will be one in which those interstitial positions are preferred whose tetragonal axes are approximately parallel to the tensile axis, since the interstitial solute atom distorts the surrounding

lattice in an asymmetrical manner, causing greater dilation along its tetragonal axis than normal to this axis. See Figure A. This tendency for solute atoms to move from randomly placed sites to favourable ones occurs at a rate dependent upon the diffusion coefficient of the solute.

Under an oscillating stress, the solute atoms will tend to jump into the preferred sites in each alternate half-cycle of stress. This process requires a finite time and in general there will be a lag between stress and strain. Energy is absorbed by the system, giving rise to internal friction or damping. This damping is a maximum when the atomic jump frequency is of the order of the period of vibration. If the atomic jump frequency is very slow compared to the period of vibration, then in a half-cycle few, if any, solute atoms will migrate to the preferential sites, hence energy absorption will be low. Conversely, if the atomic jump frequency is very fast compared to the period of vibration, in a half-cycle all the solute atoms will occupy favourable sites and stress and strain will be in phase. Only when the jump frequency of the interstitial solute atom is similar to the period of vibration of the applied stress is the damping high. Obviously the greater the number of solute atoms being stress induced to occupy more favourable sites, the greater will be the damping.[2,7,8,9]

While internal friction due to carbon and nitrogen in iron has attracted most attention, the phenomenon is general

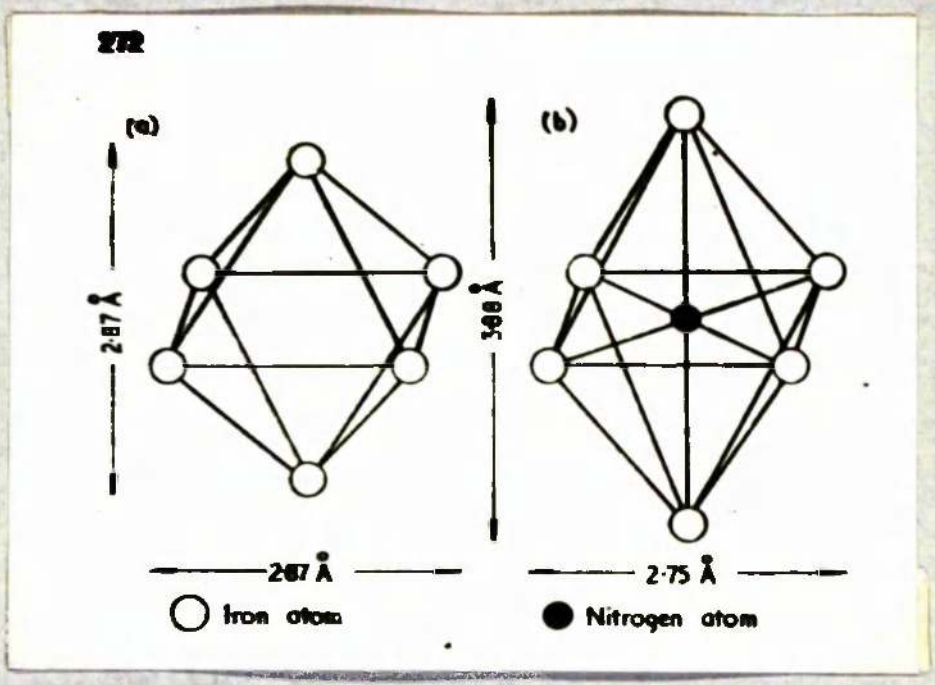

Figure A. Dilation caused by a nitrogen atom in solution in α-iron.(6)

to interstitial solutes in b.c.c. metals. Thus similar effects have been reported for carbon, nitrogen and oxygen in tantalum [10-25], niobium [25], vanadium [26, 27], and columbium [28, 29].

3. The Mathematical Treatment of Internal Friction.

If a metal be subjected to a suddenly applied and maintained force within its elastic limit, there will be a corresponding instantaneous strain which increases with time to an asymptotic value. Removal of the force produces an instantaneous decrease in strain which thereafter falls, with time, to zero. By constructing a mechanical model exhibiting this type of behaviour under the action of a force, it can be shown that its motion obeys an equation of the form

$$a_1\sigma + a_2\dot{\sigma} = b_1\varepsilon + b_2\dot{\varepsilon} \qquad (1)$$

where a_1, a_2, b_1, b_2 are constants and σ, ε are stress and strain.

Solids obeying this equation are defined as Standard Linear Solids. Further consideration of the relationship existing between stress and strain, in such solids, when these quantities are periodic, gives a relationship of the form

$$\tan\delta = DM\,\frac{\uparrow W}{1 + (\uparrow W)^2} \qquad (2)$$

where $\underline{\tan\delta}$ is the tangent of the loss angle between stress and strain.

ΔM is the relaxation strength ($\varepsilon_2/\varepsilon_1$). This factor is dependent on the amount of solute present, increasing with increasing solute content, and on texture, its value being very small for a specimen with a (111) texture. In order to obtain reproducible measurements of solute concentration, the texture dependence of ΔM must be eliminated. This is conveniently achieved by ensuring that specimens have random grain orientation.

τ is the mean time for the appropriate internal rearrangement to occur and is known as the relaxation time. It is related to the diffusion coefficient, D, for the solute atoms in a body-centred cubic lattice by

$$\tau = \frac{a^2}{36D} \qquad (3)$$

where a is the lattice parameter.

For stress induced preferential ordering, which is amplitude independent, τ obeys an Arrhenius type of equation

$$\tau = \tau_0 e^{\Delta H/RT} \qquad (4)$$

where τ_0 is a constant and ΔH is the activation energy for the diffusion process.

W is the angular frequency and is obtained by multiplying the linear frequency by 2π.

In the study of internal friction by observation of the gradual decrease in amplitude of vibration during

free oscillation, the logarithmic decrement is defined as the natural logarithm of the ratio of successive amplitudes. In the case of small $\tan \delta$,

$$\tan \delta = \frac{\text{ln.dec.}}{\pi} = Q^{-1} \qquad (5)$$

where $\text{ln.dec.} = {}^{1}/_{n} \ln ({}^{A}1/A_1 + n)$, A_1 being the amplitude of the initial vibration and $A_1 + n$, the amplitude of the vibration n cycles later.

Thus the common form of equation (2) is

$$Q^{-1} = \Delta M \frac{\uparrow W}{1 + (\uparrow W)^2} \qquad (6)$$

The variation of Q^{-1} is dependent upon the product $\uparrow W$. In this type of anelasticity where the internal rearrangement occurs by atomic diffusion, the relation shown in equation (4) is extremely convenient since it expresses the temperature dependence of $\uparrow$. Thus an internal friction peak can be obtained either by measuring Q^{-1} as a function of temperature, (and therefore of $\uparrow$, equation (4)), at constant frequency or by measuring Q^{-1} as a function of frequency at constant temperature. The former is the more convenient experimentally since the latter method necessitates the alteration of frequency over several powers of 10 in order to encompass a full damping peak. It is emphasised that the position of the peak on the temperature axis is independent of orientation and solute concentration and is governed solely by the atomic jump frequency for any given angular frequency

provided the process is described by a single relaxation time.

4. Calculation of the Activation Energy.

Internal friction peaks obtained at two different frequencies, W_1 and W_2, can be superimposed by a horizontal shift along the temperature axis. The magnitude of this shift enables the activation energy, ΔH, for the process to be calculated. Differentiation of equation (6) shows that $\uparrow W = 1$ when Q^{-1} is a maximum.

At the peak $\uparrow_1 W_1 = \uparrow_2 W_2 = 1$.

Since $\uparrow$ obeys an Arrhenius relationship

$$W_1 e^{\Delta H/RT_1} = W_2 e^{\Delta H/RT_2}$$

Hence $\ln (W_2/W_1) = \Delta H/R \left(\frac{T_2 - T_1}{T_1 T_2} \right)$ (7)

where T_1 and T_2 are the absolute temperatures corresponding to the maximum value of Q^{-1} at frequencies W_1 and W_2. The accuracy of the activation energy value calculated by this method is obviously dependent on the factor $(T_2 - T_1)$. For reliable determination of ΔH, $(T_2 - T_1)$ should be as large as possible and this, ideally, requires experiments performed at widely differing frequencies; a condition which cannot be readily satisfied in the normal torsional pendulum.

Alternatively, a second expression for the activation energy may be derived thus:-

$$Q^{-1} = \Delta M \frac{\uparrow W}{1 + (\uparrow W)^2} \qquad (6)$$

Q^{-1} is a maximum when $\uparrow W = 1$

$$\therefore \; Q^{-1}_{max} = {}^{\Delta M}/_{2}$$

$$\frac{Q^{-1}_{max}}{Q^{-1}} = \frac{1 + (\uparrow W)^2}{2 \uparrow W} = \frac{(\uparrow W)^{-1} + (\uparrow W)}{2}$$

$$= \cosh \ln (\uparrow W).$$

Since $\uparrow = \uparrow_o e^{\Delta H/RT}$

$$\frac{Q^{-1}_{max}}{Q^{-1}} = \cosh \ln (\uparrow_o e^{\Delta H/RT} . W)$$

But at the peak $w \uparrow_o e^{\Delta H/RT_m} = 1$ (T_m = Temperature of the peak)

$$\therefore \; \frac{Q^{-1}_{max}}{Q^{-1}} = \cosh \ln (e^{\Delta H/RT} e^{-\Delta H/RT_m})$$

$$= \cosh \ln \left[e^{\Delta H/R ({}^{1}/T - {}^{1}/T_m)} \right]$$

$$= \cosh {}^{\Delta H}/_{R} ({}^{1}/T - {}^{1}/Tm) \qquad (8)$$

This equation allows calculation of the activation energy from the shape of a <u>single</u> internal friction peak, utilising the experimental Q^{-1} values obtained over a range of temperature encompassing the peak. This may be useful in obtaining the activation energy for a single process in the absence of

reliable "peak shift" data. There are certain processes in which, either, more than one species of solute participates or one solute distributes itself in more than one type of interstice. In such cases τ does not assume a unique value. The existence of a range of relaxation times, no matter how narrow, in place of a single relaxation time, will always result in the broadening of the internal friction peak. Provided τ obeys an Arrhenius type equation, the distinct processes may vary from each other either by having a different activation energy, ΔH, or by a difference in the relaxation time constant τ_0. In these circumstances equation (8) may also be utilised to assist resolution of a broadened multi-relaxation time internal friction curve into its component single relaxation time peaks. In contrast, equation (7) is only useful when dealing with an internal friction peak having a unique relaxation time.

CHAPTER III.

LITERATURE SURVEY

III. LITERATURE SURVEY.

This survey deals mainly with the behaviour of nitrogen in iron and iron alloys. However, because of the similarity of the effects produced in iron by carbon and nitrogen, and because both give rise to similar internal friction peaks, many investigators report experiments involving both solutes. Reference is made, therefore, to work on carbon where this is relevant to the overall discussion.

1. Theoretical Treatises and their Experimental Verification.

Woodruff[20] was the first to notice an anomaly in the internal friction of iron as a function of temperature. Whilst studying the effect of temperature on the time of decay of steel tuning forks, a distinct minimum was observed at approximately 70° C (f = 128 c/s). Since the time of decay is inversely proportional to the internal friction, this corresponds to a maximum or peak value of damping at the above temperature. These observations were also the first to demonstrate that the temperature corresponding to the internal friction peak is frequency dependent, being higher the higher the frequency, for a given process. More than thirty years later, Snoek[22] showed that a wire loaded with nitrogen produced an internal friction peak whose height was approximately equal to the weight per cent of nitrogen, and that the peak height decreased with tempering. In a second publication[4], which

followed shortly, the mathematical treatment of internal friction was considered and the familiar equation

$$Q^{-1} = \Delta M \frac{\uparrow W}{1 + (\uparrow W)^2} \qquad (6)$$

for a single relaxation time process derived. The exact physical mechanism by which stress induced diffusion of interstitial solutes gave rise to an internal friction peak was elucidated, as discussed in the previous section.

Polder[22] elaborated on Snoek's theory for b.c.c. structures by considering a single crystal under uniaxial stress in an arbitrary direction. By postulating that the solute atoms did not interact with each other, it was shown that for 0.01% C in solution, the magnitude of the elastic after-effect, $\varepsilon_2/\varepsilon_1$, should be 0.039. Since the after-effect is related to the damping by the relationship

$$\varepsilon_2/\varepsilon_1 = 2\, Q^{-1}\,\text{max} \qquad (9)$$

this leads to a value of 0.0195 in terms of the damping peak height. Further, given that the dissolved atoms could migrate directly only from one interstice to the (four) nearest interstices, the diffusion coefficient of the solute could be represented by

$$D = \frac{a^2}{36 \uparrow} \qquad (3)$$

The theory also made the important prediction that the damping should show strong anisotropy, being zero for a crystal stressed

in a [111] direction since the interstitial positions are all equivalent in relation to the applied stress, and therefore, no stress induced diffusion should occur. Conversely, the damping should be at a maximum for a stress applied in a [100] direction.

Dijkstra[3] confirmed experimentally the salient features of Polder's theory. Purified single crystals, in the form of strips 50 x 5 x 0.15 m.m., were nitrided or carburised and their damping capacity measured. The amount of solute present in solution was estimated by comparing the electrical resistance of the specimens with a calibration graph relating percentage increase in resistance to the solute concentration. The experimental results are summarised below:

Solute	Orientation	Damping
0·01% C	[100]	0·0215
0·01% C	[111]	0·00125
0·01% N	[100]	0·016
0·01% N	[111]	0·0012

These measurements are in good agreement with the above theory. The [111] crystals showed very slight damping due to the presence of about 5% of small crystals whose orientation differed from that of the basic crystal. The assumption that mutual interaction between the dissolved particles could be neglected was also experimentally substantiated,

since Dijkstra obtained a straight line plot relating the damping to the concentration of solute. The value of 0.021$ for a crystal having a [100] orientation and containing 0.01% C compares favourably with the figure of 0.019$ predicted theoretically by Polder[22].

A second theoretical treatise on the estimation of the damping value was undertaken by Smit and Van Beuren[23] who interpreted damping as causing a change in the elastic modulii of the material. It was shown that a general relationship existed between the elastic constants of single crystals and those of polycrystalline specimens in cubic metals. Using this relationship, it was estimated that, for a polycrystalline specimen of random orientation having 0.01% N in solution, the damping at 17°C was 0.007$. A similar calculation by Rawlings and Tambini[24] yielded 0.008$, which agrees well with the previous work and with the experimentally determined values of 0.007$ [24] and 0.007$ [25].

The theoretical values of both Polder and Smit and Van Beuren are subject to uncertainties introduced by the values of the elastic constants used, which are themselves determined experimentally, and by approximations made in the course of calculation. For this reason the most reliable method of determining the proportionality factor, relating the concentration of solute to the height of the internal friction peak, is probably an experimental one. Nevertheless,

theoretical values of the proportionality factor and other theoretical predictions have been shown to be in substantial agreement with experimental results and is striking proof of the correctness of the theory.

The normal texture conferred on iron by a drawing process is [110], and much controversy exists in the literature concerning the effect of such a texture on the magnitude of the internal friction peak in polycrystals[26,27,28]. The conclusion to be drawn, however, is that for the same solute content, the internal friction will decrease with increasing texture. A second point, arising from the theory, which has been much debated, is the validity of the linear relationship between the magnitude of the effect and the solute content. The suggestion has been made that the relationship obeys a curve[29]. However, both theory and the majority of experimental investigations[22,30,31] favour a linear relationship. A study by Lagerberg and Joseffson[26] of the influence of grain boundaries on the behaviour of carbon and nitrogen in α-iron, showed that the internal friction decreased with decreasing grain size for a given solute content. This was attributed to grain boundaries trapping or absorbing adjacent interstitial atoms.

The above observations, although important theoretically, are no less important from an experimental point of view. Since both texture and decreasing grain

size lower the internal friction, reproducible results will only be obtained if the specimens have random orientation and large grains. A large grain size reduced the probability of completely random orientation and a compromise must be achieved. Fast and Verrijp[25] were able to obtain consistent results by recrystallising the specimens above the $\alpha-\gamma$ transition (950°C) which effectively removed any texture. The mean grain diameter aimed at was approximately one-tenth the diameter of the wire i.e. 0.003".

2. Solubility Measurements of Nitrogen in Iron Below the Eutectoid Temperature.

A diagram of the iron-nitrogen system is shown in Figure B. There are two stable solid solutions, namely, the face-centred cubic γ-phase and the body-centred cubic α-phase. From both a practical and a theoretical viewpoint, the $\alpha/\alpha+\gamma'$ and the $\alpha/\alpha+\gamma$ phase boundaries are extremely important since it is nitrogen in solution which causes ageing and brittleness. In order to understand and control the effects of nitrogen in steel, it is imperative that the extent of the solubility of nitrogen in α-iron be accurately known. Recent measurements have shown that the solubility of nitrogen in α-iron is much smaller and decreases much more rapidly, with decreasing temperature, than was previously thought to be the case.

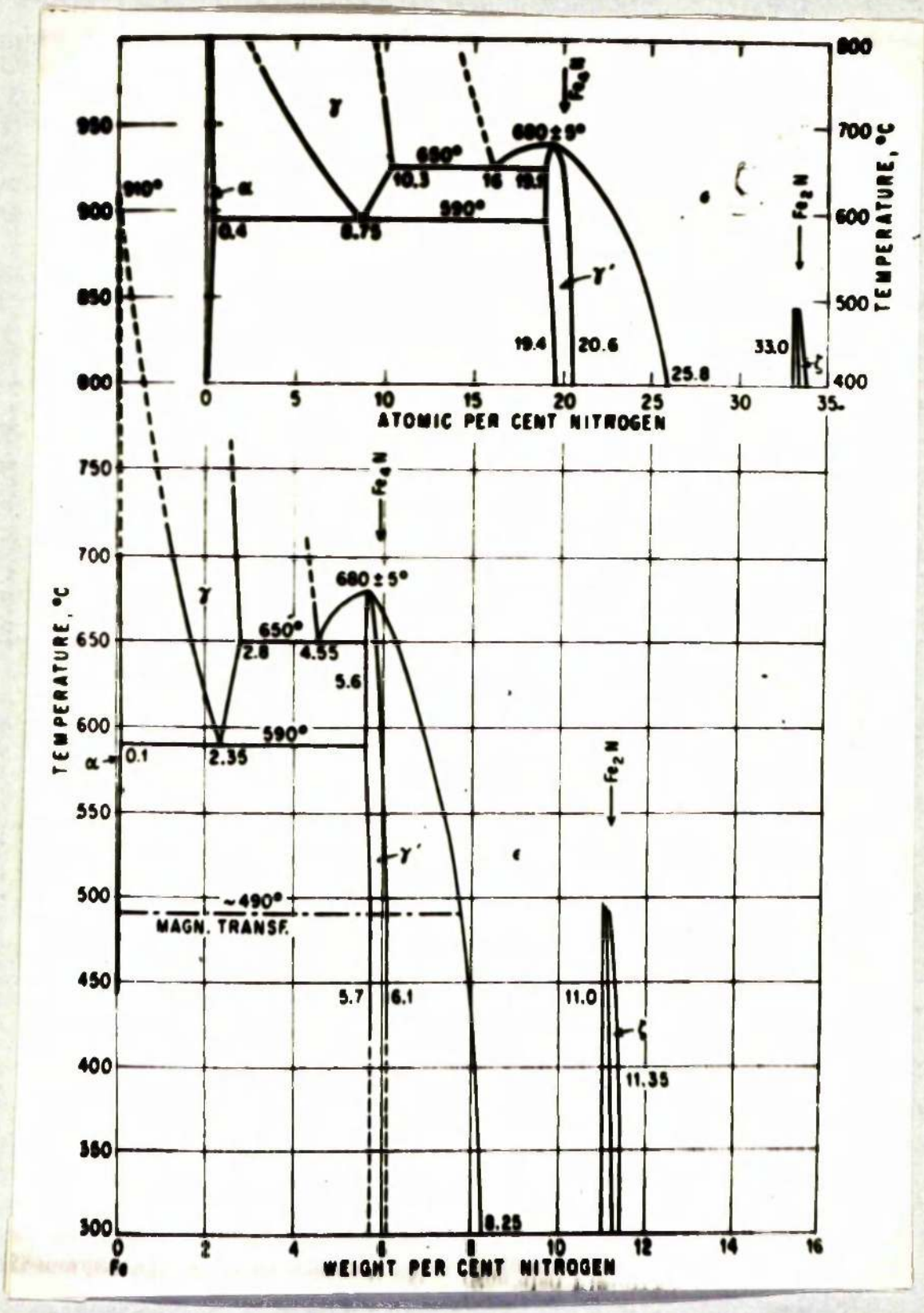

(32)

Figure B. The Iron-Nitrogen System.

In performing solubility measurements, it is important to distinguish the precipitated phase with which the nitrogen is in equilibrium. The stable phase is Fe_4N which has a f.c.c. structure. Dijkstra [33], whilst studying the precipitation of nitrogen from a supersaturated α-iron solution by the internal friction technique, observed a metastable nitride phase forming below 300°C. Jack [34,35] noted that the same precipitate occurred during the decomposition of nitrogen martensite. Using X-ray techniques, the structure of the new phase was shown to be body-centred tetragonal with a structural unit containing eight (2x2x2) distorted and expanded body-centred cubic units of the original supersaturated solution or martensite structure. The cell contains at the most two nitrogen atoms at $(0,0,\frac{1}{4})$ and $(\frac{1}{2},\frac{1}{2},\frac{3}{4})$ and for convenience may be designated Fe_8N, although up to one-half of the number of nitrogen sites may be vacant. Thus below the eutectoid temperature, nitrogen in solution may be in equilibrium with either Fe_4N or Fe_8N. Since Fe_8N is metastable, the solubility of nitrogen in equilibrium with Fe_8N is greater than for Fe_4N.

Several investigations, using various techniques, have been made to determine the solubility of nitrogen in iron below the eutectoid. These results are summarised in Table I.

TABLE I. SOLUBILITY OF NITROGEN IN α-Fe IN EQUILIBRIUM WITH Fe_4N AND Fe_2N

Results ( ) refer to equilibrium with Fe_2N

Temperature °C	Köster [39]	Elfstrom [33]	Borelius et al. [40]	Åström & Borelius [29]	Parravano et al. [41]	Fast & Verrijp [25]	Raulings & Tombini [24]	Corney & Turkdogan [44]
590					0·10			
575		0·075	0·097			0·088		
550					0·070	0·076	0·0870	
500		0·050		0·062		0·055	0·0646	0·060
450		0·035	0·059	0·047	0·053	0·038	0·0455	
400	0·020	0·025	0·045	0·034		0·025	0·0310	
350		0·015		0·024			0·0200	
330			0·026	0·020				
300	0·010	0·010	0·018	0·015			0·0115	
						(0·055)		
250		0·005	0·014	0·009			0·0054	
		(0·0255)				(0·0234)		
200	0·005	0·003	0·008					
		(0·0105)				(0·0088)		
150								
		(0·0049)				(0·0025)		
100	0·001							
						(0·0052)		

Early investigations undertaken by Fry [36], Eisenhut and Kaupp [37], and Seferian [38], yielded results which can no longer be regarded as acceptable. The first reasonably accurate determination of the solubility of nitrogen in equilibrium with Fe_4N was that of Köster [39], who measured electrical resistivity. It was found that a linear relationship existed between the resistivity and the concentration of nitrogen in solution. Unfortunately resistivity measurements are not very reliable since they are apt to be affected by other factors such as oxide films on the surface of the specimens, dispersions of fine precipitate or quenching stresses, as well as varying with solute content. These results must therefore be treated with some reservation, nevertheless the agreement with more recent values is surprisingly good.

The internal friction technique is ideal for making solubility measurements, since only atoms in solid solution contribute to the damping process, precipitates having no effect. Dijkstra [33], using this technique, obtained nitrogen solubilities in the range 200°C - 575°C. The experiments entailed quenching nitrided samples from 590°C to form a supersaturated solution. Tempering at a given temperature followed until the maximum damping value remained constant with increasing time. This final value of damping was taken as a measure of the solubility at that temperature. In order

to obtain a proportionality factor between damping and solute concentration, resistivity measurements were used in conjunction with the results of Köster[29]. This showed that Q^{-1} was equal to the weight per cent of nitrogen in solid solution to within an accuracy of $\pm$ 10%. This factor was assumed to apply up to nitrogen, concentrations of the order of 0.075 wt.%, although direct comparison with Köster's results was only possible up to 0.015 wt.%. The agreement shown between Dijkstra's and Köster's results is therefore to a large extent inherent in the method of calculation adopted.

Borelius et al.[30] measured the solubility by an isothermal calorimetry method. These results were much higher than those obtained by Dijkstra and cannot be considered as reliable in view of the subsequent work by Åstrom et al.[29], who repeated Borelius' work and obtained results which were 17% lower than those obtained in the first investigation. Further, by measuring the elastic after-effect Åstrom also obtained results which confirmed the revised calorimetric results. The elastic after-effect experiments utilised a relatively large specimen in the form of a coil. The nitrogen content of the coil was determined from the increase in its weight after nitriding. One end of the coil was rigidly fixed whilst the other was twisted through a fixed angle, held in that position for a sufficiently long time, released, and the damping measured in terms of the after-effect.

The relation found between damping and nitrogen concentration was not linear but curved. The deviation from linearity, however, was exactly of the type to be expected if accidental precipitation occurred at higher temperatures. This was more than likely, since it is known that quenched iron-nitrogen solutions are extremely unstable at high nitrogen contents, and as the specimen was very cumbersome, efficient quenching was not achieved. According to the results, a wire quenched from the eutectoid temperature at 585°C and containing 0.1 wt.% nitrogen in solution could never show a damping value greater than 0.055 at -18°C. The work of Fast and Verrijp [25] showed that values of Q^{-1}_{max} higher than 0.07 could easily be obtained at room temperature by quenching a wire containing 0.1 wt.% nitrogen from 580°C. In view of this, the findings of Åstrom are suspect.

Paranjpe [41] investigated the whole of the iron-nitrogen system by a chemical equilibrium method in conjunction with X-ray diffraction. At any given temperature, carbonyl iron powder was brought into equilibrium with NH_3-H_2 mixtures of progressively higher ammonia potentials before quenching into water. Micro-Kjeldahl analyses and X-ray diffraction measurements were made. The solubility limit was detected by the appearance of a second phase. The results were in reasonable agreement with those of Dijkstra [33], although small discrepancies existed which were probably due to differences

in the physical nature of the specimens.

From the above work it is apparent that there is a reasonable measure of agreement between investigations using different techniques. The internal friction method, however, is the most attractive experimentally and is probably more accurate than other techniques. Fast and Verrijp [25] were the first to use the internal friction technique to make a comprehensive study of the solubility of nitrogen in iron. The damping of wire specimens, 10" long x 0.030" diameter, was measured by observing the decay of the amplitude during free vibration in a torsional pendulum apparatus similar to that devised by Kê [26]. As in all the internal friction experiments reviewed in this section, the reliability of the solubility data depends largely on the accuracy of the factor relating damping to concentration. Two series of experiments were undertaken to determine this factor. In the first series, the wire samples were nitrided at 950°C in 99% N_2 + 1% H_2 for varying times, quenched, solution treated at 570°C and quenched. The height of the damping peak measured after the last quench increased initially with increasing time of heating, but after 2 - 3 hours a constant value was reached. Ten peak heights measured after 3, 4, 8 hours were all found to lie within the range Q^{-1} max = 0.021 $\pm$ 0.0005. Micro-Kjeldahl analyses showed the nitrogen content to be wt.% N = 0.0265 $\pm$ 0.001. In the second series, the wires were nitrided at 950°C, as above, and

then at 570°C in NH_3-H_2 mixtures to raise the nitrogen content still further. These peak heights were found to lie in the range $Q^{-1}max = 0.0585 \pm 0.0008$, analyses gave wt.% N = 0.074 ± 0.001. These two series showed that the wt.% N = 1.26 ± 0.04Q^{-1}max. at 22°C.

In general their method of determining solubilities consisted of tempering a supersaturated solution of nitrogen in iron at any given temperature in the range 380°C - 580°C, and observing Q^{-1}max as a function of time until no further change occurred. The final value of Q^{-1}max was taken as a measure of the nitrogen solubility at that temperature. The results are summarised in Table I. At high nitrogen contents, the supersaturated solutions became extremely unstable and reproducible results were not obtained with nitrogen contents above 0·08%. With nitrogen contents between 0.05 - 0.08% reproducible results could only be obtained by measuring very quickly a small number of points on the internal friction curve, situated on both sides of the peak, whilst no special precautions were needed for nitrogen contents lower than 0·03%.

Results that are too high may be obtained for the $\alpha/\alpha+Fe_4N$ phase boundary by the presence of either finely divided Fe_4N precipitates or by Fe_8N formation. Fast and Verrijp guarded against the former by slow cooling their wires from 580°C prior to resolution and against the latter by

performing the experiments at temperatures higher than 300°C. Their solubilities are much higher than those reported by Dijkstra [33]. This, however, is almost entirely due to the difference in the proportionality constant used in the two investigations. If the proportionality factor of Fast and Verrijp is applied to the results of Dijkstra, this yields solubility values which are greater than those obtained by Fast and Verrijp. This in fact suggests that their results may be low due to accidental precipitation.

Rawlings and Tambini [34] also made a study of the $\alpha/\alpha+$ Fe_4N equilibrium in iron using internal friction but approached equilibrium from the opposite direction by nitriding a wire containing little or no nitrogen. Ammonia was passed through a cracking furnace in series with the furnace containing the wire specimens. The ammonia potential in contact with the wires, and hence the quantity of nitrogen absorbed, was controlled by variation in the cracking furnace temperature. Hydrogen can also be absorbed in this method of nitriding since the reaction may be represented as

$$2NH_3 \rightarrow \underline{2N} + \underline{6H}$$

However, it has been shown [43] that the hydrogen peak, at the frequency used, is at 100°K and its contribution to the nitrogen peak is negligible. The Q^{-1}_{max} was measured as a function of the ammonia potential at temperatures in the

range 250°C - 550°C. At any given temperature, the damping first increased with increasing ammonia potential and then decreased due to the formation of a case of Fe_4N. The maximum damping obtained at each temperature was taken as the true measure of solubility at that temperature. The proportionality factor was determined by analytical methods and found to be 1.28 at 17°C.

The results obtained were higher than those of Fast and Verrijp partly due to the slightly greater proportionality factor, but mainly due to the more efficient quench obtained by Rawlings and Tambini, who used a smaller and thinner specimen (2" x 0.02" diameter). If the factor of 1.28 is applied to the results of Dijkstra [33], they agree exactly with those of Rawlings and Tambini above 300°C. At lower temperatures complications are introduced due to the possibility of the formation of Fe_8N. The values quoted by Rawlings and Tambini for 250°C and 300°C could refer to equilibrium with Fe_8N as the authors did not offer evidence to the contrary. However, as they nitrided their wires and did not measure the solubility by the precipitation technique, the results probably do in fact refer to equilibrium with Fe_4N. This suggests that the low temperature results of Dijkstra are high due to incomplete precipitation.

The single solubility measurement by Corney and Turkdogan [34] deviates less from the results of Rawlings and

Tambini than from those of Fast and Verrijp. In view of the foregoing discussion there is strong evidence in favour of the results of Rawlings and Tambini being the most reliable. The solubility of nitrogen in α-iron in equilibrium with Fe_4N, from their data, may be represented by

$$\log N = -\frac{1649}{T} + 0{\cdot}942 \quad \text{wt.\%}$$

The values reported by Fast and Verrijp[85] for Fe_8N are more reliable than those of Dijkstra, and may be expressed by

$$\log N = -\frac{2160}{T} + 2{\cdot}518 \quad \text{wt.\%}$$

Similar internal friction experiments have been performed on iron-carbon alloys[86] with equally encouraging results.

3. Precipitation Studies by Internal Friction Techniques.

In metallography, the most widely studied precipitation process is that which occurs in age-hardening alloys. The systems which have received most attention have been aluminium-copper, iron-carbon and iron-nitrogen. Physical properties of alloys such as hardness and electrical resistance change during precipitation and such changes have been used to follow ageing processes. However, these measurements are unreliable since the size, shape and distribution of the precipitated phase influences their values.

Internal friction measurements have no such drawbacks and the technique has been used extensively in the study of precipitation from the α-iron solid solutions of nitrogen and carbon.

In studying precipitation rates by internal friction, some important considerations should be borne in mind. A nitrogen atom will only contribute to the normal internal friction peak if its jump rate corresponds to that for normal interstitial sites. If its jumping rate changes by a factor of approximately 100, its contribution will be negligible. Wert[46] has suggested that nitrogen atoms residing in distorted regions of the lattice adjacent to grain boundaries or surrounding precipitates might not be properly measured, since the mean time-of-stay in such positions would differ from that in normal sites. The grain boundary effect may be neglected if specimens are not fine grained. The trapping of solute atoms in the disturbed regions surrounding precipitates will only occur in the initial stages of the process when the precipitates are likely to be coherent, since bulk precipitates do not cause severe lattice distortion. Atoms removed from solution as precipitates will not contribute to the damping.

The precipitation process is observed by measuring $Q^{-1}_{max.}$ as a function of time. The decrease in $Q^{-1}_{max.}$ accompanying the tempering of a supersaturated solution corresponds to the removal of solute from solid solution and

the formation of a precipitate.

Dijkstra [33] made a detailed study of nitrogen precipitation in α-iron below the eutectoid temperature. In the first series of experiments the effect of differing initial nitrogen contents on the rate of precipitation was examined at a fixed temperature. Results indicated that the rate of rejection of nitrogen from solution was strongly dependent on the initial concentration and increased with increasing concentration. In a second series, wires of constant nitrogen concentration were tempered at temperatures in the range $0^{\circ}C$ - $500^{\circ}C$ and the damping measured as a function of time for each temperature. From Dijkstra's observations it appeared that nitrogen was rejected from solid solution by two distinct mechanisms, one predominating at low temperatures and the other at high. The two processes occurred independently of each other, at different rates, and had different dependencies on temperature. Micro-examination revealed that both phases showed a Widmanstatten structure, but whereas the first structure (Fe_8N) had a (001) orientation, the second (Fe_4N) had an orientation associated with a higher order plane probably (210), supporting the view that the two precipitates occurred independently. The obvious conclusion was that the nucleation of Fe_4N must be extremely difficult at low temperatures. This is feasible since, it is known from the later work of Jack [34,35], the atoms of Fe_8N have the same arrangement as in α-iron. Therefore, the formation

of its nuclei demands a much smaller activation energy than the formation of Fe_4N nuclei, in which the iron atoms have the face-centred cubic arrangement of γ-iron.

The observations of Dijkstra may therefore be explained as follows. When the temperature is relatively low (below 250°C) and if the iron is supersaturated with respect to both Fe_4N and Fe_8N, precipitation starts with the formation and growth of Fe_8N. After a much longer time, the more stable Fe_4N nuclei appear and grow at the expense of the first formed precipitate. At higher temperatures, above 300°C, thermal agitation of the atoms in greater and Fe_4N nuclei form without much delay. It was also confirmed that the precipitation rates at varying temperatures and nitrogen contents were in agreement with the standard nucleation theory [47].

Wert [48] also studied the precipitation of nitrogen from supersaturated iron solutions with a view to obtaining a mathematical expression which would accurately describe the ageing process. Precipitation to form Fe_8N and Fe_4N was studied at temperatures in the range 25°C - 150°C and at 315°C respectively. A preliminary attempt was made to use an expression of the form

$$W = kt^n \qquad (10)$$

where n is a constant and W the amount of precipitate formed in time t, to describe the experimental results. It was shown that this equation was only valid up to approximately 40% of

the total precipitation. This was attributed to interference between adjacent particles of precipitate with the accompanying general depletion of solute in the iron lattice in the later stages.

Clearly, an equation which will account for precipitation in the later stages must take into account the depletion of the solute atoms from the matrix. An alternative equation of the form

$$\frac{\Delta C\,(t)}{Co} = 1 - \left[\exp \; -(t/\uparrow)^{n}\right] \qquad (11)$$

where $\Delta C(t)$ is the amount of material precipitated in time t. Co is the original solute content, $\uparrow$ and n are constants, was applied by Wert. The Fe_8N results plotted according to this equation showed three distinct portions. The first stage extended up to approximately 20% of the total precipitation, the second stage up to 80 - 90% and the third stage accounted for the remainder. The n values for the first and second stages were 2.45 and 1.0. The third stage was poorly defined and no n value was obtained. Studies of the precipitation of Fe_4N showed only one stage with $n = 1.6$. In these experiments there were two main sources of error. Firstly, during the early stages of the precipitation process, small errors in the determination of Co and $\Delta C(t)$ were reflected as large percentage errors in $\ln \frac{\Delta C(t)}{Co}$. Secondly, there was difficulty in determining the exact tempering time, especially at high temperatures, since the

time of heating and quenching may not be small compared to the total measured tempering time. Nevertheless, the experimental data fitted the above Law, equation (11), up to about 80% of the total precipitation. More complex equations[49] have been derived in attempts to describe the precipitation process over a still wider range. None of these expressions, however, appear to lead to a satisfactory physical interpretation of the precipitation process.

Zener[50] postulated that the value of n obtained by applying equation (11) to precipitation results could be interpreted in terms of the shape of the precipitated particles. Working on this premise, he showed that for spherical growth, the volume increased in proportion to $(t - to)^{3/2}$; for cylindrical growth as $(t - to)^{4/2}$ and for discoidal growth as $(t - to)^{5/2}$, where to is the time required for the formation of the nucleus. Wert found that in the case of Fe_8N, n was approximately 5/2, thus by Zener's reasoning, Fe_8N precipitated as discs and to was zero i.e. there was no incubation period. This conclusion concerning spontaneous precipitation is contrary to the findings of Dijkstra[33] who reported the existence of an incubation period for tempering temperatures lower than 250°C. Wert also predicted that carbon precipitated as spheroids, but an electron microscopy study[51] has shown that these precipitates are discoidal. Further, Pitch and Lücke[52] obtained n values for carbide precipitation which were smaller

than the minimum predicted by Zener.[50] Thus the attractive model of Wert and Zener, that the factor n was indicative of the shape of the precipitate, appears to be unfounded. A theoretical treatment by Hsun[53] in which two stages of precipitation were assumed, showed that the value of n should be 1·5 for all particles, regardless of shape, in the initial stage, and 1·0 for the second stage provided the size of the precipitated particles was small compared to their distance of separation.

Wert[54], studying the simultaneous precipitation of nitrogen and carbon, showed that the rate of ageing of one type of interstitial was influenced by the presence of the other. When both solutes were present, the precipitation rate of the slower was increased to equal that of the faster precipitating solute. This rate increase could be explained either by an increase in the number of nuclei available for precipitation or by an increase in the diffusion rate. Since the shape and position of the individual nitrogen and carbon internal friction peaks were found to be unaltered by the presence of both in solution, the diffusion rates of these solutes are also unaltered. Wert therefore concluded that the increased rate of precipitation must be accounted for by an increase in the number of nuclei, and suggested that carbon or nitrogen could nucleate massive precipitates of each other or that a mixed carbonitride could nucleate and precipitate.

Recent work [56] on carbon precipitation showed that the kinetics of precipitation changed when the ageing temperature was below about 60°C for iron-carbon alloys containing 0.022%C. This was manifest by an increase in n, the exponential in the Wert and Zener Law, (equation (11)), and a decrease in the activation energy associated with precipitation, the latter effect being attributed to a change in the mode of nucleation. A more comprehensive study was undertaken by Chollet and Crussard [56] who observed carbon precipitation in the range 23°C - 225°C for alloys containing 0.005 to 0.022%C. By plotting $t1/_2$ vs $1/T$, it was shown that three temperature ranges existed where the kinetics of precipitation was different; the limits of these ranges increased with increasing carbon content. These phenomena depended in a complex way on the nucleation and growth of the precipitates. The authors conceded that the transition between the lower and middle range was due to a change in the mode of nucleation as proposed by Doremus [55], whilst they attempted to explain the transition between the middle and highest ranges in terms of the growth factor.

4. Determination of Diffusion Coefficients by Internal Friction Techniques.

As shown earlier, the diffusion coefficient of an interstitial solute in iron is given by

$$D = \frac{a^2}{36\tau} \qquad (3)$$

To ascertain the diffusion coefficient at any temperature, it is sufficient to observe the relaxation time τ at that temperature. This value is found immediately from the position of maximum damping, since at the peak $w\tau = 2\pi f \approx 1$. By varying the frequency, the coefficient of diffusion at other temperatures can be determined and, by plotting ln D vs $^1/T$, the activation energy for diffusion can be estimated. Both carbon and nitrogen diffusion coefficients obtained at low temperatures by internal friction techniques agree well with values extrapolated from results obtained by conventional diffusion experiments at higher temperatures. This agreement confirms the hypothesis on which equation (3) depends i.e. that the interstitial atoms, in α-iron, move only $^a/_2$ cms. to nearest neighbour interstices in each jump. Since the Snoek relaxation depends on very small displacements, measurements of internal friction allow the determination of diffusion coefficients which are very much smaller than those determined by the conventional method, where numerous jumps are necessary to produce a measurable difference in a concentration gradient. If, for example, the diffusion coefficient of nitrogen in α-iron at room temperature was to be measured by conventional methods, this would entail nitrogen diffusing from a nitrogen rich alloy into pure iron to a minimum depth of 0·1 - 0·2 cms. This distance is approximately equivalent to 10^7 elementary jumps of a nitrogen atom, and it has been estimated[57] that, since the

atoms move randomly, this would require a period of a million years. Such a calculation illustrates vividly the advantages offered by internal friction methods in this field.

Wert[58] made a study of the diffusion of carbon in α-iron, in the range -35°C to 200°C, using relaxtion phenomena. In order to measure $\perp$ over this range of temperature it was necessary to vary the frequency up to approximately 1000 c/s. A single internal friction technique could not be employed, and use was made of the elastic after-effect for sub-zero temperatures, the torsion pendulum for ambient temperatures and a magnetically driven torsion pendulum for higher temperatures. In addition, a precipitation technique was used to deduce the diffusion coefficient in the range 150°C - 200°C, since precipitation occurred too rapidly to allow relaxation peak measurements to be made with certainty. The results of Stanley[99], obtained by conventional methods at 500°C - 700°C, were taken in conjunction with the other values to give a plot of ln D vs $^1/_T$. This gave a straight line, indicating the constancy of the activation energy for diffusion, 41 kJ, over this wide range of temperature. Similar techniques were used in the determination of nitrogen diffusion coefficients[60] but the temperature range investigated was much shorter, -30°C to 50°C. Wert and Zener[61] also reported values for Do and the activation energy for diffusion.

In addition to determining the diffusion coefficient of nitrogen at room temperature from the position of the relaxation peak, Fast and Verrijp[62] also reported values for higher temperatures in the α and γ ranges. They utilised the fact that desorption of nitrogen from iron wires by hydrogen is diffusion controlled[85]. Iron wires loaded with nitrogen were held for varying periods at different temperatures in a stream of wet hydrogen to allow desorption to occur. The wires were subsequently quenched, given a homogenising treatment and the height of the internal friction peak measured to give the residual nitrogen content. Fast and Verrijp showed that a plot of log $\frac{Q^{-1}_{max}(t)}{Q^{-1}_{max}(t=o)}$ ($<-$ o.3) versus time gave a straight line plot from which the diffusion coefficient of nitrogen at a given desorption temperature could be calculated. These measurements showed that the diffusion coefficient of nitrogen in α-iron was much greater than in γ-iron. At 540°C, the diffusion coefficient of nitrogen in α-iron had already surpassed the 950°C value for nitrogen in γ-iron, while at 950°C, the extrapolated value of diffusion coefficient in α-iron was about 50 times greater than for γ-iron.

The results of the investigations discussed above are shown in Table II in terms of the constants ΔH and D_0 in the diffusion equation. The work of Busby[63], who obtained

TABLE II. ACTIVATION ENERGY FOR THE DIFFUSION OF NITROGEN IN α - IRON

Diffusion equation of the form $D = D_0 e^{-\Delta H/RT}$

	Fast and Verrijp [62]	Wert [60]	Busby [63]	Wert and Zener [61]	K [64]
ΔH	18,600	18,200	15,600	17,700	20,000
D_0	0.0066	0.005	0.0012	0.0014	

his results by analysing specimens after nitriding for various times, calculating the fractional saturation and hence the diffusion coefficient, is included for comparison together with the activation energy obtained by Kê[64].

In Table III actual values for the diffusion coefficient of nitrogen, according to various investigators, are shown for several temperatures. Wert and Zener[61] gave only a few results over a small temperature range, while Wert[60] obtained several results but only at low temperatures. These results have been extrapolated in Table III to give a comparison with those of Fast and Verrijp[62] who obtained a few values over a very wide temperature range. On balance, there is little to choose between the results of Fast and Verrijp and those of Wert, the discrepancies in their results can be explained by the difference in their values of Do. There is also reasonable agreement with the results of Busby[63].

5. The Study of Ternary Systems by Internal Friction Techniques.

This discussion, so far, has dealt with effects produced by nitrogen atom movements associated with a unique type of site in the iron lattice. The introduction of a substitutional atom into the iron lattice generally produces alternative sites in which the nitrogen atom can reside. This may result in either the normal Snoek peak being broadened or the formation of an additional separate peak. Fast and Dijkstra[65] compared the shape of the internal friction peaks

TABLE III. DIFFUSION COEFFICIENTS OF NITROGEN IN α - IRON

Temperature °C	Fast and Verrijp [62]	Wert [60]	Busby [63]	Wert and Zener [61]
20	1×10^{-16}			
50		1.9×10^{-15}		
100	8.5×10^{-14}	7.6×10^{-14}		
400			1.1×10^{-8}	2.5×10^{-9}
500	3.6×10^{-8}	2.1×10^{-8}	4.7×10^{-8}	1.4×10^{-8}
600	1.4×10^{-7}	8.5×10^{-8}	1.5×10^{-7}	4.9×10^{-8}
700	4.4×10^{-7}	2.5×10^{-7}	7.8×10^{-7}	1.47×10^{-7}
950(α)	3.1×10^{-6}			

and the rates of precipitation of nitrogen in iron and iron containing 0.5 at.% manganese. They reported that manganese shifted the nitrogen peak from 25°C to 32°C and increased its half-width from 25 C° to 36 C°, clearly indicating that more than one relaxation time was operative. This broadened peak could be resolved into two single relaxation time curves, one of which passed through a maximum at the same temperature as the pure iron nitrogen alloy whilst the maximum of the other was at a temperature about ten degrees higher. Therefore, for a given temperature, the second peak had a longer relaxation time than the first and consequently the nitrogen atom had a longer mean time-of-stay in the interstitial positions associated with this second peak. It was natural to regard this phenomenon in terms of the relative affinities of manganese and iron for nitrogen. The heat of formation of Fe_4N is 0.9 Kcal/mole and that of $Mn_{2.5}N$ is - 23 Kcal/mole. This suggests that nitrogen atoms may reduce their energy by occupying interstitial positions where one or more of their immediate neighbours is an atom of manganese. Damping measurements show that once "imprisoned" in this way, the nitrogen atoms remained capable of jumping (or there would be no peak) but at a reduced jump frequency. It was noted that manganese inhibited the precipitation of nitrogen from solution.

Later work, by Dijkstra and Sladek[66], confirmed the findings of Fast and Verrijp[65] and attempted to explain the

results. In order to conceive a mechanism which could give rise to the manganese peak, it was postulated that the six interstitial positions surrounding a manganese atom in the lattice had, for nitrogen, a free energy level lower than for a normal site, giving rise to a new relaxation time, τ_{Fe-Mn}. Thus, the manganese peak was attributed to jumps between a Fe - Fe interstice and a Fe - Mn interstice. In order to explain the decreased rate of nitrogen precipitation caused by manganese, distinction had to be made between the two types of equilibria which could exist due to the great difference in the diffusion rates between substitutional and interstitial atoms. Dijkstra and Sladek interpreted their results by considering that, when conditions were such that the substitutional atom participated in diffusion, nitrides with a different alloy content from that of the matrix were formed, (ortho-precipitate). If the substitutional atom did not diffuse, the nitride precipitate inherited its alloy content from the matrix, (para-precipitate). They suggested that manganese slowed para-precipition of nitrides by reducing the number of available nuclei.

More detailed studies [47,48] suggested that it was not possible to explain the marked retardation of precipitation caused by manganese simply by postulating that the nitrogen jump frequency was reduced in the presence of manganese. Fast [37] stated that this phenomenon could only be satisfactorily

explained by taking into consideration the interaction of nitrogen and pairs of manganese atoms. He suggested that due to this interaction a third maximum in the damping curve should exist at temperatures much lower than that of the normal peak. Whilst this peak would only show as a shoulder on the damping curve in a 0.5 at % Mn alloy, it should become the dominant peak in a 2 at % Mn alloy, since 15% of all the manganese atoms have a manganese atom as a nearest neighbour. It was, therefore, postulated that the greater part of the nitrogen in solution was bound to pairs of manganese atoms.

Investigations[49] of iron-carbon alloys containing 0.5 at % Ni; 0.9 at % Mo; 0.5 at % Cr; 0.5 at % Mn; and 0.5 at % V, showed that the position and shape of the carbon peak was the same for each of these alloys as for pure iron and that there were no subsidiary peaks in the range - 35°C to 200°C. It was reported that the carbon content as determined by analyses and by peak heights did not agree, analyses gave results which were very much higher than the damping peaks suggested. Although no explanation was offered it would appear to be obvious that in some cases carbide formation had occurred, however in the case of nickel and manganese which do not form stable carbides, the results are rather surprising.

In iron-vanadium-nitrogen and iron-molybdenum-nitrogen alloys no peak comparable to the Mn - Mn - Fe peak

was produced[67,68], but a distinct peak at a much higher temperature than the normal nitrogen peak was observed[66]. Fast and Meijering[70] made a close study of iron-nitrogen alloys containing 0.5 at % V. It was argued that since manganese produced a broadened peak, an element having a higher chemical affinity for nitrogen would produce an abnormal peak at a very much higher temperature. Vanadium was chosen since it has a much higher chemical affinity for nitrogen than manganese. An abnormal peak was obtained at approximately 88°C (f = 0.7 c/s.), which was in agreement with the previous observations of Dijkstra and Sladek[66] except that the abnormal peak appeared to be governed by more than one relaxation time, whereas the former workers considered the abnormal peak to be described by a single relaxation time. Fast and Meijering[70] found that the vanadium acted differently from manganese in two respects. Firstly, the vanadium alloy, unlike the manganese alloy, could contain large amounts of nitrogen (up to one atom nitrogen/atom vanadium) without showing any internal friction. Two damping peaks were found only when the alloy contained free nitrogen as well as chemically combined nitrogen. Secondly, vanadium increased the rate of precipitation of nitrogen. It was found that with increasing time of nitriding at 950°C, the abnormal peak reached its maximum first and then remained stationary until the maximum of the normal peak was attained. The abnormal

peak was also shown to move towards higher temperatures with increasing nitrogen content. Peak heights were lower than expected from chemical analyses, this being due to the formation of VN precipitates and to precipitation occurring during the measurement of the peaks. They suggested that the abnormal peak was due to the presence of finely distributed precipitates of vanadium nitride creating "abnormal" interstices in their environment, where nitrogen atoms were more strongly bound than in normal interstices. The low temperature peak was at the same temperature as for iron-nitrogen alloys and was undoubtedly due to the normal type of interstitial jumps.

While the present work was in progress (1961), Fast [57] in the light of work done on vanadium solubility in the Fe-V-N system by Fountain and Chipman [71] altered his interpretation of the mechanism associated with the abnormal peak. He reported previously unpublished work on the effect of aluminium and titanium on damping in iron-nitrogen alloys which failed to show abnormal peaks in the presence of AlN and TiN precipitates. Experiments using copper additions were also quoted, which indicated broadening of the normal peak when copper was in solid solution but showed no effect when copper was present as a precipitate. In view of these results, the mechanism proposed for the Fe-V-N abnormal peak [70] could no longer be considered valid. Since Fountain and

Chipman had shown that the solubility of VN in iron at 950°C was measurable, Fast accepted that a mechanism involving vanadium and nitrogen atoms in solution could be responsible for the abnormal peak. He obtained evidence for this by showing that wires containing vanadium and nitrogen heated at 950°C and quenched gave an abnormal peak, whereas wires held in the α-range at 830°C, where dissociation of VN was negligible, showed only the normal peak.

6. Thermodynamic Investigations of the Fe-V-N System.

While thermodynamic data on the formation of VN is available[72], little work has been done on the Fe-V-N system.

Pearson and Ende[73] derived a theoretical expression which allowed calculation of nitrogen solubilities in the presence of vanadium in α- iron. This, however, was based on the assumption that the solutes behaved ideally. In view of the strong chemical affinity between vanadium and nitrogen this would appear to be unlikely except in the case of extremely dilute solutions.

Turkdogan et al[74] investigated the effect of 0.016 and 0.057 %V on the solubility of nitrogen in iron. They concluded that vanadium nitride did not appear to form at nitrogen potentials lower than those required for the formation of iron nitride (Fe_4N) and that Henry's Law was obeyed for solutions containing up to 0.05 %V. The former conclusion is surprising, in view of the high nitrogen absorption rates

found by Fast and Meijering[70] in iron-vanadium alloys using very low nitrogen potentials.

Fountain and Chipman[71] carried out the most comprehensive investigation of the Fe-V-N system and determined many thermodynamic properties. In the context of the present work, their values for the solubility product of vanadium nitride in equilibruim with dissolved nitrogen and vanadium in the α and γ ranges is of particular interest.

From $\underline{V} + \underline{N} \rightarrow VN$; $K = [\% \underline{V}][f_N \% \underline{N}]$

it was shown that for γ-iron $K = -\frac{7070}{T} + 2.27$

and for α - iron $K = \frac{-7830}{T} + 2.45$

The activity coefficient of nitrogen in iron (f_N) was shown to be strongly influenced by vanadium content. At 950°C Fountain and Chipman give the relationship

$$\log f_N = -0.47 [\%V].$$

which indicates strong negative deviation from ideality, as might be expected from the high chemical affinity between nitrogen and vanadium. Recent Russian work[75] has suggested that the activity coefficient of nitrogen is independent of vanadium content. Thus considerable uncertainty still appears to exist on the thermodynamic properties of these alloys.

7. The Present Investigation.

Only two previous investigations, by Dijkstra and Sladek[66] and by Fast and Meijering[70], have included work on

the internal friction of Fe-V-N alloys. In both cases only a single vanadium content was studied and Fast and Meijering alone have attempted to discuss the nature of the "abnormal" high temperature damping peak. No attempt has been made to determine the activation energy associated with the peak or to explain the reported shift of the peak with varying nitrogen content. It is also rather surprising that no similar peak has been reported in the Fe-V-C system since the effects of nitrogen and carbon are usually similar in their internal friction effects. The effect of vanadium on nitrogen precipitation has also received little attention. In view of this situation the present investigation was undertaken in the hope of obtaining further information on the behaviour of nitrogen in alloys containing varying amounts of vanadium.

CHAPTER IV.

EXPERIMENTAL APPARATUS

AND

SPECIMEN PREPARATION.

IV. EXPERIMENTAL APPARATUS AND SPECIMEN PREPARATION.

1. Vacuum Casting Unit.

Since specimens of the highest possible purity were desired in the present work, the raw materials used were the purest obtainable and the iron-vanadium alloys were produced in a vacuum melting and casting unit. A line diagram and photograph of this equipment is shown in Figure 1. The apparatus consisted of three parts, namely (1) the melting chamber, (2) the casting chamber, and (3) the pumping system.

The melting chamber was constructed from a thick silica tube, 18" high x 4·5" diameter, one end of which was cemented, by means of black wax, into a steel flange which formed an o-ring seal with the top of the casting chamber. The upper end of the tube carried a steel head into which was fitted thermocouple and observation ports. Attached to the underside of the head was a radiation shield. The steel head and flanges at the ends of the tube were water cooled. Around the middle of the silica tube was wound the copper induction coil.

The casting chamber was a large cylindrical steel vessel, approximately 17" high x 17" diameter, sealed at its lower end and having a demountable top. Set into this top, in addition to the silica tube, was a large observation port,

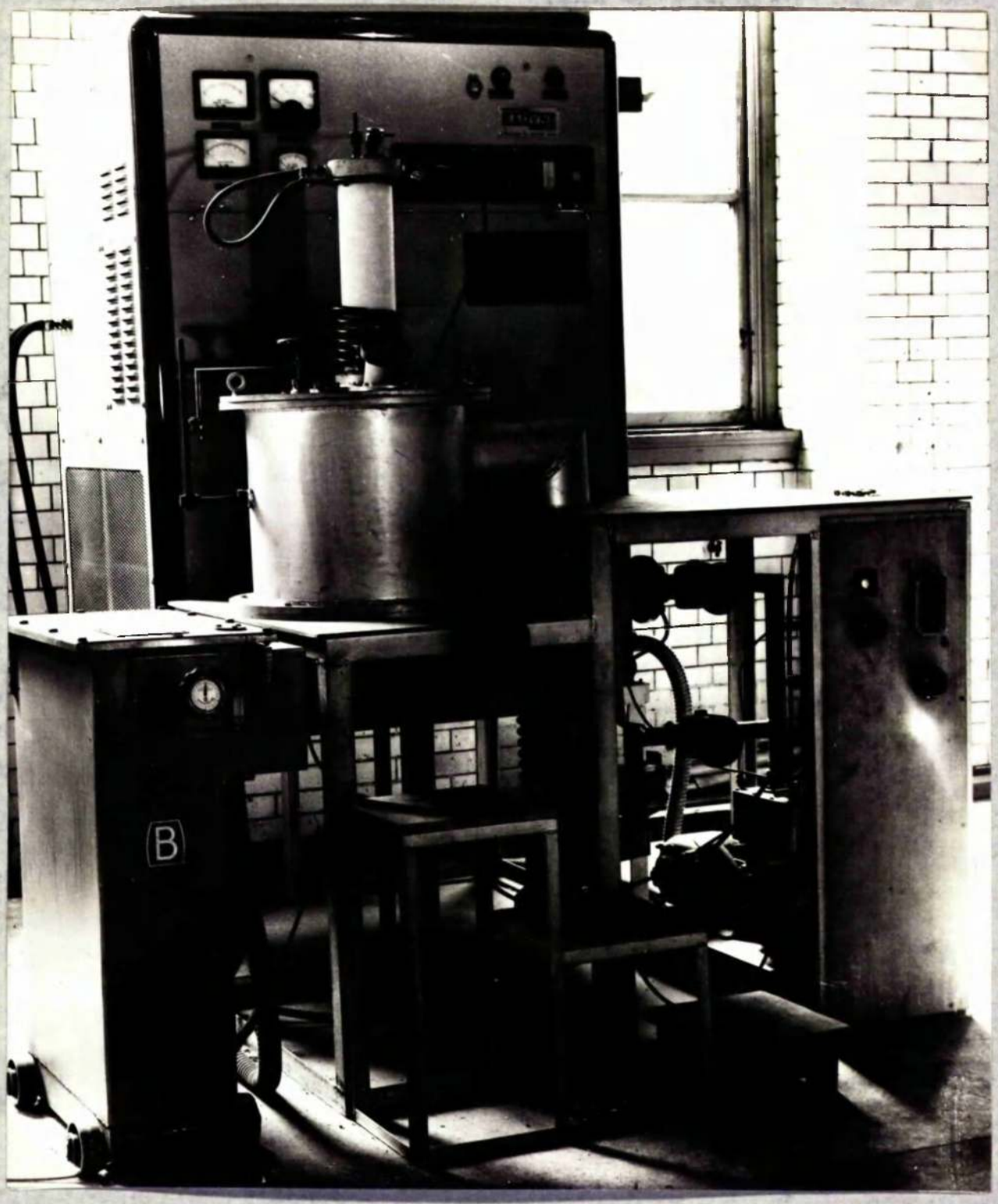

VACUUM CASTING UNIT

KEY TO FIGURE 1. VACUUM CASTING UNIT

a - Observation port.

b - Silica tube.

c - Copper induction coil.

d - Handle for rotating alloying addition containers.

e - Port for filling containers.

f - Casting handle.

g - Chute retracting spring.

h - Copper tube enclosing rachet and pinion arrangement.

i - Rachet.

j - Casting basket stand.

k - Swivelling casting basket.

l - Alundum sleeve and base plate.

m - Crucible.

n - O-ring seals.

o - Copper water pipe connecting top and bottom flanges.

p - Thermocouple port.

q - O-ring seals.

r - Oil diffusion pump.

s - Rotary backing pump.

t - Vacuum valves.

u - Flap valve.

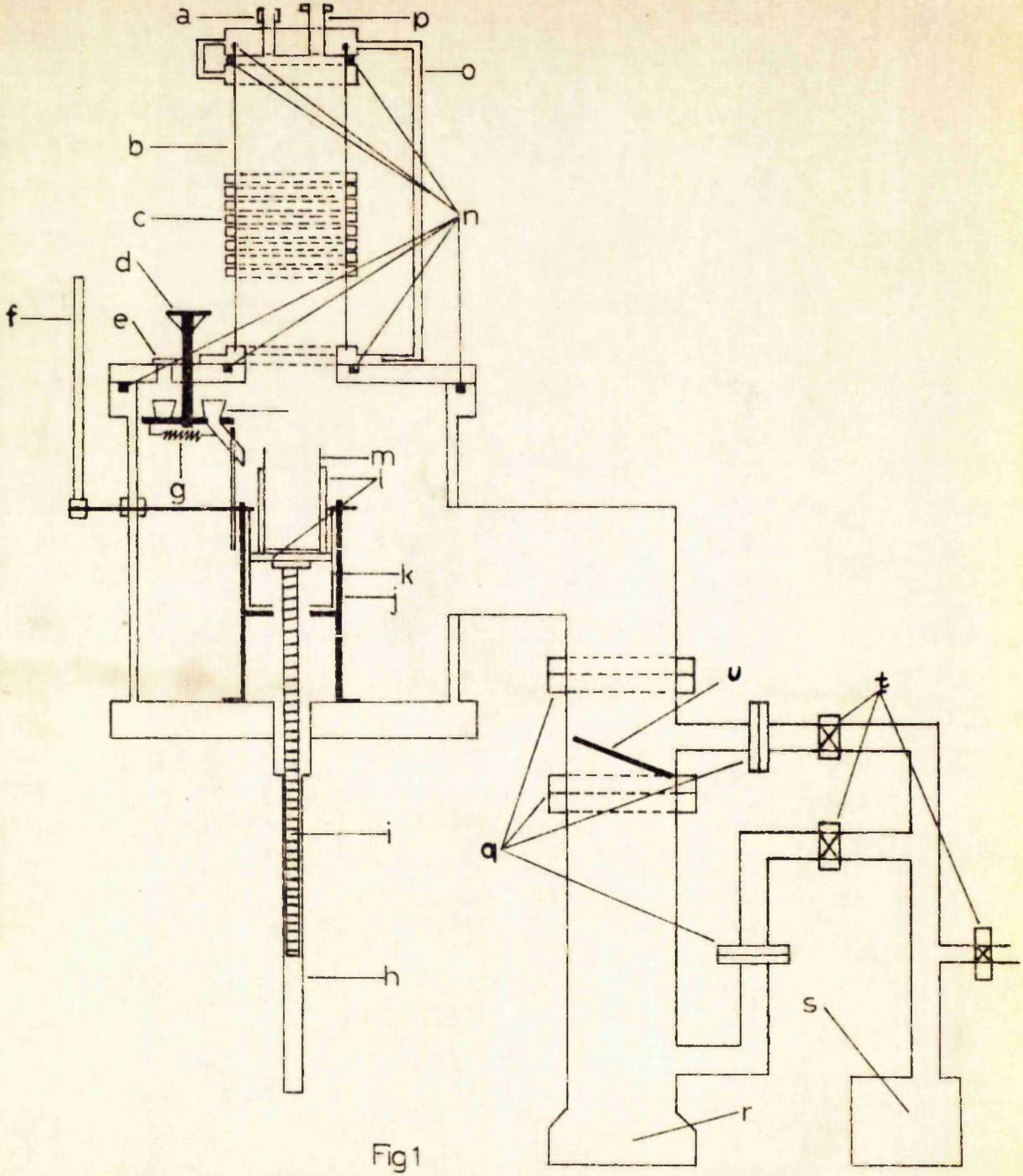

Fig 1

a device for making alloy additions under vacuum, and an extension which allowed a Penning Gauge head to be attached in a position unaffected by the electric field of the induction coil. The alloy addition mechanism consisted of four small bottomless buckets bearing on a brass plate. By rotating the buckets, their contents could be discharged into the 6" x 3" diameter crucible via a chute. The chute was retracted during casting by a suitable mechanism. Positioned centrally inside the chamber was the casting basket. The crucible could be raised from this basket, by means of a rack and pinion, into the induction coil. Once the charge was molten, the crucible was lowered to its former position and the metal poured into a cast iron mould. It was found necessary to heat the mould in order to obtain sound bars and power for this purpose was supplied to a mould heater via two electrodes inserted into the side of the chamber. Approximately 2 lbs. of alloy was obtained in each heat and this was cast into a bar 1" diameter x 9" long.

The pumping system consisted of a three stage oil diffusion pump, 36" high x 7" diameter, rated at 800 litres/min. at 10^{-4}, backed by a single stage rotary pump, rated at 700 litres/min. The valves in the pumping system were so arranged that it was possible to isolate the diffusion pump both when commencing to pump and when admitting air into the system. A Pirani gauge-head was located on the high vacuum side of the diffusion pump.

Pressure measurements were effected by both the Pirani gauge (range 0·5 - 0·001 mm.Hg) and the Penning gauge (range 5 - 0·1 μ). Pressures of the order of 0.1 - 0·2 μ were realised in this unit.

Power was originally supplied by a Philips high frequency induction unit (10 kw, 400 k c/s.). This unit was not satisfactory as the gases evolved from the charge ionised under the combined effect of the low pressure and the electric field, causing a glow discharge within the silica tube. This discharge was auto-catalytic and had the effect of absorbing all the available power, resulting in the resolidification of the charge, thereby giving rise to cracking of the crucible. Various rates of heating and periods of soaking at red heat were used in attempts to overcome this difficulty but these measures proved inadequate. Finally, a Radyne medium frequency heater (20 Kw, 1-10 K c/s) was obtained which obviated this difficulty.

2. Production of Alloys.

Difficulty was experienced in obtaining a crucible which would not erode, nor crack nor contaminate the metal by chemical reaction. Theoretical choice, from the point of view of stability of the oxide, favoured magnesia as a crucible material. Magnesia had the added advantage that any decomposition which did occur would not contaminate the melt with magnesium metal since magnesium is insoluble in iron and would volatilise under vacuum.

Attempts were made to manufacture slip cast magnesia crucibles, the raw material being pure magnesia which was carefully washed and dried before grinding in a ball-mill for several days to ensure a fine particle size. Magnesia crucibles were slip cast from a colloidal dispersion of magnesia in absolute alcohol using tapered plaster-of-paris moulds. Contrary to expectations, the shrinkage of the crucibles was so small that even with tapered moulds stripping of the crucibles could only be achieved by breaking away the mould. Several crucibles were thus obtained but they all cracked either whilst drying or during firing. This technique was abandoned.

At 1600°C alumina is as stable as magnesia and, as an alternative, high purity recrystallised alumina crucibles were obtained in the knowledge that there was a possibility of the decomposition of alumina occurring, resulting in contamination of the melt. An estimation of the possible extent of the reaction may be made as follows.

The reaction concerned is $Al_2O_3 \rightarrow \underline{Al}^2 \cdot \underline{O}^3$

At 1600°C $\log K = -12.3$ (76)

$\therefore [\%\ Al]^2 \cdot [\%\ O]^3 \sim 10^{-13}$

It is obvious that the amount of aluminium contamination will depend on the degree of oxidation of the melt. The iron used was very high in oxygen (0.15%) so that initially the equilibrium amount of aluminium is negligibly small ($\sim 5 \times 10^{-4}\%$).

However, since the melt was deoxidised with carbon, the final oxygen content is much less ($\sim 10^{-5}\%$) and, under these circumstances, considerable aluminium pick-up would be possible. The extent of reaction would be dependent on kinetics, nevertheless some aluminium pick-up could be expected if the metal was held molten for long periods after the deoxidation by carbon had ceased.

The pure alumina crucibles used were extremely unsatisfactory in that all the crucibles cracked before, or just as, melting of the charge occurred. This was puzzling and rather difficult to explain. It was possible that this was due to the way in which the charge melted in the induction coil, since it was noted that the middle melted first and this probably led to molten metal falling onto the bottom of the crucible and causing spalling. No explanation could be offered for the few cases where cracks were observed, on the bottom and side of the crucible, before there was any evidence of melting having occurred.

Attention was given, next, to ramming mixtures in the hope that a mechanically sound crucible could be produced. Zircosil (Associated Lead Development) ramming mix allowed strong crucibles to be made with relative ease. The green crucibles were oven-dried (100°C) before being fired in the induction coil of the melting unit, under vacuum, using a graphite susceptor to heat the crucible. Crucibles so produced were successful in so far that they did not crack,

did not evolve large quantities of gas, and resisted erroaion, allowing the charge to be held molten for lengthy periods (15 - 30 mins.) to ensure homogenisation of the melt after alloying. The mix consisted of a zirconium silicate (an extremely stable compound) with ammonium phosphate added as a bond. There was little possibility of silicon pick-up from the zirconium silicate, however, the ammonium phosphate bond, even after firing under vacuum, was only partly volatilised, and the casts made in these crucibles were contaminated with phosphorus by as much as 0·09%P. It was hoped to reduce the amount of phosphorus pick-up from these crucibles by making several casts in the same crucible and, by analysing successive casts for phosphorus, establish whether the increase in phosphorus content could be gradually reduced, and eventually eliminated, due to the scavenging action of the preceding casts. This programme was unsuccessful since it was impossible to obtain two consecutive casts from the same crucible due to cracking. Experiments with high temperature sintered zircon crucibles with no bond were unrewarding, their mechanical properties being inferior to the bonded type. The spalling resistance was much lower than for rammed crucibles, resulting in failure by cracking. Zirconia crucibles contained in larger rammed zircosil crucibles finally proved satisfactory. Whilst these difficulties were being resolved, several casts were made by courtesy of Via-Vac Ltd. in their plant at Wishaw. The casts were made in a 24"

vacuum furnace using zirconia crucibles.

Initially electrolytic iron was used as the base material until it was discovered that the metalloid content was higher than the preliminary analysis had indicated. High purity Swedish iron, kindly supplied by B.I.S.R.A., having the analysis shown in Table IV was finally used.

The oxygen content of the iron was extremely high necessitating deoxidation with spectroscopically pure carbon due to the hazards involved in the use of hydrogen as a deoxidant. The quantity of carbon added was slightly in excess of the stoichiometric amount, to ensure complete removal of oxygen. It was thought that the excess carbon could be removed from the specimens, later, by treatment with hydrogen. The deoxidation reaction may be written $\underline{C} + \underline{O} \rightarrow CO$ (gas)

$$K = \frac{pCO}{aC\ aO} \qquad (77)$$

This equilibrium constant is given by $\log K = \frac{2065}{T} + 1.643$

At $1600^{\circ}C$, $K = 5.55 \times 10^{2}$.

Since pCO = pressure in the vacuum system $\sim 1.3 \times 10^{-7}$ atmospheres, the solubility product aC. aO $\sim 2.5 \times 10^{-8}$. The residual carbon content in the casts is approximately 0.01%, so that the residual oxygen content in the metal should be approximately 10^{-5}%, a negligible value.

The general procedure adopted in producing the alloys was to place the carbon in the crucible first and then place the

TABLE IV. ANALYSES OF SWEDISH IRON

C = 0.02%	Si = 0.005%	Mn = 0.0027%
S = 0.009%	P = 0.001%	Ni = 0.0067%
Cr = 0.0025%	Mo = 0.003%	W = <0.01%
V = 0.0004%	Ti = 0.0009%	Co = 0.0065%
Al = 0.0018%	Cu = 0.0037%	Sn = <0.01%

O_2 = 0.15%

With C and O_2, Fe = 99.7651%

Without C and O_2, Fe = 99.9551%

The analyses of the vanadium used for alloying were

C = 0.026%	O_2 = 0.055%
N_2 = 0.039%	H_2 = 0.0018%

V = balance

iron charge on top. Due to the high oxygen content, the carbon-oxygen reaction was extremely vigorous, the effervescence on melting being such that most of the charge was thrown either out of the crucible or up onto the sides where the iron bridged and would not melt. It was therefore necessary to melt slowly and to introduce an atmosphere of argon at 50 cms. pressure into the melting chamber. Towards the end of the boil, the pressure was slowly reduced until eventually it was less than 0·5μ. Only when the metal was quiescent was the vanadium added. A further small release of gas usually followed. The average charge was approximately 950 gms. of iron. Six alloys with vanadium contents in the range 0-1% V were cast. The analyses of the various casts are shown in Table V.

3. Working of Alloys.

The cast bars were machined until a smooth surface free from blemishes was obtained. Reduction by cold rolling followed, in stages of 0·01" per pass, until the final diameter of 0·5" was obtained. Before drawing, the bars were vacuum annealed for 1 hour at 700°C. The mechanical and thermal history of the bars during drawing was as follows.

Drawn from 0·5" - 0·268". Vacuum annealed at 700°C for 1 hour after every 45% reduction of area.

Drawn from 0·0268" - 0·047". Vacuum annealed at 700°C for 1 hour after every 25% reduction of area.

Drawn from 0·047" - 0.031". No intermediate anneal. Reduction of area was 57%

TABLE V. ANALYSES OF CASTS

Cast No.	Carbon	Silicon	Sulphur	Phosphorus	Vanadium
Originally	0·02	0·005	0·009	0·001	0·0004
18	0·010	0·030	0·012	0·007	(0·004)
19	0·010	0·025	0·011	0·002	0·157
20	0·010	0·025	0·010	0·005	0·395
21	0·011	0·025	0·015	0·005	0·620
22	0·007	0·025	0·012	0·005	0·690

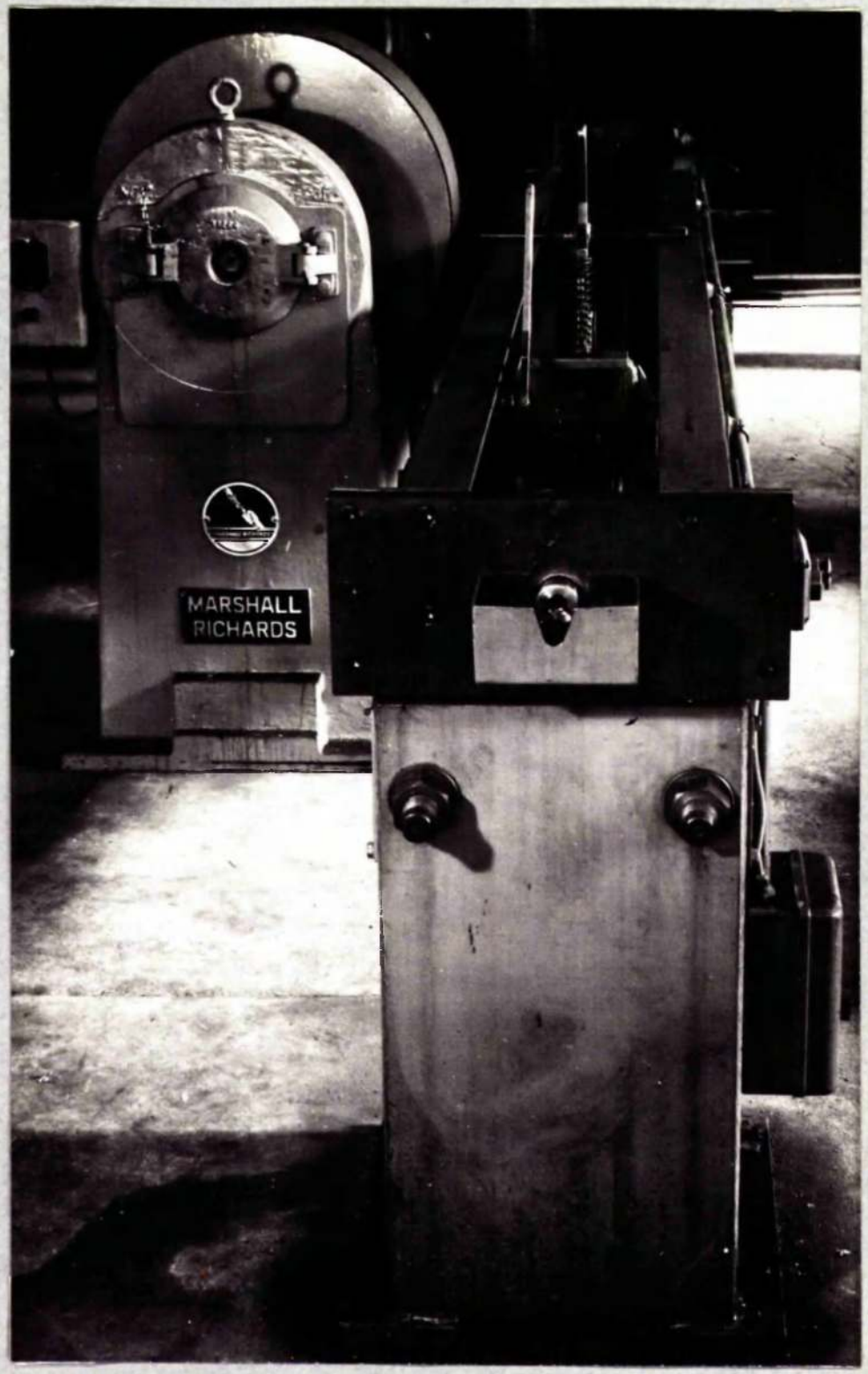

The Draw-Bench.

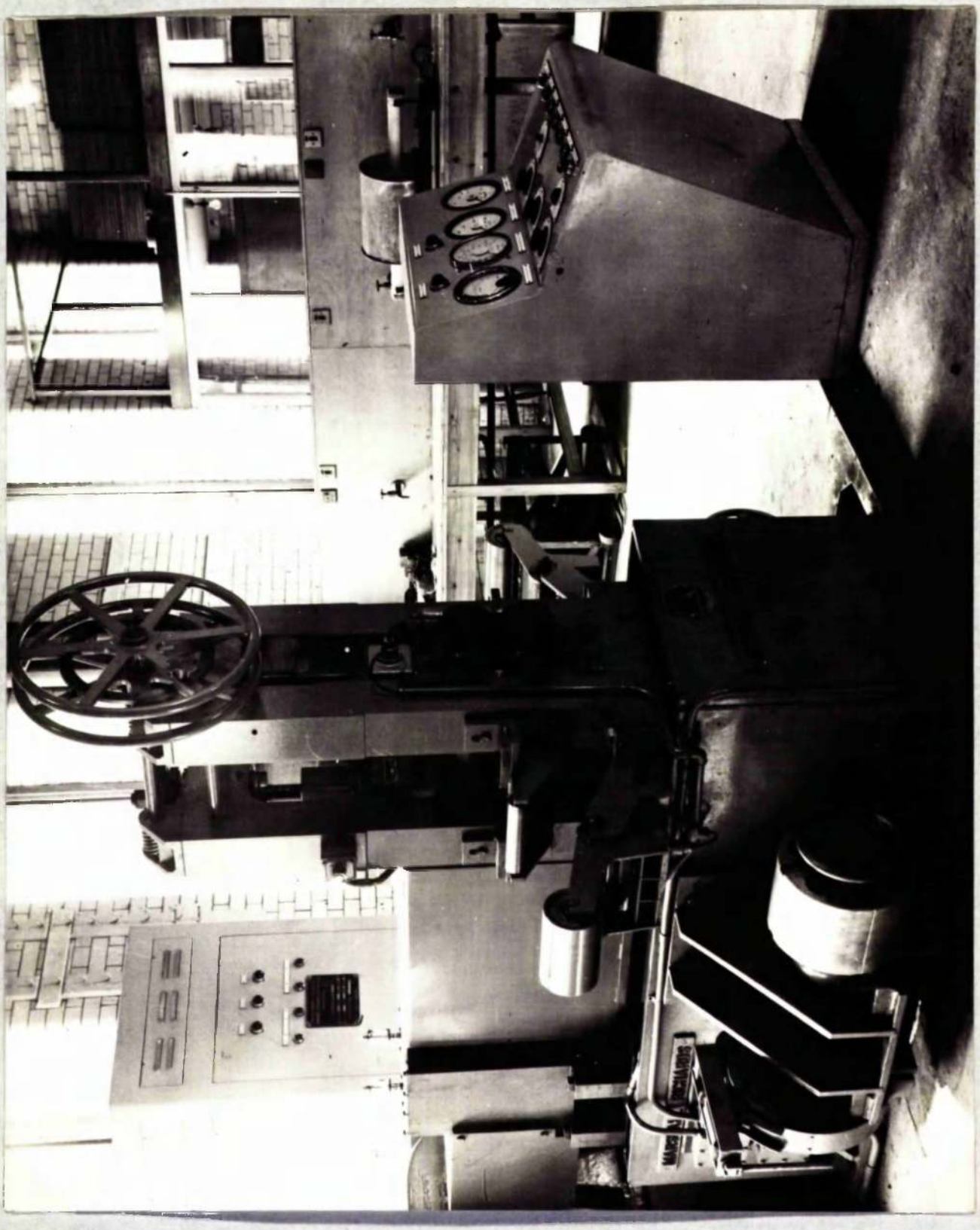

The Rolling Mill.

4. Grain Size and Grain Orientation of Alloys.

It will be recalled that the internal friction is dependent both on the orientation and grain size. Consistent results were obtained by having a mean grain diameter equal to approximately one-tenth the diameter of the wire and random orientation. Since both these conditions were reported to be satisfied by recrystallising the wires at 900°C - 950°C, this treatment was adopted in the present work.

Specimen wires from each cast were sealed in evacuated silica tubes and soaked at 920°C for 10 minutes then normalised. Longitudinal sections of wires were etched in 3% nital and examined through a Vickers-Projection microscope at X200. The viewing screen had an area of 12·25 sq.ins. Approximately eight grain counts were performed on each wire and the arithmetic mean taken, fractions of a grain being counted as unity. The mean grain diameters were found to lie in the range 0·00329" - 0·00478", compared to the diameter of the wire, 0·031."

The orientation of the specimens was checked using a flat-film camera of the Laué type. The conditions used were 30 minute exposures at 40 Kv, 30 ma, using a cobalt target. Transmission photographs were taken both with the wire specimen stationery and rotating. In both cases, the diffraction rings were of constant intensity, although rather spotty due to the influence of the grain size [70]. No evidence of preferred orientation was found.

5. Heat Treatment Furnaces.

(i) Horizontal Furnaces.

Two horizontal furnaces were constructed for the purpose of treating the wires with hydrogen and annealing them in vacuum. The silica furnace tube, 2·5" diameter x 36" long, was wound with nichrome wire, 0·028" diameter, so that the temperature gradient along a 12" length in the centre of the furnace was not greater than $\pm 5^{\circ}C$ from the set temperature. A control couple was cemented onto the surface of the tube, at the mid-point of the hot zone. The furnace resistance was approximately 50 ohms. By means of asbestos wool packing the furnace tube was held centrally in a "Sindanyo" (type of asbestos) casing 12" diameter x 24" long.

The two furnaces were connected to a common pumping system consisting of an oil diffusion pump (rated at 25 litres/sec) backed by a single-stage, gas-ballast, rotary pump (rated at 28 litres/min.). Valves were so arranged that the furnaces could be evacuated either together or singly, and the oil diffusion pump could be isolated both when admitting air into the system and at commencement of evacuation. Pressure measurement of the system was effected by a discharge tube which blacked out at 10^{-3} m.m.Hg. When the pumping system was not required, gas could be passed through the furnaces. The water supply to the diffusion pump was checked by a "Flowtrol" unit to guard against failure of the water supply.

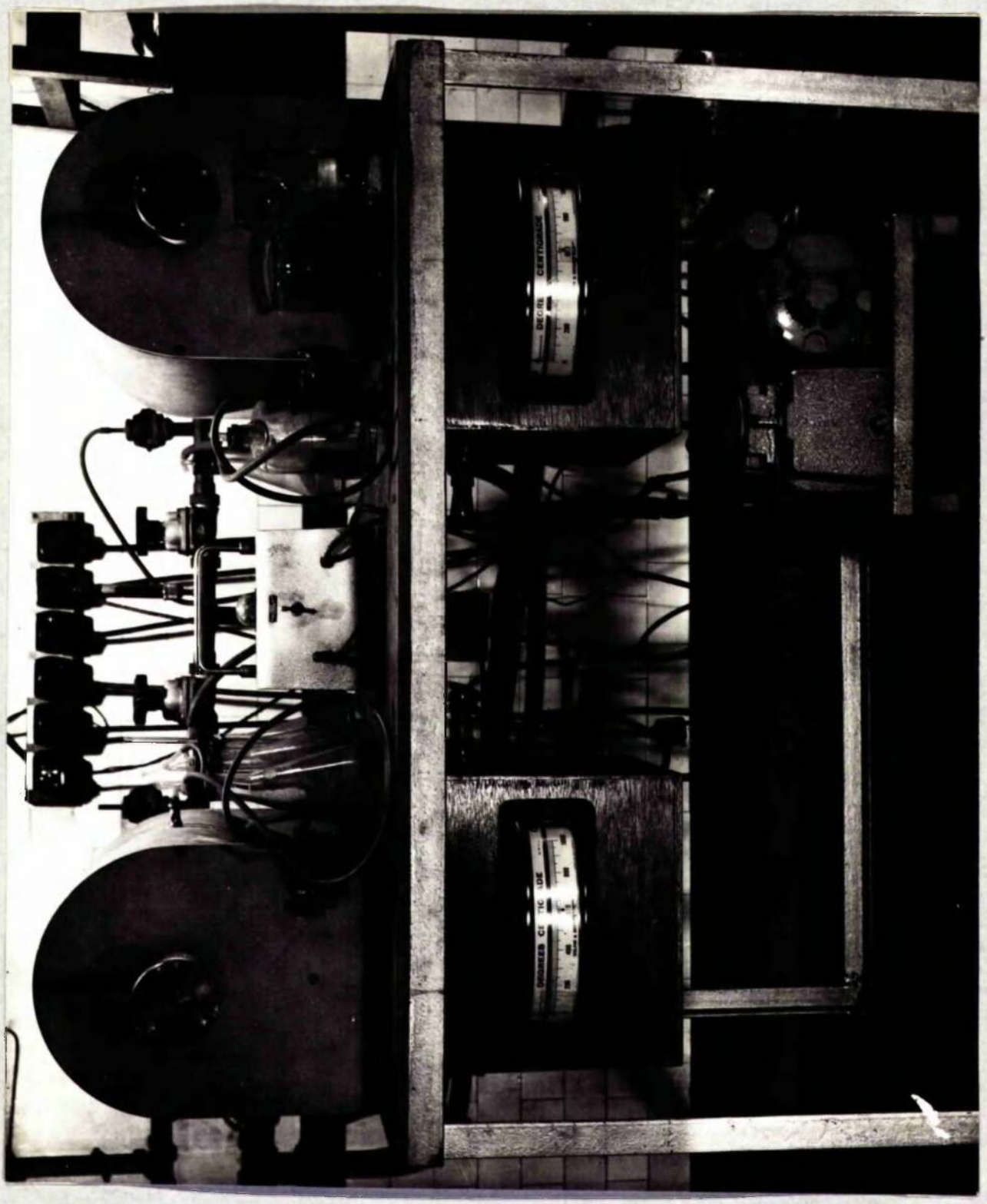

The Horizontal Heat Treatment Furnaces.

The temperature in each furnace was controlled by a Kelvin-Hughes proportional controller to within $\pm 2^{\circ}C$ of the set temperature. Each controller had a broken thermocouple system which automatically switched off the power in such an eventuality. Since the current load was too large to be safely handled by the instrument, a mercury switch was incorporated into the circuitry. The furnaces were capable of a maximum temperature of $950^{\circ}C$. Careful calibration of the set temperature on the instrument panel against the temperature in the middle of the furnace, as indicated by a chromel-alumel thermocouple and potentiometer, was made for each furnace.

(ii) Vertical Furnaces.

A photograph and line diagram of this apparatus (Figure 2) is shown. Two vertical furnaces, with facilities for quenching, were built for nitriding the specimens. These furnaces, apart from being 12" longer, were identical in construction, temperature control and pumping system as the horizontal furnaces. In order to facilitate quenching, the specimen carrier, within the furnace, was suspended by a fine wire connected to two electrodes in the top flange which sealed the furnace tube. Application of a voltage across the electrodes caused the wire to melt and the specimen carrier fell into a quenching bath which formed an extension of the furnace tube.

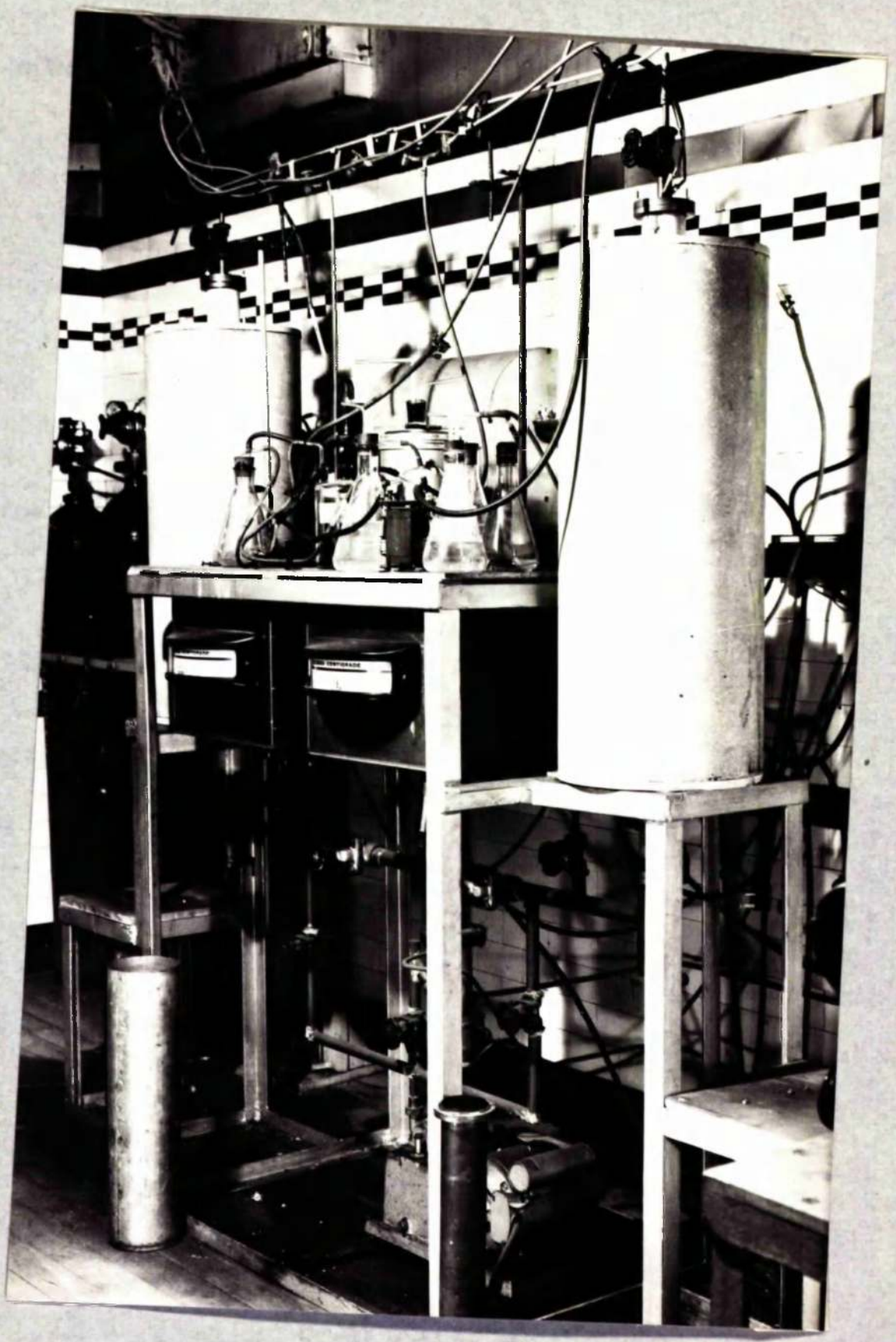

VERTICAL HEAT TREATMENT FURNACES.

KEY TO FIGURE 2. VERTICAL HEAT TREATMENT FURNACES

a - Venturi meters.

b - Stopcocks.

c - Vacuum flask.

d - Solid CO_2

e - Glass tube containing absorbent.

f - Saturator.

g - Asbestos wool packing.

h - 'Sindanyo' case.

i - Control thermocouple.

j - Vacuum valves.

k - Electrodes.

l - Fine nichrome wire.

m - Specimen holder.

n - O-ring seals.

o - Quenching medium.

p - Demountable quenching tank.

q - Discharge tube.

r - Vacuum seal.

s - Oil Diffusion pump.

t - Rotary backing pump.

u - Demountable flanges.

v - Gas mixers.

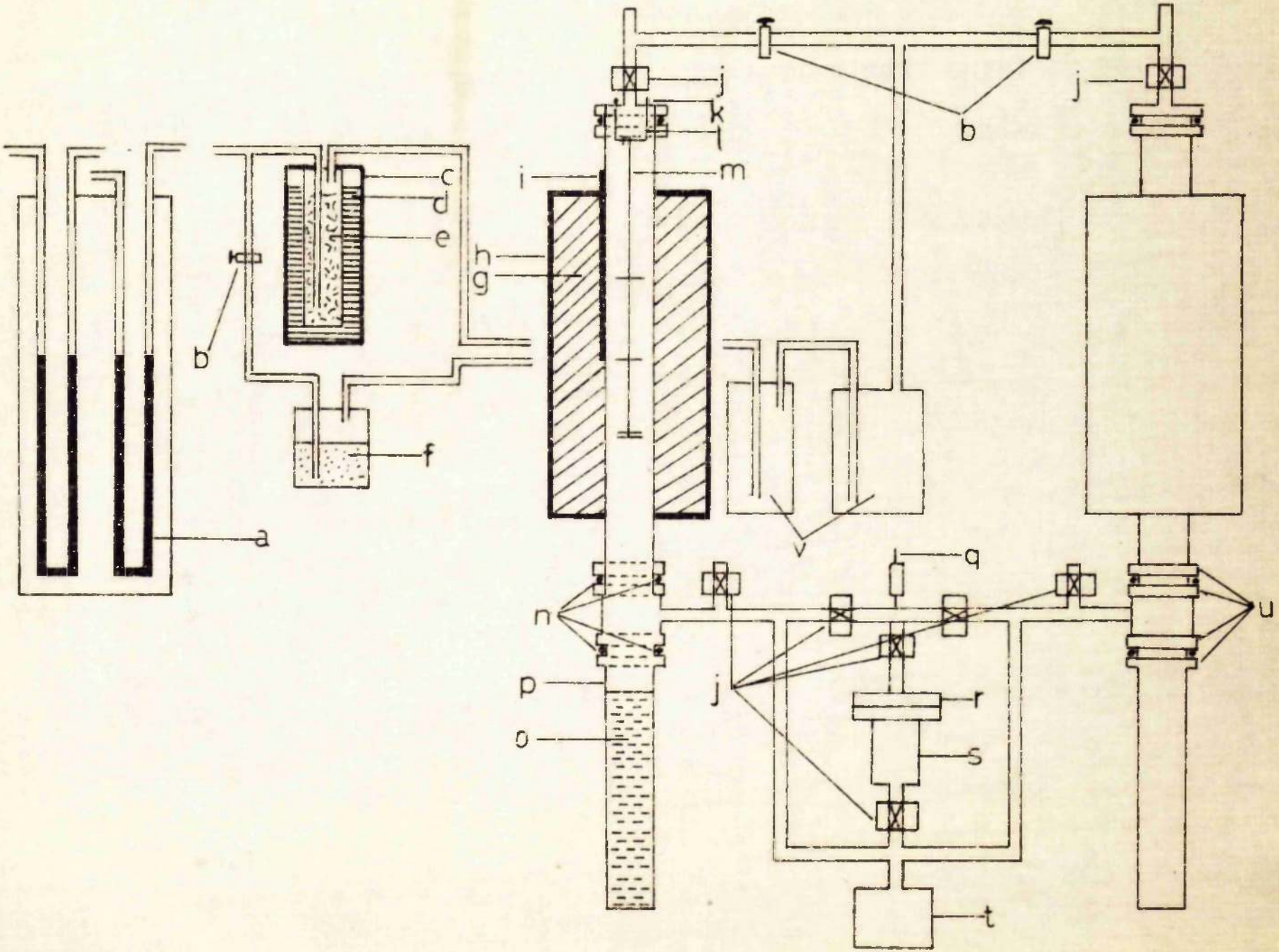

Fig 2

Gas lines for hydrogen, ammonia and argon were fitted to the furnaces. The gas system was flexible in that any combination of gases, either dry or saturated with liquid, could be used. Description of the gas system is best achieved by considering a flow diagram. (Figure C).

The various parts of the purification and metering system are described below.

DEOXO. This is a patent platinised catalyst to remove oxygen from hydrogen by the reaction.

$$2H_2 + O_2 \longrightarrow 2H_2O$$

DESSICATOR (1) This contained magnesium perchlorate.

DESSICATOR (2) This contained a zeolite (alumino-silicate) molecular sieve material which is a very effective dehydrant and absorbant for hydrocarbons.

VENTURI METERS. Calibration of the hydrogen Venturi was achieved by using a rotating drum gas meter. The ammonia meter was calibrated by absorbing the ammonia, for a measured period of time, in standard hydrochloric acid and backtitrating the excess acid with standard sodium carbonate, using methyl orange as indicator. Calibration graphs, relating the rate of flow to the pressure difference across the Venturi, were obtained for hydrogen and ammonia.

SATURATOR. This contained either distilled water for wet hydrogen treatment or toluene for carburisation experiments.

COLD TRAP. This consisted of a tube, filled with either a

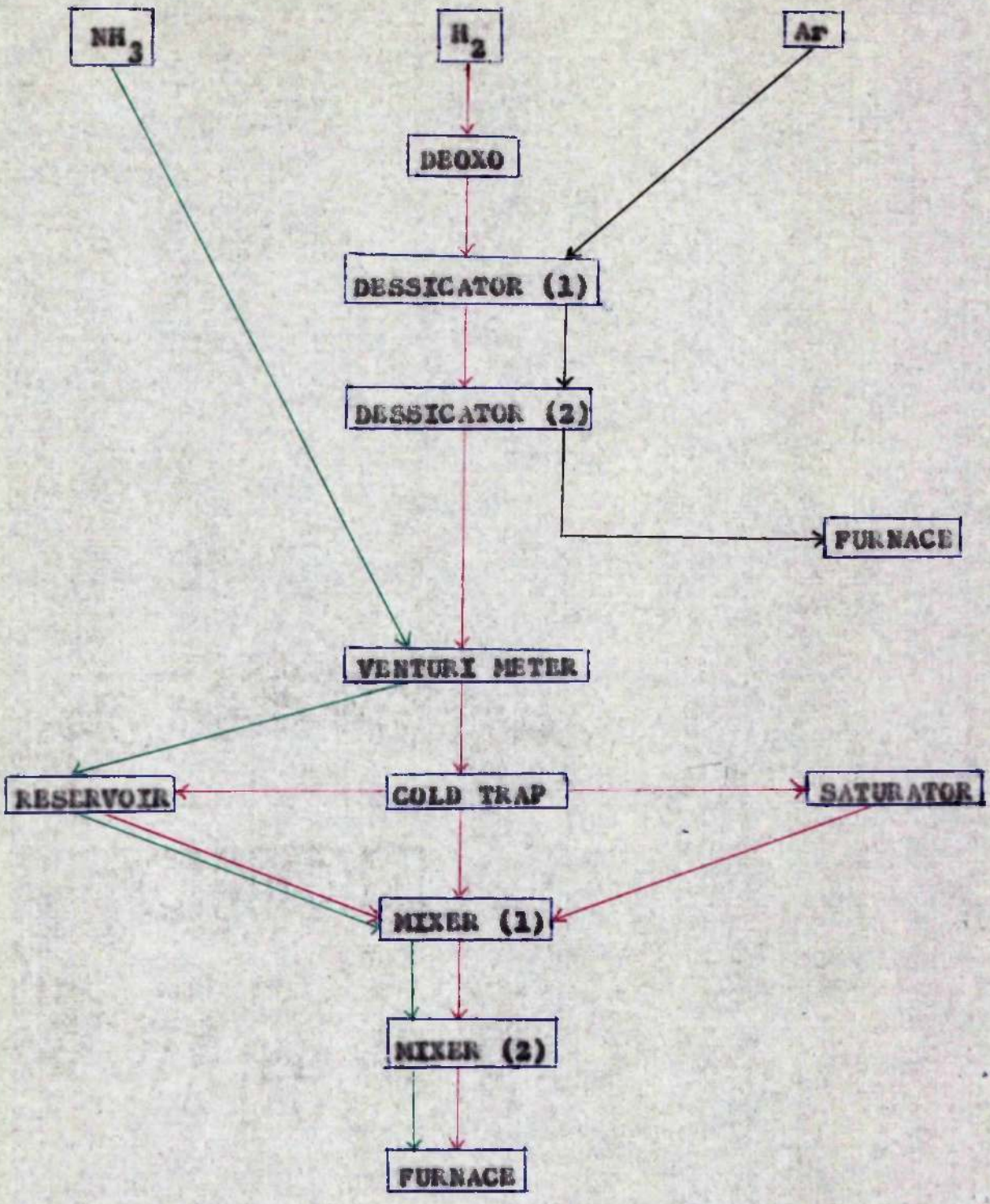

Figure C. GAS SYSTEM FOR VERTICAL FURNACES.

zeolite or activated charcoal, inside a Dewar flask packed with crushed CO_2.

RESERVOIR. The purpose of this was to damp any pressure fluctuations in the ammonia line, thereby ensuring a constant ammonia potential in the gas mixture.

MIXER (1) This was a flask containing two inlets, one for ammonia and the other for hydrogen. Since the percentage of hydrogen in the gas mixture was much higher than that of ammonia, it was necessary to draw the ammonia inlet tube down to a fine nozzle. This ensured that the ammonia had a high exit velocity and was unaffected by the relatively high hydrogen back-pressure.

MIXER (2). This was a tube containing glass beads to cause intimate mixing of the gases.

The exit gases, from the furnace, were passed through a cracker furnace at 600°C to guard against free ammonia polluting the atmosphere.

6. Torsional Pendulum.

The pendulum was similar to that described by K$\hat{e}$ [42], Figure 3. Essentially, the wire specimen, 11" long x 0·031" diameter, was held at one end in a steel pin-vice attached to a rigid steel frame. Clamped to its lower end was an inertia bar, 8" long, with a small moveable surface mirror at the centre. Small weights fitted onto the bar and could be adjusted to any position along its length. This enabled the frequency to be

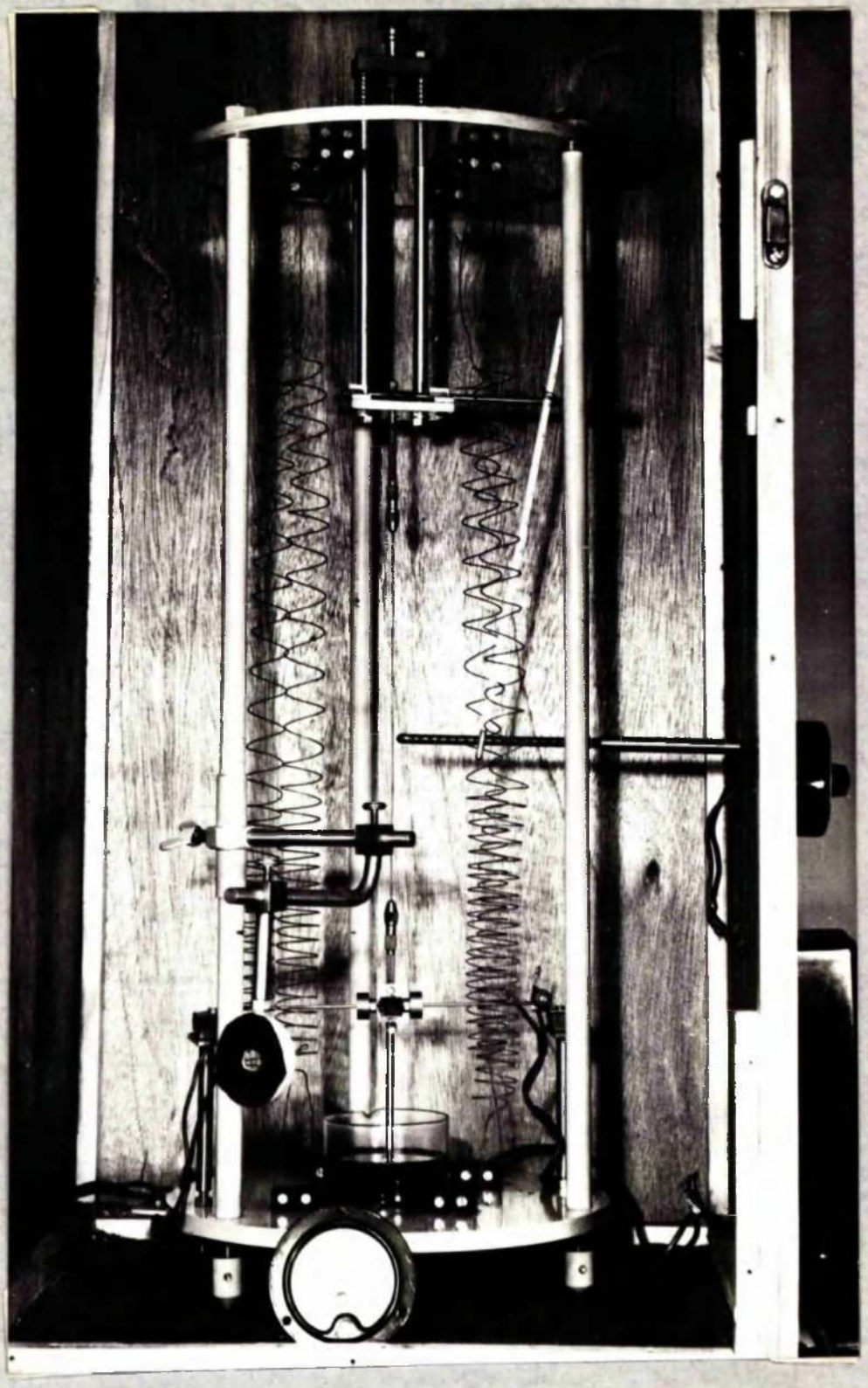

TORSIONAL PENDULUM.

KEY TO FIGURE 3. TORSIONAL PENDULUM

a - Fan motor
b - Wooden cabinet.
c - Gear wheel.
d - Upper steel vice.
e - Thermometer.
f - Wire specimen.
g - Lower steel vice.
h - Mirror.
i - Springs.
j - Adjustable weights.
k - Oil.
l - Levelling screws.
m - Glass dish.
n - Electromagnet stands.
o - Inertia bar.
p - Electromagnets.
q - Relay.
r - Bimetallic thermostat.
s - Wire heating coils.
t - Rotational control.
u - Steel frame.
v - Vertical adjustor.
w - Fan.
X - Plane focussing lens.
x - Lens with focal length of 3 metres.
Y - Rotating recording drum.
y - Stand.
Z - Synchronous motor.
z - Projector lamp.

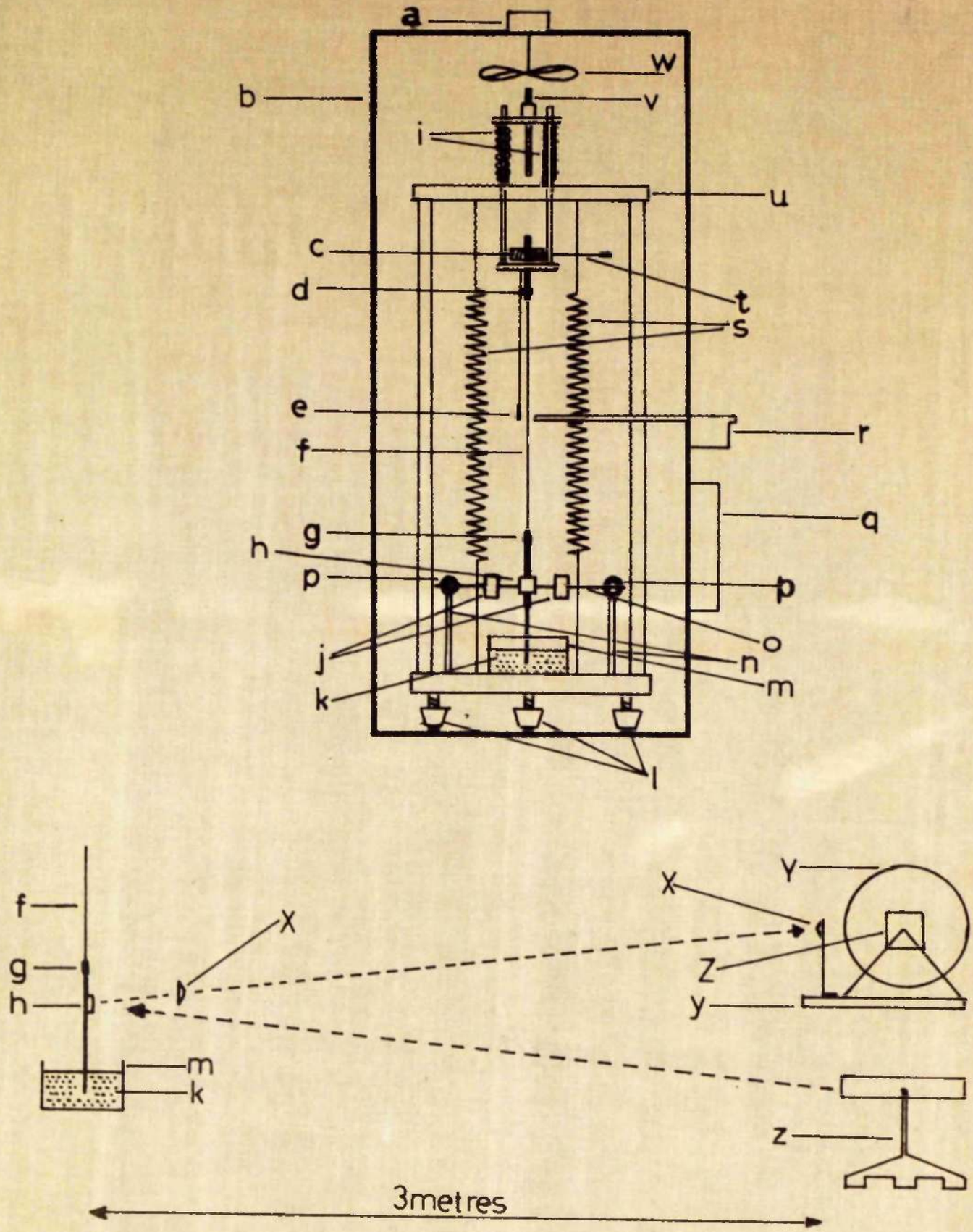

Fig.3

varied from approximately 0·7 C/S to 2·5 C/S. The tip of the upright of the inertia bar dipped into an oil-dashpot which damped out non-torsional vibrations. The wire was set in torsional vibration by energising a pair of strategically placed electromagnets. In order to facilitate rapid alignment of the optical system, facilities were provided for raising, lowering and rotating the wire in addition to which the mirror could be swivelled about a horizontal axis. The positions of the electromagnets were made variable to accommodate this adjustment.

Four heating coils surrounding the specimen provided means of varying the temperature. Power to the coil was supplied from a Variac transformer. Incorporated into the circuitry was a relay operated by a bimetallic thermostat, so that it was possible to vary the temperature from ambient to approximately 45°C. Temperatures lower than ambient could be obtained by cooling with solid CO_2. The temperature was controlled to $\pm$ 0·5°C with a maximum gradient along the length of the specimen of $\pm$ 2°C. The whole system was enclosed by a wooden cabinet, 40" high x 20" deep x 18" wide, having a glass door. Set into the roof of the cabinet was a small fan which aided convection. Care had to be exercised in setting the fan speed, as too fast a speed caused excessive air currents giving rise to lateral movement of the wires.

A slit of light from a lamp (12v, 24w), approximately three metres distant, was projected onto the mirror on the

inertia bar. The reflected image passed through a concave lens, a few inches in front of the pendulum, which focussed the image onto a plane focussing lens which, in turn, condensed the slit into a spot on the surface of a recording drum. The recorder consisted of a brass drum, 10" long x 6" diameter, driven by a synchronous motor at 0.5 r.p.m. A permanent trace was obtained by wrapping a sheet of Ilford B3-1P bromide paper around the drum. All the experiments were performed in specially constructed dark-rooms. Sample traces obtained are shown in Figure 4.

For high temperature work, a similar, but smaller, pendulum was built. (See photograph). The suspension mechanism was constructed into the top of a "Sindanyo" cylinder 12" diameter x 15" high. Shorter 6" length specimens were used in this apparatus, the clamping, energising, optical and recording systems being as described above. The lower half of the inner surface of the casing was wound with 0.028" diameter nichrome wire, its current being controlled by a variable transformer. Three thermometers were inserted through holes drilled down the side of the casing, corresponding to positions at the top, middle and bottom of the wire, so that the bulbs were no more than 0.25" distant from the wire specimen surface. To ensure good circulation, and so minimise temperature gradients along the length of the specimen, a small fan was inserted at the top of the container. In addition a miniature rotary

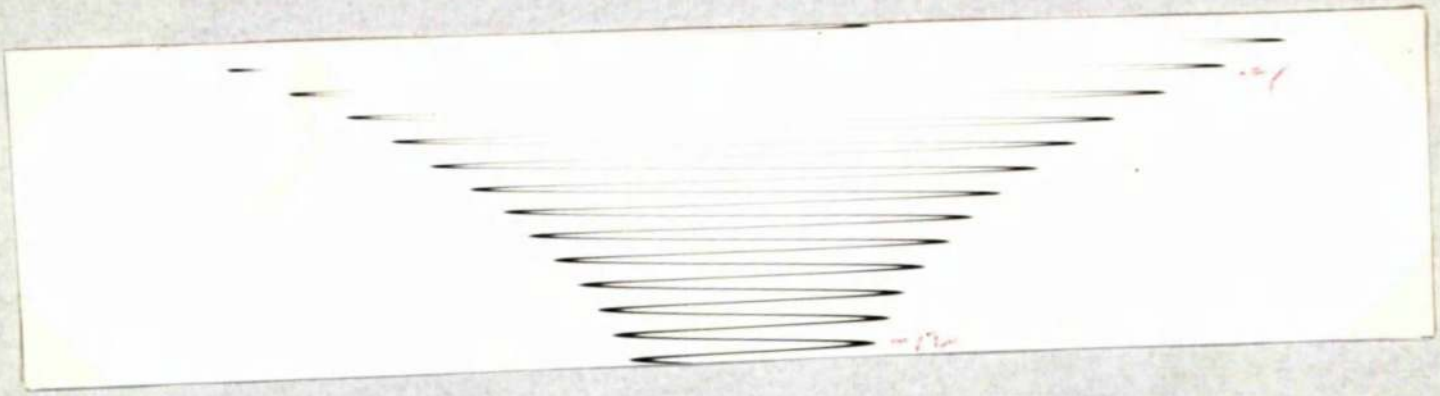

DAMPING = 4×10^{-2}, f = 1.2 c/s

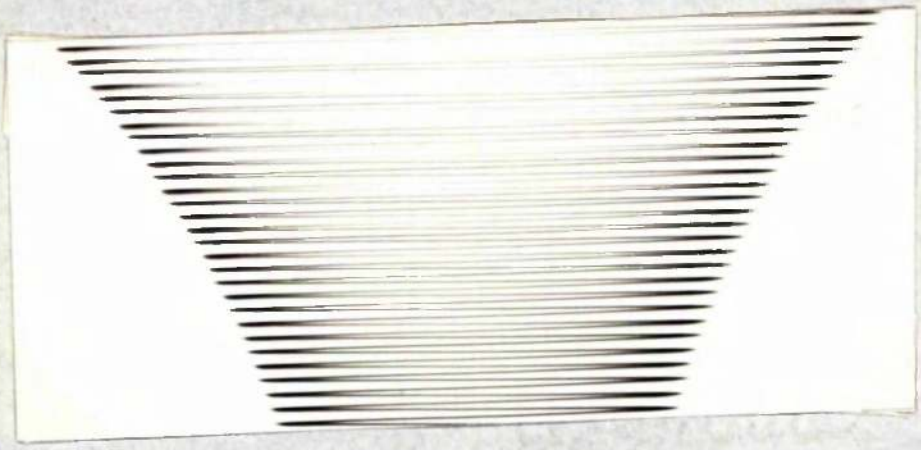

DAMPING = 8×10^{-3}, f = 2.45 c/s

DAMPING = 6×10^{-4}, f = 1.3 c/s

Figure 4. Sample traces obtained using the internal friction apparatus.

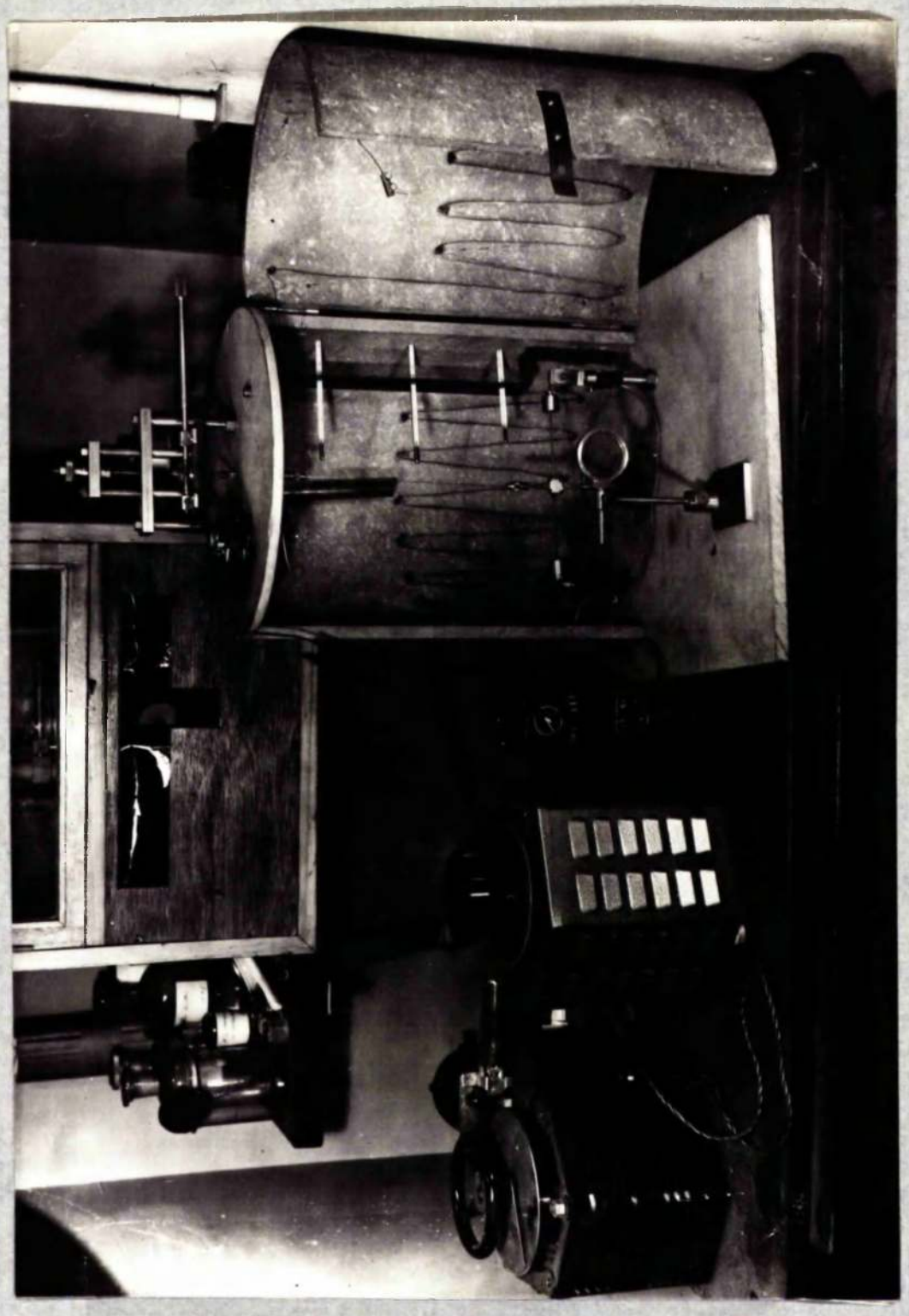

THE HIGH TEMPERATURE TORSIONAL PENDULUM

blower supplied air at ambient temperature into the top of the apparatus. Again care was needed in adjusting conditions to prevent disturbance of the pendulum. The temperature was controlled manually and could be maintained within $\pm$ 0.5°C of any desired temperature. The maximum gradient along the length of the specimen was less than $\pm$ 1°C.

The shear strain on the surface of the wire whilst being tested in either pendulum was not greater than 5×10^{-5}. Conservatively estimating the yield point of iron as 10,000 lbs/ins., the stress on the wire due to the weight of the inertia bar was less than 2% of the yield stress. These conditions always ensured that the damping was amplitude independent, this being verified by a plot of the logarithm of the amplitude of vibration against the ordinal number of vibration. A typical plot is shown, Figure 5.

The amplitudes of vibration on the photographic traces were measured by ruler to within $\pm$ 0.05 cms. Before calculating Q^{-1}, each measurement was corrected to account for the width of the light spot. No amplitude greater than 12 cms. or smaller than 4 cms. was measured and the maximum estimated error in Q^{-1} was less than 1%. Clearly, it was desirable to measure amplitudes which were as large as possible. The amplitude ratio was usually calculated on the basis of ten cycles, the first few cycles being discarded wherever possible, to eliminate any influence of non-torsional motion or remanent magnetism

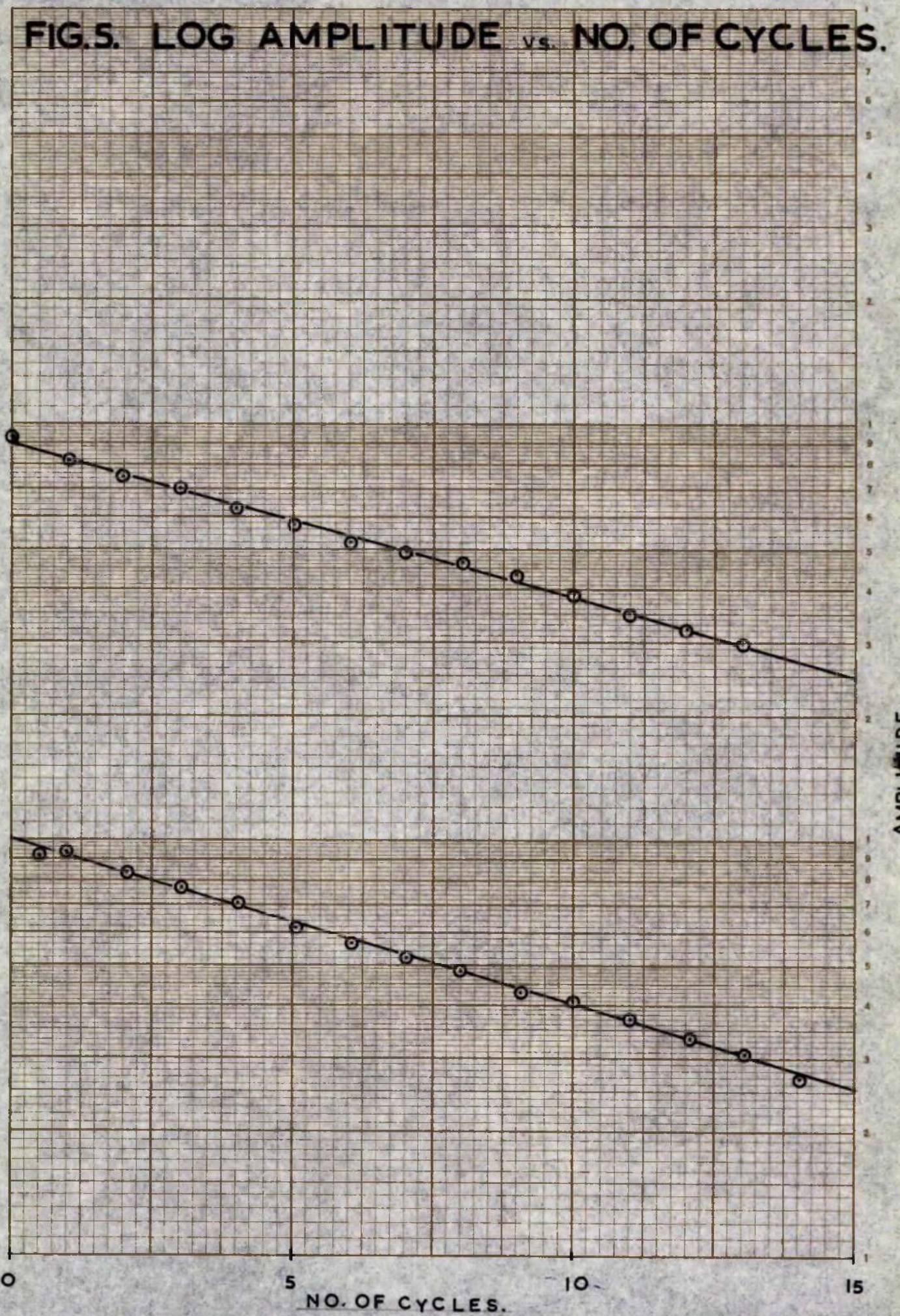
FIG.5. LOG AMPLITUDE vs. NO. OF CYCLES.
AMPLITUDE.
0
5
10
15
NO. OF CYCLES.

affecting the damping. From each trace at least four values of Q^{-1} were measured, the arithmetic mean of the results being used. The frequency was measured by observing the number of cycles occurring in one complete revolution of the recording drum. All the values of Q^{-1} quoted have been corrected for background damping. This was measured on purified wires prior to nitriding and was generally of the order of 1×10^{-3}.

7. Purification Treatment.

Since it was necessary, during the manufacturing of the alloys, to deoxidise the iron with carbon, the wires had a small residual carbon content. As carbon itself gives rise to internal friction it must be removed from the wire specimens. A convenient method, for carbon removal, is to treat the wires in a stream of moist hydrogen for long periods at a temperature where diffusion of carbon readily occurs. Under these conditions carbon is removed by two reactions:-

$$C + O_2 \longrightarrow CO_2 \qquad (1)$$

$$C + 2H_2 \longrightarrow CH_4 \qquad (2)$$

the reaction (1) being the more favourable.

Moist hydrogen (saturated in distilled water at ambient temperature) was passed over the wires at 700°C at a rate of 120 c.c./min. (3.8 cms./min. linear velocity) for long periods. Pure iron wires showed a background damping of approximately 5×10^{-4} after treatments lasting 20 hrs. It was not considered desirable to purify the vanadium alloy wires

with wet hydrogen since it would possibly internally oxidise the vanadium. Dry hydrogen was used, the carbon being removed by reaction (2). This reaction is not very efficient and even after 50-60 hours the alloy wires showed a background damping of the order of 1.3×10^{-3}, however, the sample wires tested did not show any carbon peak. Since the background damping varied from cast to cast, it was assumed that the higher background damping was inherent in the alloy and not due to carbon. The wires were therefore considered purified after a treatment of at least 60 hours.

CHAPTER V.

EXPERIMENTAL.

V EXPERIMENTAL

1. Solubility Measurements.

Throughout the present work, Ammonia was used in preference to nitrogen as the nitriding medium. It is known that the nitrogen/iron equilibrium is unfavourable, due to the activation energy barrier of the surface reaction and, at temperatures below 600°C, this reaction is extremely slow. A more rapid method of nitriding is to use ammonia which decomposes on the iron surface to produce highly active nascent nitrogen.

A series of experiments, using pure iron wires, was undertaken to determine a suitable $NH_3 - H_2$ gas mixture in which to nitride the samples. The ammonia potential desired would just supersaturate the wires at 590°C, if sufficient time for equilibrium to be established was allowed. Using the diffusion coefficient for nitrogen in α-iron determined by Wert[60], it was calculated that the samples would be homogeneous after 8 hours nitriding. The work of Lehrer[77] suggested that 10% NH_3-H_2 mixtures should be in equilibrium with saturated α-iron at 590°C. Using data obtained by Fast and Verrijp[62] a frequency was calculated which caused the nitrogen peak to occur at a temperature a few degrees above ambient.

A number of wires were nitrided at 590°C in 10% NH_3-H_2 mixtures for times varying from 4 to 12 hours. The gas flow of 15⁰ c.c./min.(4.8 cms./min.. linear velocity)

ensured that marked decomposition of the ammonia did not occur. After quenching into oil at 4°C, the damping was measured at 23°C using a frequency of 1.34 C/S. The results obtained for treatments longer than 6 hours lay within the range $Q^{-1}max$ = 3.72×10^{-2} to 4.24×10^{-2}. These values corresponded to nitrogen contents very much lower than the solubility of nitrogen in α-iron at 590°C. It was considered that three factors could account for the low results.

1. The Ammonia potential was too low and saturation was not attained. In this case, a higher Ammonia potential should produce higher damping values.

2. The wires had been overnitrided although no definite nitride case was observed microscopically. A nitride case would give low results since, although the nitride itself does not cause damping, it has the effect of reducing the volume in which energy can be dissipated within the wire, but does not produce a corresponding decrease in the energy required to cause torsional vibration. Thus the value of

$$Q^{-1} = \frac{\text{Energy dissipated within the wire}}{\text{Energy imparted to the wire.}}$$

will decrease.

3. Since a highly supersaturated solution of nitrogen is unstable, precipitation might have occurred before and during damping measurements. However, the results obtained were approximately half the expected value, and as only 10-15 minutes elapsed before the damping was measured, it was

considered that precipitation alone could not account for such a large discrepancy.

To test the possibility that the ammonia potential was too low, new wires were treated under the same conditions as above in 20% NH_3-H_2 mixtures. For a given time of treatment the damping was lower for a wire treated in 20% NH_3-H_2 than for one treated in 10% NH_3-H_2. After 6 hours treatment, the damping was 3.02×10^{-2} which decreased to 5.21×10^{-3} after 14 hours treatment. Micro-examination revealed a thick nitride case. It was therefore concluded that both 10% NH_3 and 20% NH_3 gas mixtures produced nitrogen potentials which were too high causing the wires to be overnitrided. This indicates that the values of ammonia percentage suggested by Lehrer [79] are high for a given temperature. This is confirmed by Busby [68] who noted nitride formation in samples nitrided at ammonia potentials recommended by Lehrer.

New wires were nitrided in 3, 5.5, 8, 10% NH_3 for 10, 16, 22, 28 hours total time. Initially the damping increased with increasing ammonia potential up to a maximum at 8% NH_3, thereafter falling rapidly at the higher potentials. It appears that ammonia-hydrogen mixtures containing 8% NH_3 provide a potential which will saturate the specimens at 590°C without causing excessive nitride formation.

It was desirable at the outset to know the capabilities of the apparatus and in order to determine this, and the

accuracy of the technique employed in measuring the damping, it was decided to perform a few solubility measurements. The $\alpha/\alpha+\gamma'$ phase boundary was investigated since this has been accurately determined by Rawlings and Tambini [24], and, Fast and Verrijp [25].

The method employed was similar to that used by Fast and Verrijp in that precipitation was allowed to occur from a supersaturated solution. Four wires were nitrided in 8% NH_3-H_2 mixtures at 590°C for 8 hours and quenched into water. The practice of quenching into oil was abandoned since, to ensure accurate results, it was of vital importance that no precipitation occurred during quenching or measurement of the damping. Water provided a much more effective quench than oil. The water was cooled to 4°C before quenching and the damping was measured at 21°C using a frequency of 0.92 C/S. Two wires were used to determine the nitrogen solubility at 350°C, 400°C and 450°C and the other two wires were used at 500°C. At each temperature, the specimens were held in a still atmosphere of cracked ammonia for periods of 0.5 hours to 3 hours. In calculating the results use was made of the proportionality factor obtained by Fast and Verijp. In Figure 6 in addition to the results obtained in this investigation also shown are those of Rawlings and Tambini [24], and, Fast and Verrijp [25]. Good agreement was obtained between the present results and those of other investigations. It could therefore be assumed that the experimental technique was accurate.

FIG.6. SOLUBILITY MEASUREMENTS.

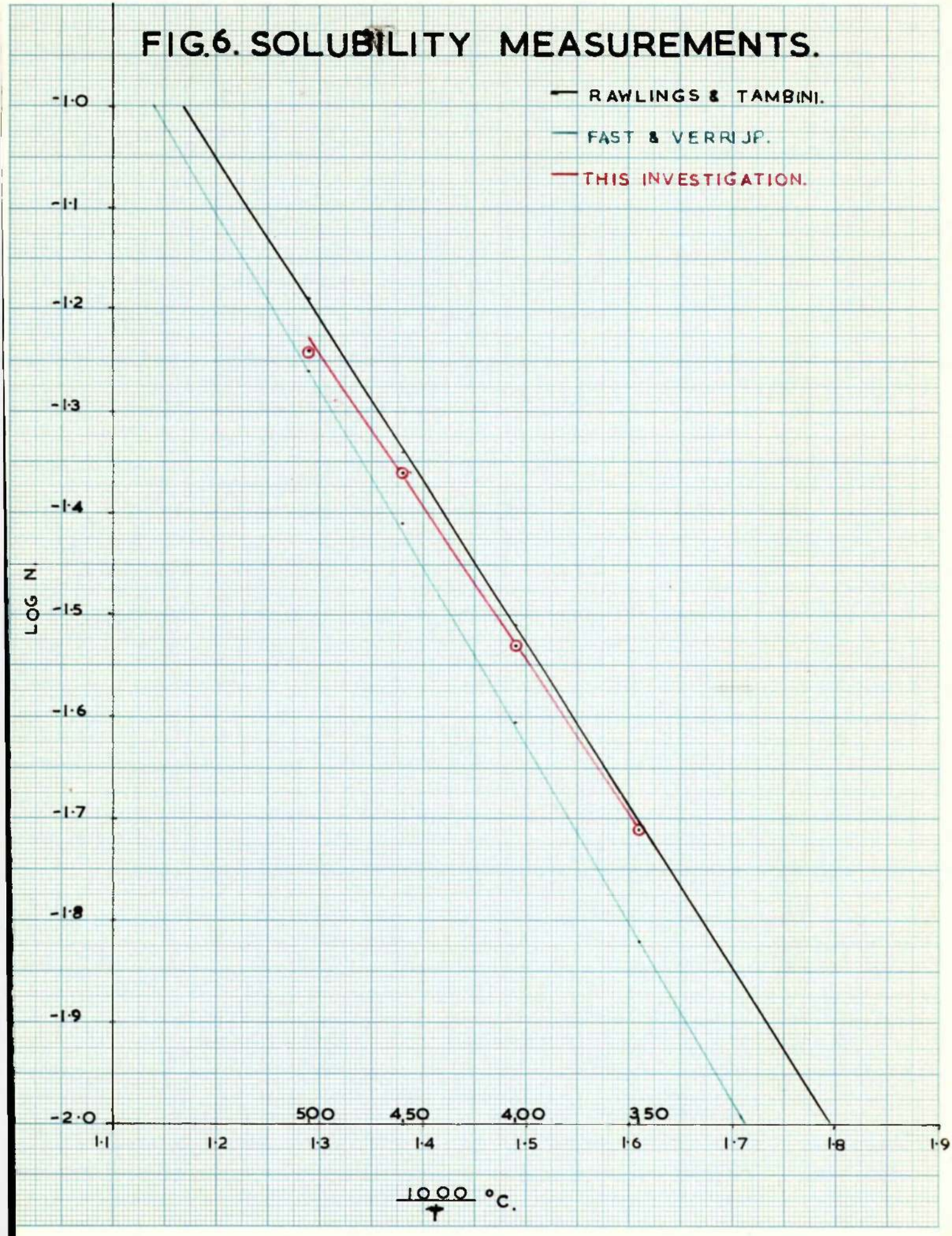

Attempts were then made to determine the effect of vanadium (0.15%V) on the solubility of nitrogen in α-iron. The method employed was similar to that described above. Care was taken to ensure that precipitation was complete at each temperature and solubilities were measured at progressively lower temperatures so that at no stage in the experiments was re-solution of precipitate required. The damping corresponding to each temperature was measured at 21°C within 10-15 minutes after quenching using a frequency of 0.9 C/S.

Figure 7 shows the solubility values obtained compared to the solubility of nitrogen in pure iron. The results indicated that vanadium apparently lowered the solubility of nitrogen in α- iron. In an attempt to confirm this, the experiment was repeated using several different nitriding treatments viz, 2 hrs in pure NH_3; 2 and 8 hrs. in 6% NH_3. These results are also included in Figure 7 and it is obvious that certain treatments gave solubilities very close to those obtained for pure iron. These results are discussed fully later but in view of the data obtained it was considered that further experiments would not be fruitful.

2. The Activation Energy for the Diffusion of Nitrogen in α-Iron.

The activation energy of a process is an important function as, in addition to allowing calculation of other data, it can be used to distinguish different processes. To determine ΔH, duplicate wires of pure iron, 0.157%V and 0.69%V, were loaded

FIG.7. SOLUBILITY OF N IN Fe+0·157 %V.

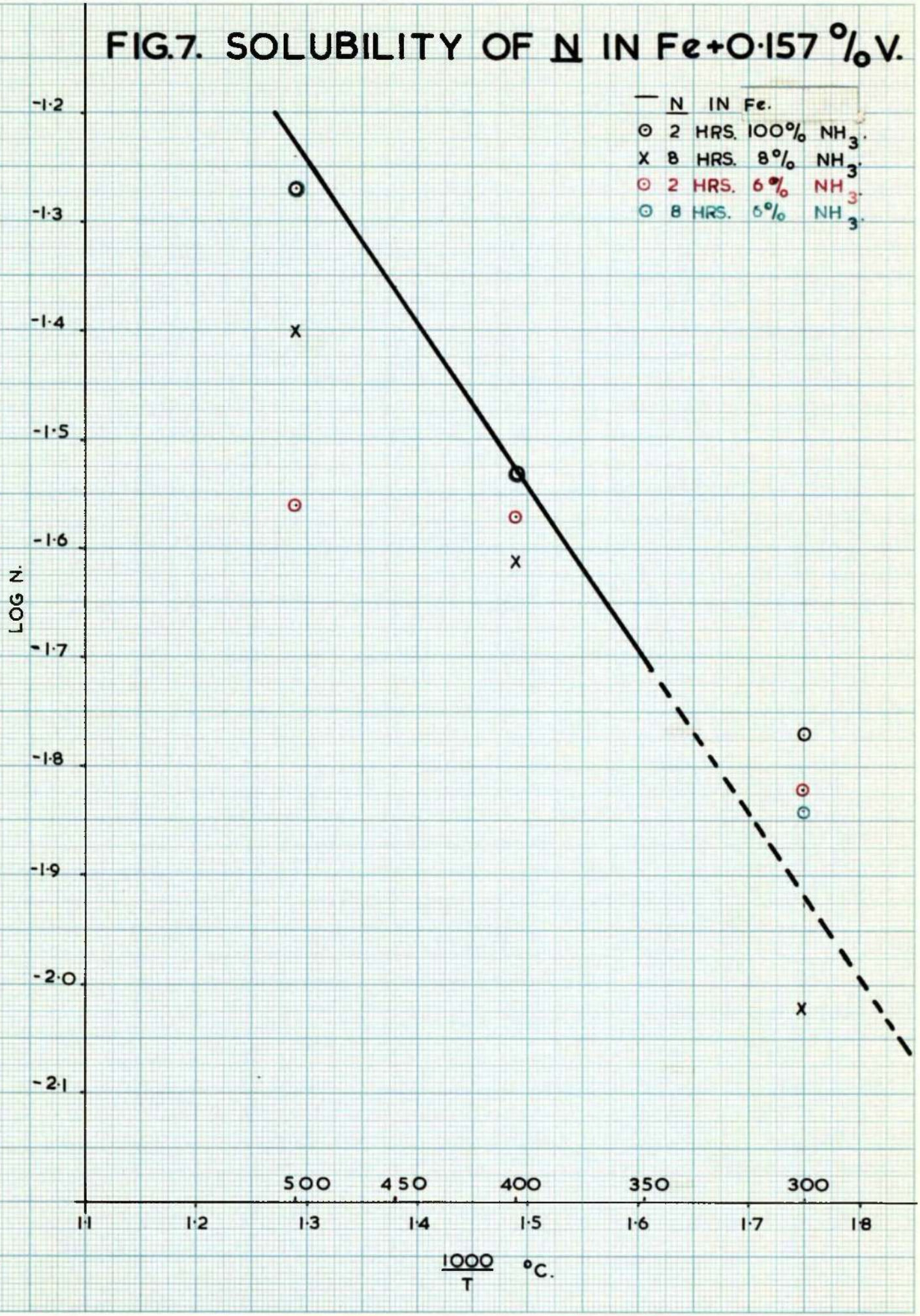

with nitrogen at 590°C (8 hours in 8% NH_3-H_2 mixtures). Quenching was followed by a re-solution treatment at 300°C to 400°C for 0.5 hours to 3.5 hours. After quenching into water at 4°C, the damping was measured over a range of temperature of approximately 10 C° at frequencies of 0.91 C/S to 2.24 C/S. Each set of wires was tested at two frequencies, one wire being used at each frequency. Figures 8 and 9 show the results obtained for pure iron and 0.157% V respectively, and the relevant data is summarised in Table VI. The curves shown are the best fit curves calculated by equation (8) using computer facilities. Unreliable results were obtained for the 0.69% V alloy; it aged appreciably in the time required for the determination of the peak (45-80 minutes). The levels of confidence were calculated for each set of results. The effect of a change in $\underline{\Delta H}$ on the shape of the theoretical damping curve is shown in Figure 10, in which curves D and H of Figures 8 and 9, (ΔH = 21,000 cals/mole and 16,000 cals/mole respectively), are shown in relation to a theoretical curve of ΔH = 18,500 cals/mole, (the value reported by Fast and Verrijp [62]), through the same experimental points. This indicates that a small change in shape causes an appreciable change in $\underline{\Delta H}$.

For calculation of $\underline{\Delta H}$, by the alternative peak shift method, the curves with the greatest difference in peak temperature were used to obtain the most reliable $\underline{\Delta H}$; the experimental error here is estimated to be less than 10%.

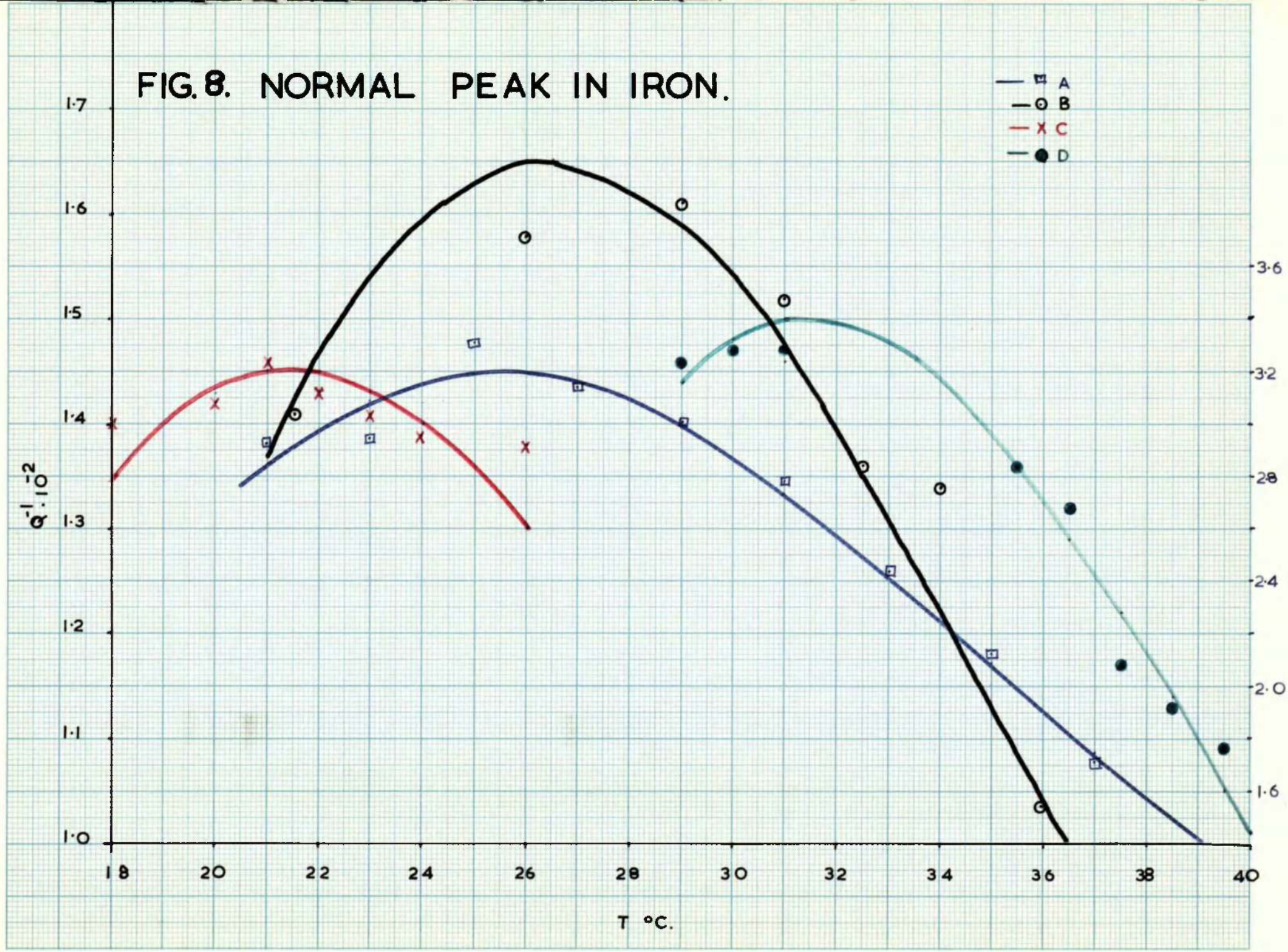
FIG. 8. NORMAL PEAK IN IRON.
A
B
C
D
1·7
1·6
1·5
1·4
1·3
1·2
1·1
1·0
Q⁻¹ · 10⁻²
3·6
3·2
2·8
2·4
2·0
1·6
18
20
22
24
26
28
30
32
34
36
38
40
T °C.

FIG. 9. NORMAL PEAK IN IRON WITH 0·157% V.

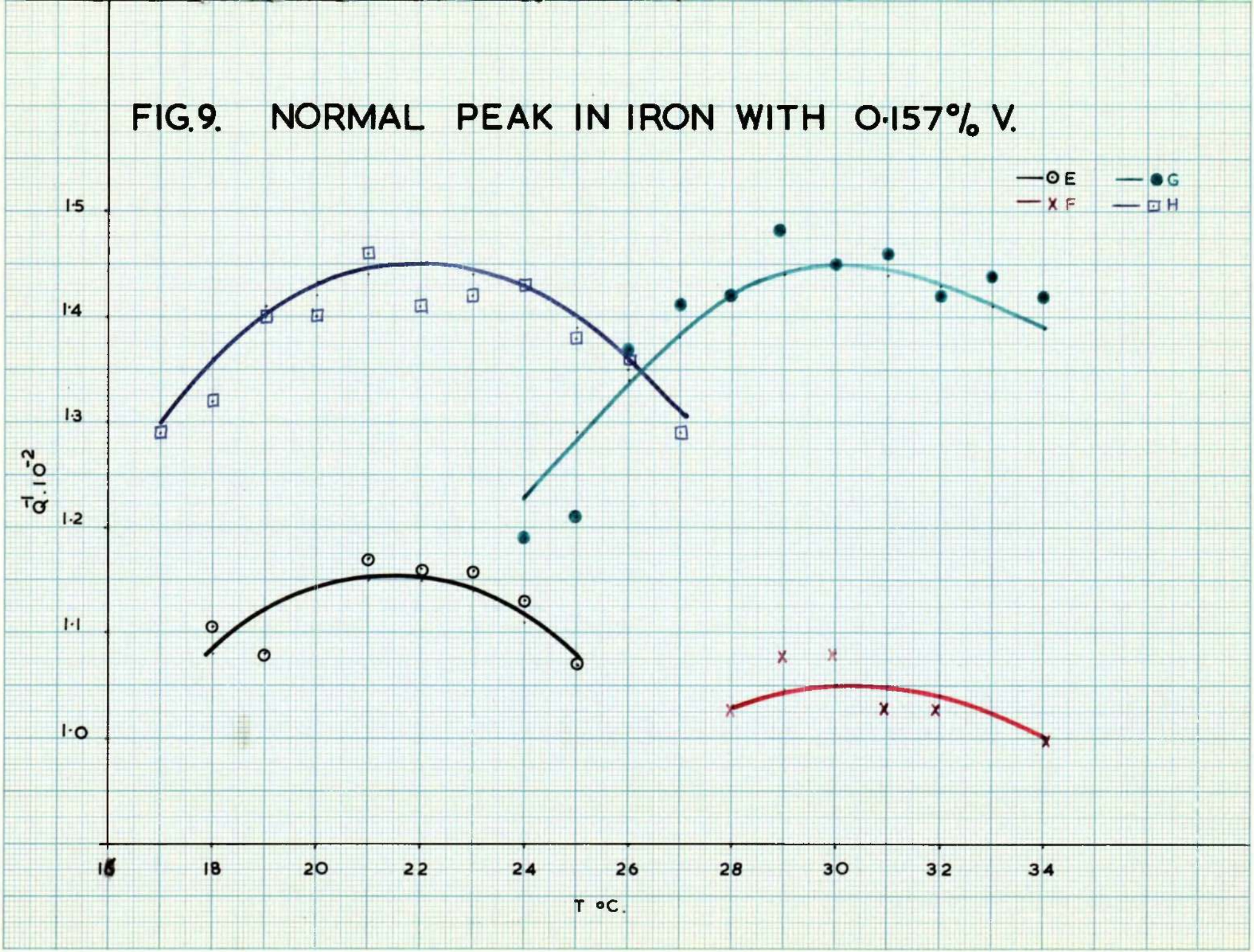

TABLE VI. THE ACTIVATION ENERGY FOR DIFFUSION OF NITROGEN IN PURE IRON AND ALLOYS CONTAINING 0.157% V.

Graph No.	% V	f	Computed Results Q^{-1} max	T peak °C	ΔH	Mean ΔH	Peak Shift ΔH
8A	Pure Fe	1.57	0.032	25.5	19,000		C - D
8B	Pure Fe	1.54	0.0165	26.5	20,000	19,800 ± 500	18,000
8C	Pure Fe	0.92	0.0145	21.5	18,500		
8D	Pure Fe	2.35	0.015	31.5	21,000		
9E	0.157	0.9	0.0115	21.5	18,000	16,100 ± 500	E - G
9F	0.157	2.24	0.0105	30	14,500		18,000
9G	0.157	2.25	0.0145	30.5	16,000		
9H	0.157	0.9	0.0145	22	16,000		

FIG.10. SHAPE COMPARISON.

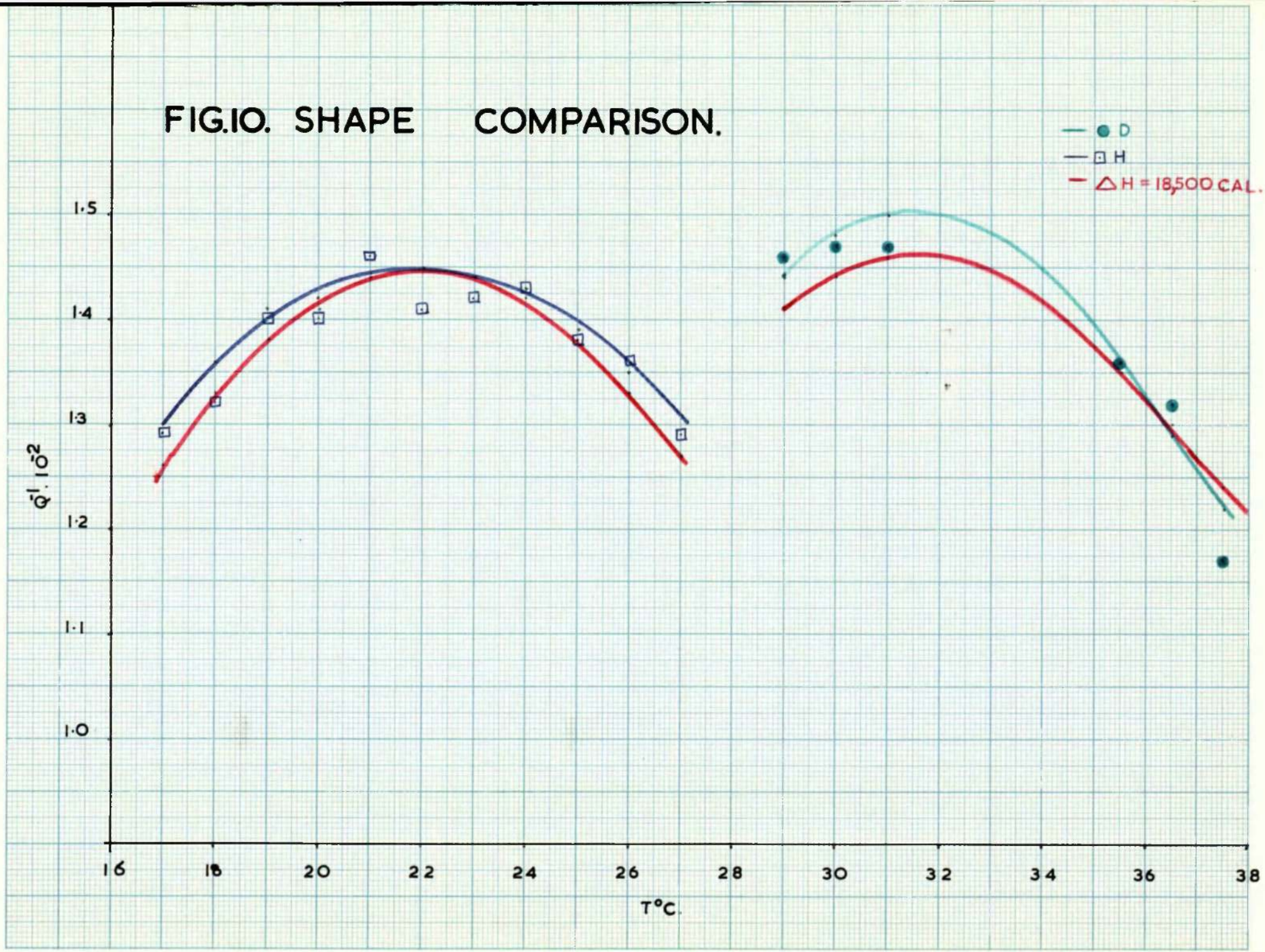

3. The Abnormal Peak in the Fe-V-N System.

In the following investigations vanadium alloy wire specimens, 6" long, were used in the specially constructed high-temperature pendulum. Difficulty was experienced in adjusting conditions so that the temperature could be varied quickly and a minimum temperature gradient maintained. Many experiments were unsuccessful due to convection currents causing the pendulum to vibrate non-torsionally. This movement was so slight that it could not be observed by the naked eye. Its discovery only came after the experiment was completed and all the traces had been developed. However, if great caution was exercised it was possible to obtain satisfactory traces. Initial experiments revealed that the background damping did not alter significantly in the range 20°C to 100°C.

Preliminary experiments revealed that no abnormal peak was produced when the vanadium alloys were nitrided at 590°C and quenched. This was in agreement with the results of Fast [57] who found that the abnormal peak was evident only in wires which had been quenched from a temperature in the region of 950°C.

Subsequently wires of varying alloy content were loaded with nitrogen at 590°C (8 hours in 6% NH_3-H_2 mixture) and quenched. They were then sealed in thin silica tubes and solution treated at approximately 950°C for 1-2 hours. After quenching the damping was measured from 15°C to 110°C.

The results are shown in Figures 11 to 13 and the relevant data summarised in Table VII.

High temperature peaks were obtained in some of these experiments, however, one surprising feature was immediately evident from the results. The low temperature peaks in some cases occurred at much higher temperatures than expected from previous experiments at similar frequencies. This suggested that more than one relaxation mechanism was operative and that the experimental curve was the sum of two or more relaxation peaks. While this peak shift might be attributed to V-N interaction, no such effect has been reported by previous investigators.[66] [70]. In view of results 11B and 11C, which gave low temperature peaks at approximately 36°C, close to the normal carbon peak, it was considered that a much more likely explanation was that the wires contained residual carbon in solid solution. From the position of the peak maximum it appeared that wires 11B and 11C contained practically no nitrogen whilst wire 11A contained little carbon. The remaining wires showed peaks at temperatures between those of nitrogen and carbon and gave lower computed ΔH values, reflecting broadening of the peak. Using the computer (Programme 3), it was shown that these broadened curves could be explained accurately as the sum of two peaks, a nitrogen peak occurring at 22°C and having a ΔH = 18,000 cals/mole and a carbon peak having a peak temperature of 35°C and an activation energy of ΔH = 20,500 cals/mole [2].

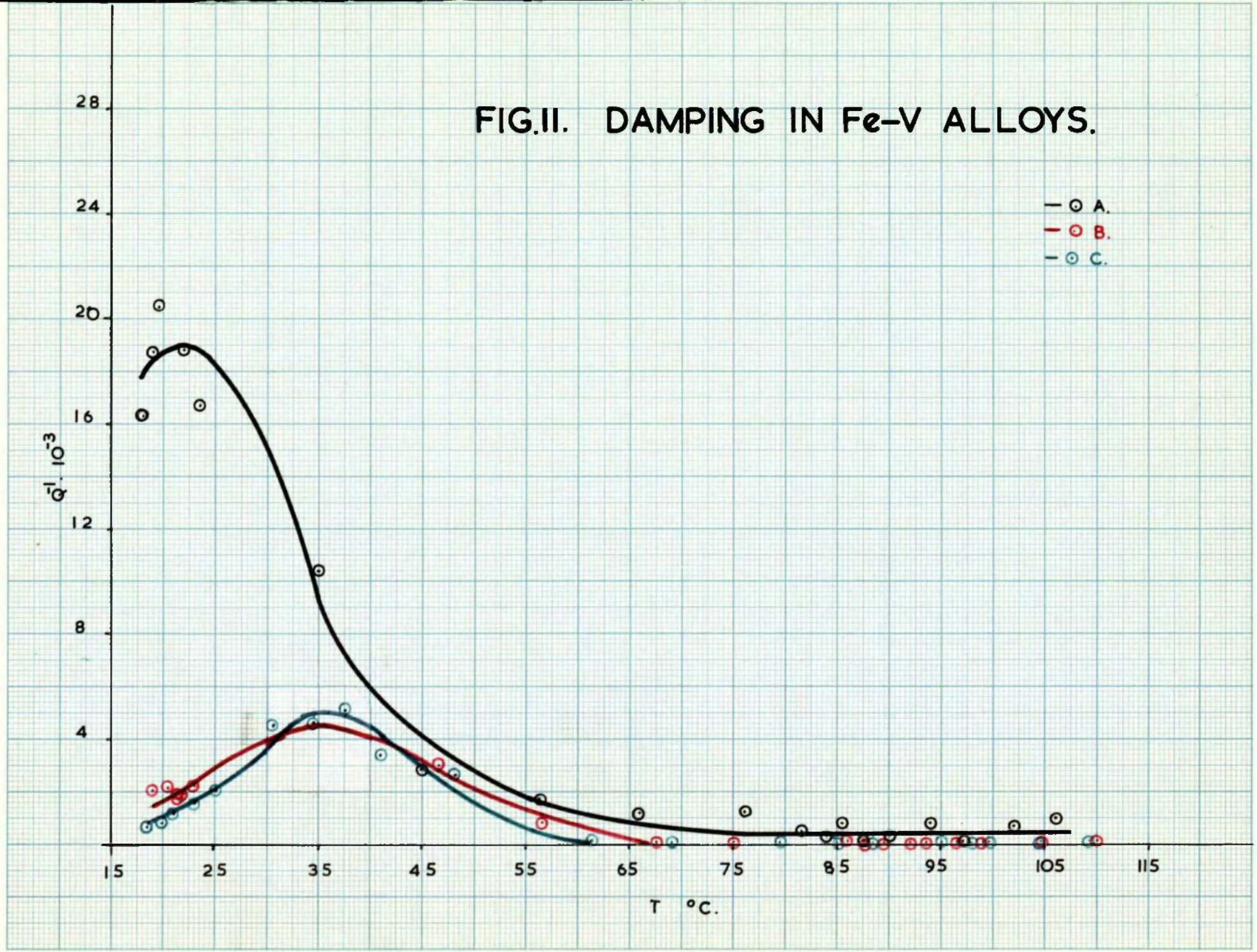
FIG.II. DAMPING IN Fe-V ALLOYS.
A.
B.
C.
28
24
20
16
12
8
4
$\frac{1}{Q} \cdot 10^{-3}$
15
25
35
45
55
65
75
85
95
105
115
T °C.

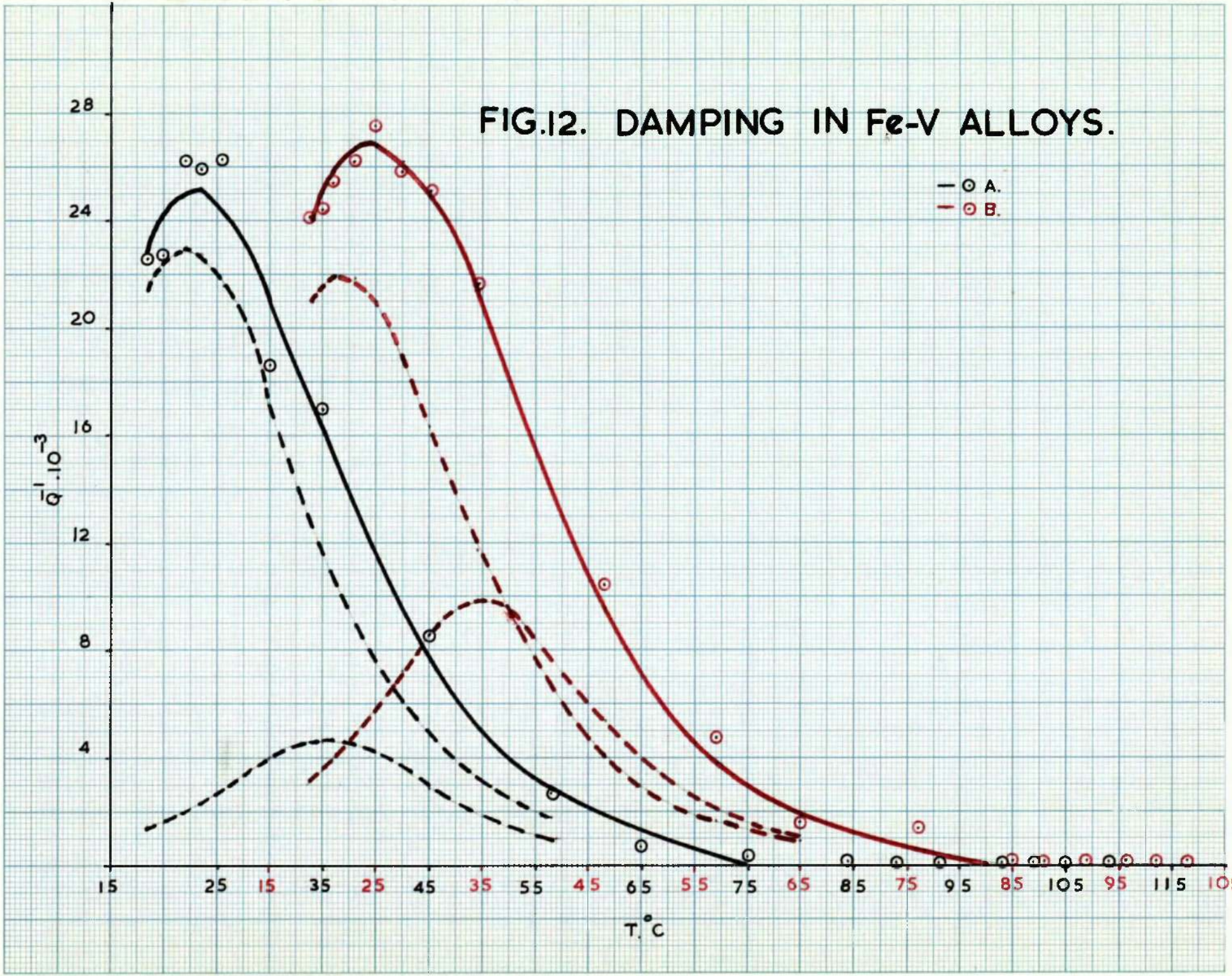
FIG.12. DAMPING IN Fe-V ALLOYS.
A.
B.
$\frac{1}{Q} \cdot 10^{-3}$
28
24
20
16
12
8
4
15
25
15
35
25
45
35
55
45
65
55
75
65
85
75
95
85
105
95
115
105
T. °C

FIG.13. DAMPING IN Fe-V ALLOYS.

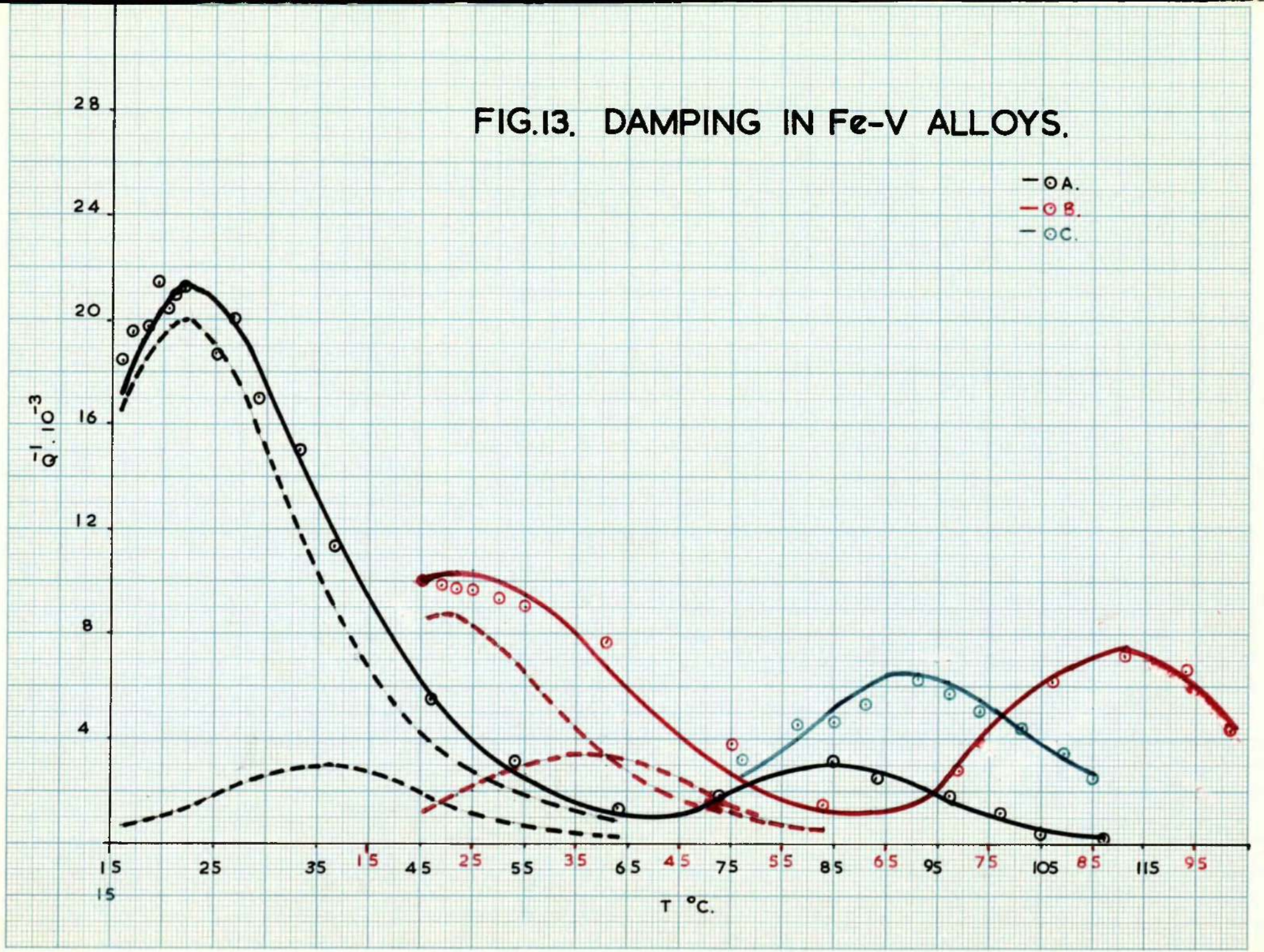

TABLE VII. COMPOSITE CURVES IN IRON - VANADIUM ALLOYS.

Graph No.	% V	Time of Soak Hours	Quenching Temp. °C	f	Normal Peak Computed Results Q^{-1}max	T peak °C	ΔH	Abnormal Peak Computed Results Q^{-1}max	T peak °C	ΔH	Resolved Peaks N Q^{-1}max	C Q^{-1}max
11A	0·157	0	940	0·94	0·019	21·5	17,500					
11B	0·69	1	982	0·90	0·0045	35·5	18,500					
11C	0·69	1	975	0·94	0·005	36	25,000					
12A	0·157	1	960	0·94	0·0255	23·5	16,500				0·025	0·0046
12B	0·395	1	950	0·94	0·0275	25·5	15,000				0·022	0·0099
13A	0·62	2	950	0·94	0·021	22	15,500	0·005	84	28,000	0·02	0·005
13B	0·415	2	950	0·94	0·01	25·5	12,000	0·0075	87·5	26,000	0·0087	0·0055
13C	0·415	2·25	963	0·94				0·0065	92·5	24,500		

12A, 11C and 13C refer to subsequent experiments on the same wires as in 11A, 11B and 13B respectively.

(In the cases of resolved peaks, the computed values of Q^{-1}max, T peak and ΔH lose their significance since such peaks are explained in terms of a nitrogen and carbon peak. These computed values have been included since, initially, they indicated that the experimental peaks were broadened).

It was now clear that carbon was exerting an influence on the results and further attempts were made to eliminate residual carbon. New wires were treated at 700°C for 50 hours in purified dry hydrogen and also at 600°C, at which temperature the methane reaction is more efficient, for 60 hours. It was found that no carbon peak could be discerned after quenching from 950°C.

At this juncture, it was considered important to determine whether carbon, present alone in an iron - vanadium alloy, would give rise to an abnormal peak similar to that obtained with nitrogen. The literature offers only one investigation concerned with carbon in iron-vanadium alloys [69] and no abnormal peak was reported.

Initially the wires were carburised at 720°C in an atmosphere of hydrogen saturated with toluene. The rate of carbon pick-up appeared to be slow and therefore the temperature of carburising was raised to 800°C. Abnormal peaks were produced on quenching as shown by results 14B and 14D. However, when these wires were sealed in silica tubes and homogenised at 950°C for 12 hours both the normal and abnormal peaks disappeared. These results are shown in Figure 14 and the relevant data summarised in Table VIII.

Subsequent to these experiments further work was carried out using wires which had been given the prolonged decarburisation treatment described above. Previously, the

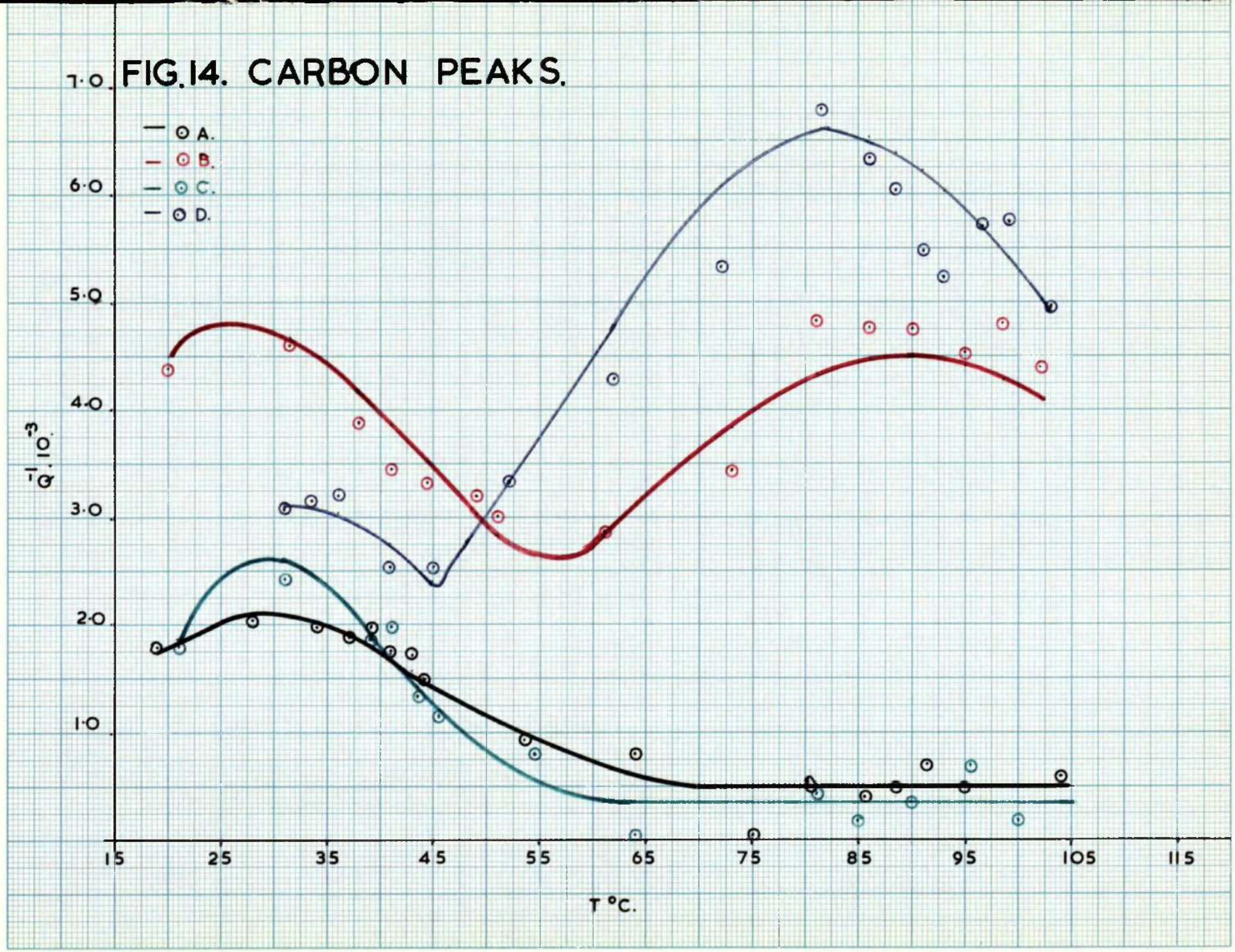
FIG. 14. CARBON PEAKS.
A.
B.
C.
D.
7·0
6·0
5·0
4·0
3·0
2·0
1·0
$\frac{1}{Q} \cdot 10^3$
15
25
35
45
55
65
75
85
95
105
115
T °C.

TABLE VIII. PEAKS OBTAINED IN IRON - VANADIUM - CARBON ALLOYS.

Graph No.	% V	Treatment	f	Normal Peak Computed Results			Abnormal Peak Computed Results		
				Q^{-1}_{max}	T peak °C	ΔH	Q^{-1}_{max}	T peak °C	ΔH
14A	0.157	½ hr. H_2- toluene at 720°C Homogenised at 720°C for 17 hrs.	0.96	0.0021	29	11,000			
14B	0.62	2½ hrs. H_2- toluene at 800°C	0.89	0.0048	27	9,000	0.0045	89	9,000
14C	0.62	1½ hrs. H_2- toluene at 800°C	0.95	0.0026	30	17,000			
14D	0.62	4 hrs. H_2- toluene at 800°C	0.88	0.0031	33	12,000	0.0006	82	11,000

attempts to produce a high temperature nitrogen peak had involved nitriding the samples at 590°C and then soaking above 900°C to obtain decomposition of vanadium nitride. In an attempt to avoid this re-solution, a new series of nitriding experiments were performed using 1% NH_3 and 6% NH_3 mixtures, at temperatures in the range 850-950°C, for sufficiently long times to produce a homogeneous wire. After quenching the damping was measured in the range 15°C to 110°C. These results are shown in Figures 15 to 20 and the relevant data summarised in Table IX.

Resolution of these peaks by Programme 3 indicates that trace amounts of carbon still exist in solution. Since the nitrogen contents in this series of experiments are low, these traces of carbon still produce considerable broadening, as indicated by the very low ΔH values computed for the experimental curves. Abnormal peaks were only obtained in those wires quenched from the γ-range, even so the peak heights were extremely small. Because of these small abnormal peaks, it was felt that little reliance could be placed upon their activation energy values. It was therefore decided to revert to the previous method of nitriding at low temperature and soaking at high temperature to decompose the vanadium nitride and so produce an abnormal peak. The time taken to determine a composite curve from 15°C to 110°C was approximately 50-80 minutes, and since it was possible that considerable ageing of

FIG.15. ALLOYS NITRIDED AT 850 °C IN 6% NH_3.

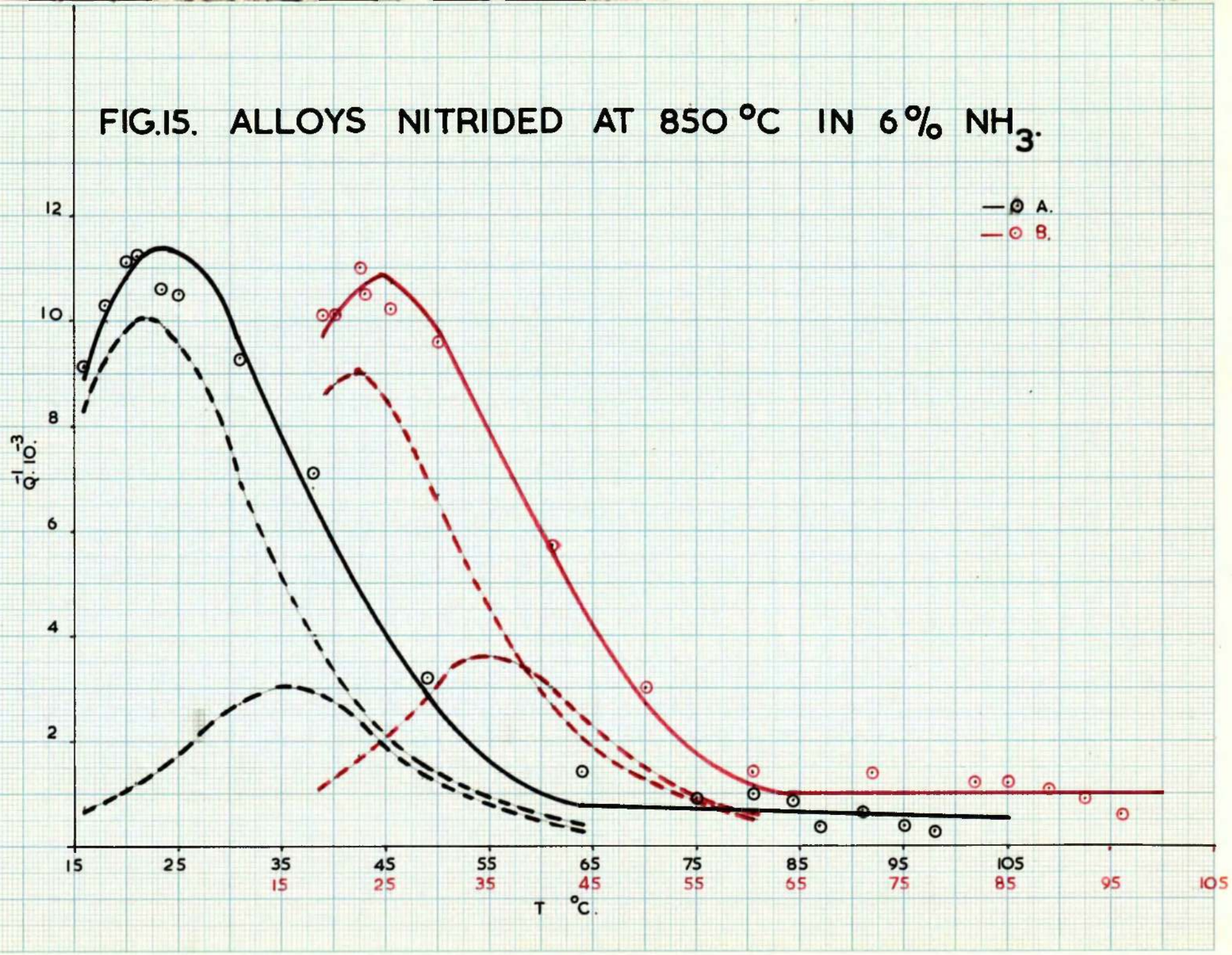

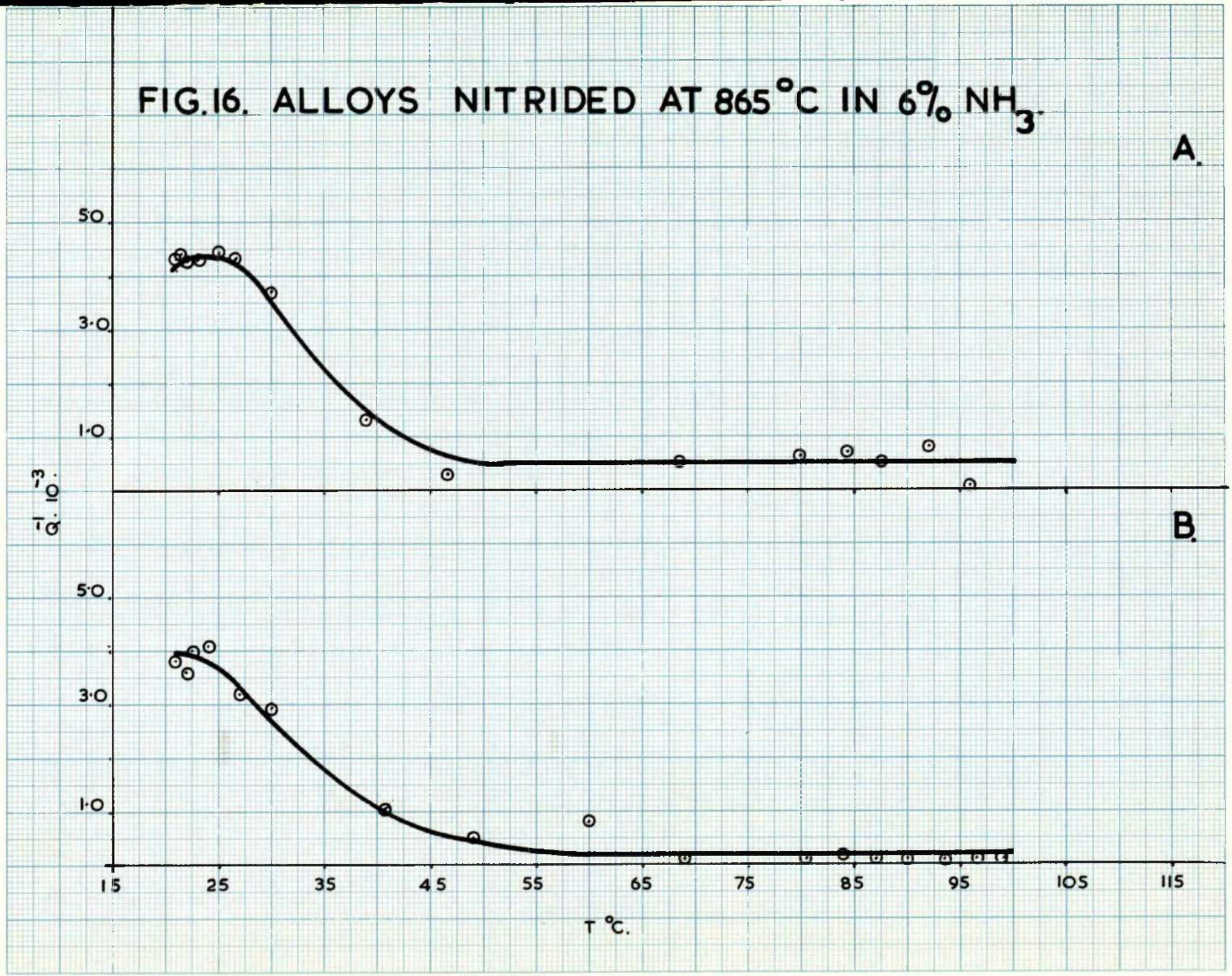
FIG. 16. ALLOYS NITRIDED AT 865°C IN 6% NH3.
A.
B.
5·0
3·0
1·0
$\frac{1}{Q} \cdot 10^3$
15
25
35
45
55
65
75
85
95
105
115
T °C.

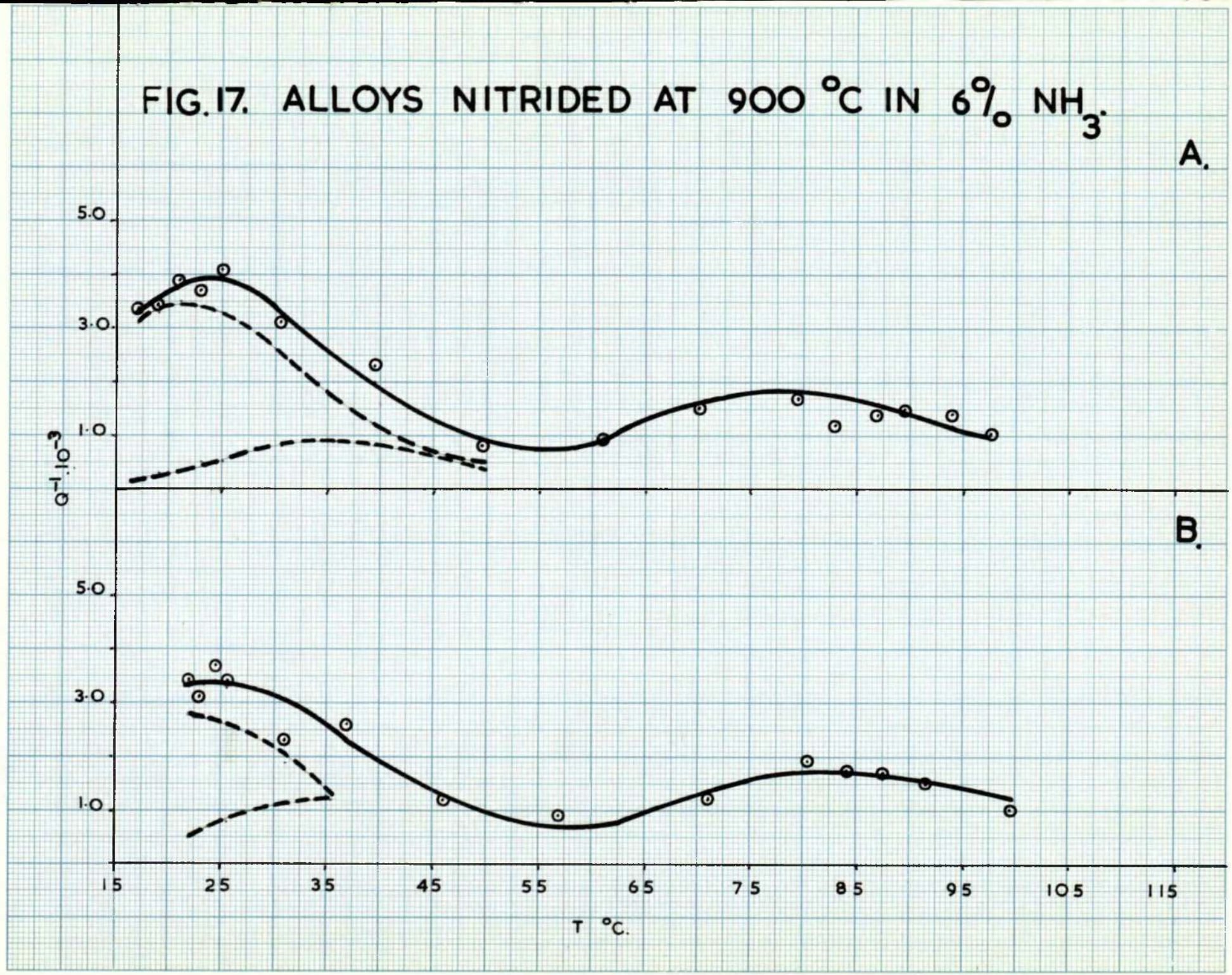
FIG. 17. ALLOYS NITRIDED AT 900 °C IN 6% NH3.
A.
B.
5·0
3·0
1·0
$10^{-3}/T$
15
25
35
45
55
65
75
85
95
105
115
T °C.

TABLE IX. DAMPING OF HIGH VANADIUM ALLOYS HYDRIDED AT HIGH TEMPERATURES.

Graph No.	% V	Treatment	f	Normal Peak: Computed Results Q^{-2}_{max}	Normal Peak: Computed Results T peak °C	Normal Peak: Computed Results ΔH	Resolved Peaks: H Q^{-2}_{max}	Resolved Peaks: C Q^{-2}_{max}	Abnormal Peak: Computed Results Q^{-2}_{max}	Abnormal Peak: Computed Results T peak °C	Abnormal Peak: Computed Results ΔH
15A	0.69	6% TiH_{3}-H_{2} at 850°C for 1 hr	0.93	0.0212	23	14,000	0.01	0.003			
15B	0.335	6% TiH_{3}-H_{2} at 850°C for 1 hr	0.95	0.011	20	14,000	0.009	0.0036			
16A	0.35	6% TiH_{3}-H_{2} at 865°C for 27 hrs	0.93	0.0044	24	21,000					
16B	0.69	6% TiH_{3}-H_{2} at 865°C for 27 hrs	0.98	0.0039	22	20,000					
17A	0.69	6% TiH_{3}-H_{2} at 900°C for 20 hrs	0.96	0.0039	24	15,000	0.0035	0.00087	0.0018	79	27,000
17B	0.335	6% TiH_{3}-H_{2} at 900°C for 20 hrs	0.93	0.0032	21	7,000	0.00275	0.00124	0.0017	82	24,000

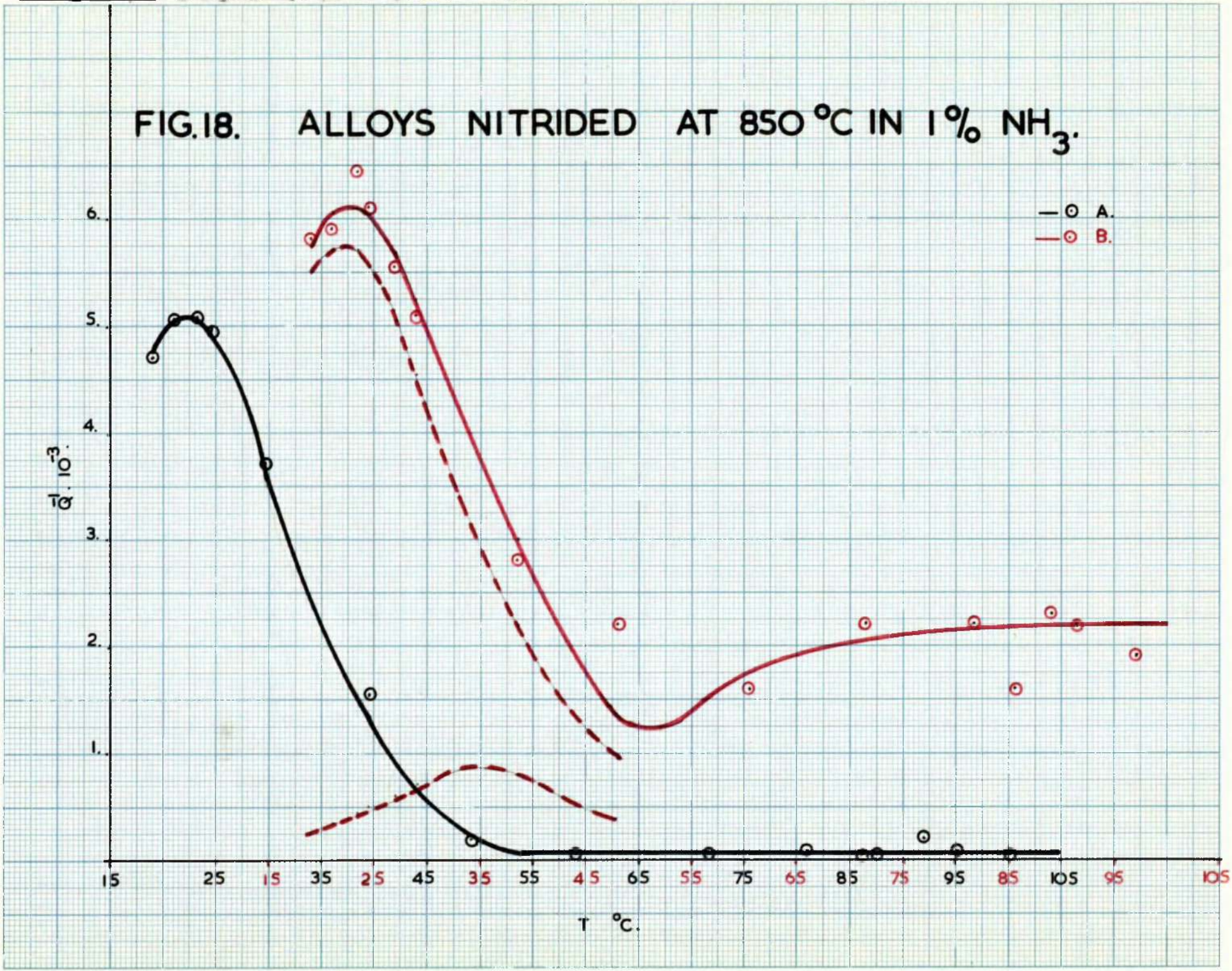
FIG. 18. ALLOYS NITRIDED AT 850 °C IN 1% NH_3.
A.
B.
$\frac{1}{\sigma} \cdot 10^{-3}$
6.
5.
4.
3.
2.
1.
15
25
15
35
25
45
35
55
45
65
55
75
65
85
75
95
85
105
95
105
T °C.

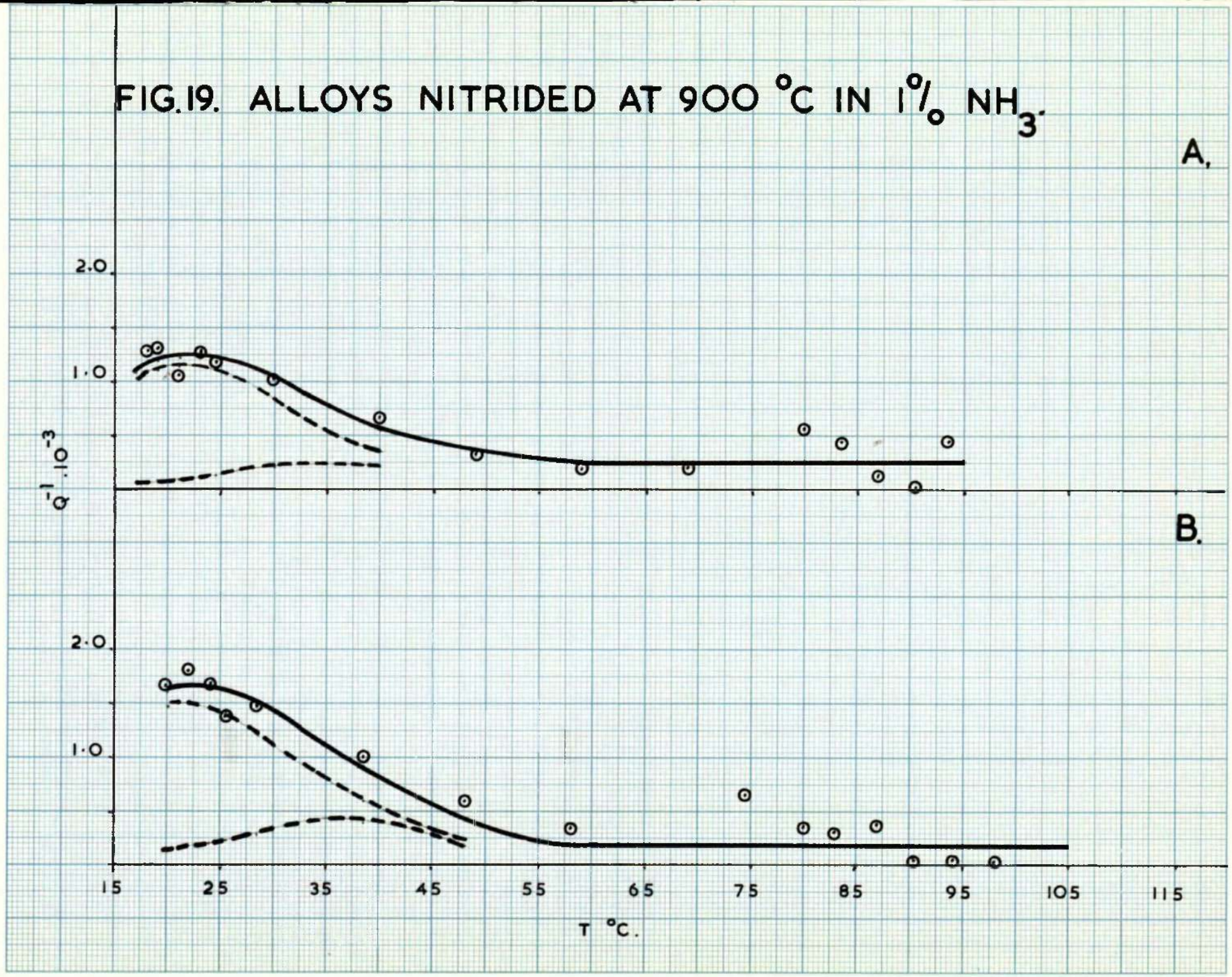
FIG. 19. ALLOYS NITRIDED AT 900 °C IN 1% NH3.
A.
B.
2.0
1.0
2.0
1.0
$10^{-3}/Q$
15
25
35
45
55
65
75
85
95
105
115
T °C.

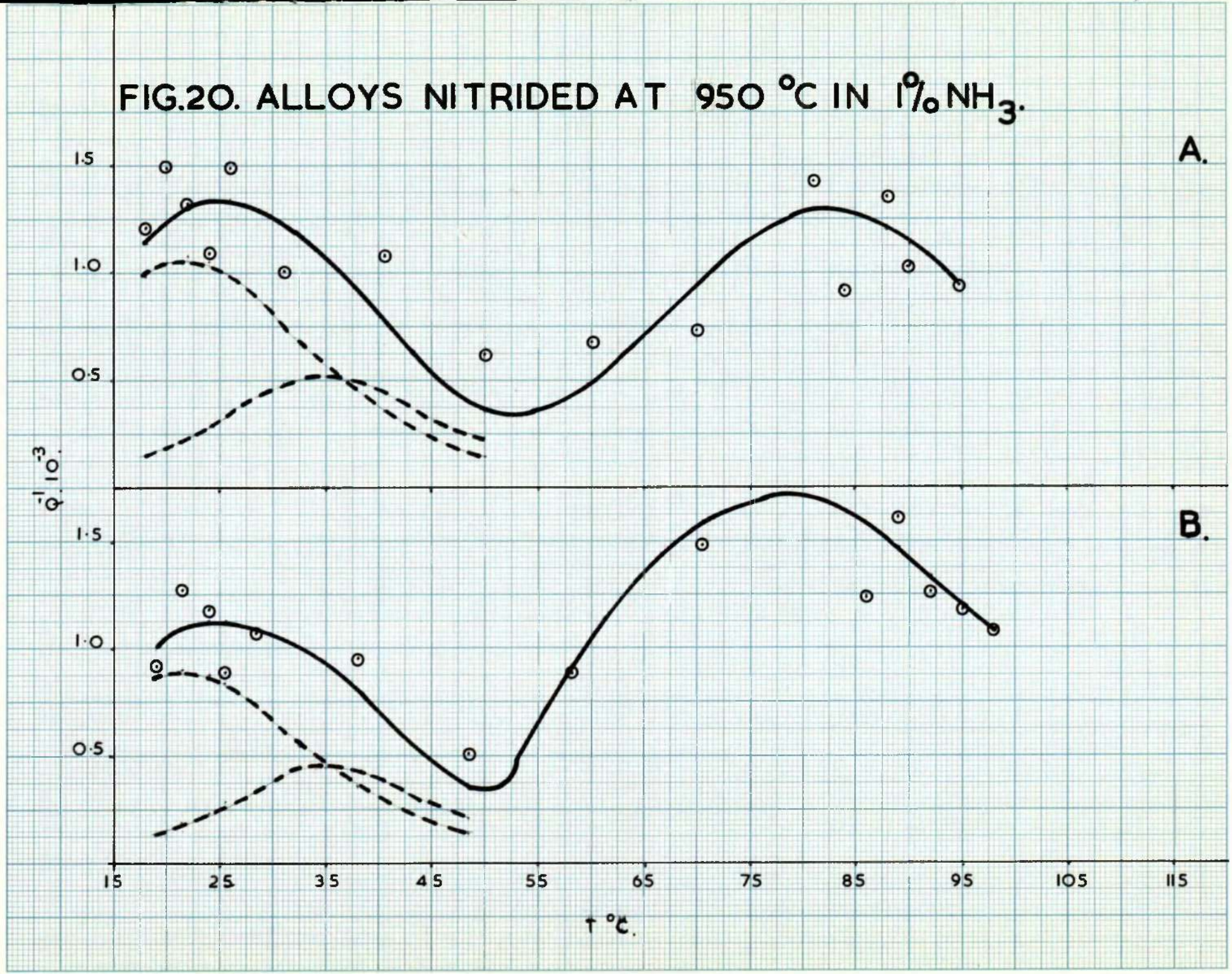
FIG.20. ALLOYS NITRIDED AT 950 °C IN 1% NH3.
A.
B.
1.5
1.0
0.5
$\frac{1}{Q} \times 10^{-3}$
15
25
35
45
55
65
75
85
95
105
115
t °C.

TABLE IX continued.

Graph No.	β V	Treatment	f	Normal Peak Computed Results α^{-1}_{max}	T peak °C	ΔH	Resolved Peaks H α^{-1}_{max}	Q α^{-1}_{max}	Abnormal Peak Computed Results α^{-1}_{max}	T peak °C	H
18A	0.62	25 Mn_3Al_2 at 850°C for 1.5 hrs	0.96	0.0051	22	21,000					
18B	0.357	25 Mn_3Al_2 at 850°C for 1.5 hrs	0.96	0.0061	22	14,000	0.00575	0.00086			
19A	0.69	25 Mn_3Al_2 at 900°C for 24 hrs	0.95	0.0012	20	11,000	0.00115	0.00023			
19B	0.345	25 Mn_3Al_2 at 900°C for 24 hrs	0.93	0.0017	24	14,000	0.0015	0.00037			
22A	0.62	25 Mn_3Al_2 at 950°C for 8 hrs	0.96	0.0023	23	9,000	0.00207	0.00053	0.0023	82	18,000
22B	0.34	25 Mn_3Al_2 at 950°C for 8 hrs	0.94	0.0011	24	11,000	0.0009	0.00045	0.0017	79	14,000

the high temperature peak could occur before measurement, it was advantageous to determine only the high temperature peak. This reduced the time required to approximately 30 minutes. To ensure that equilibrium decomposition of vanadium nitride occurred, much longer soaking times than previously used were allowed.

Wires were nitrided in 6% NH_3-H_2 mixtures at 590°C for 8 hours and quenched. They were then sealed in silica tubes and re-solutioned at 950°C for up to 16 hours before quenching into water (4°C) and storing in liquid nitrogen. Wires of each vanadium content were used, although no abnormal peak was obtained in the case of wires containing 0.157% V. Separate experiments showed that an abnormal peak could not be produced in pure iron-nitrogen alloys irrespective of the treatment given. These results are shown in Figures 21 and 22 and summarised in Table X.

The abnormal peak heights were generally higher than obtained previously. The peak temperature however was not constant at constant frequency, suggesting that there was more than one process operating and that the peak was broadened. These results are discussed fully later.

4. Ageing in Fe-V-N Alloys.

Ageing experiments were performed on both the normal and abnormal peaks. The wires, previously loaded with nitrogen, were quenched from 590°C or 950°C and aged at 30°C for the

FIG. 21. ABNORMAL PEAK IN Fe–V ALLOYS.

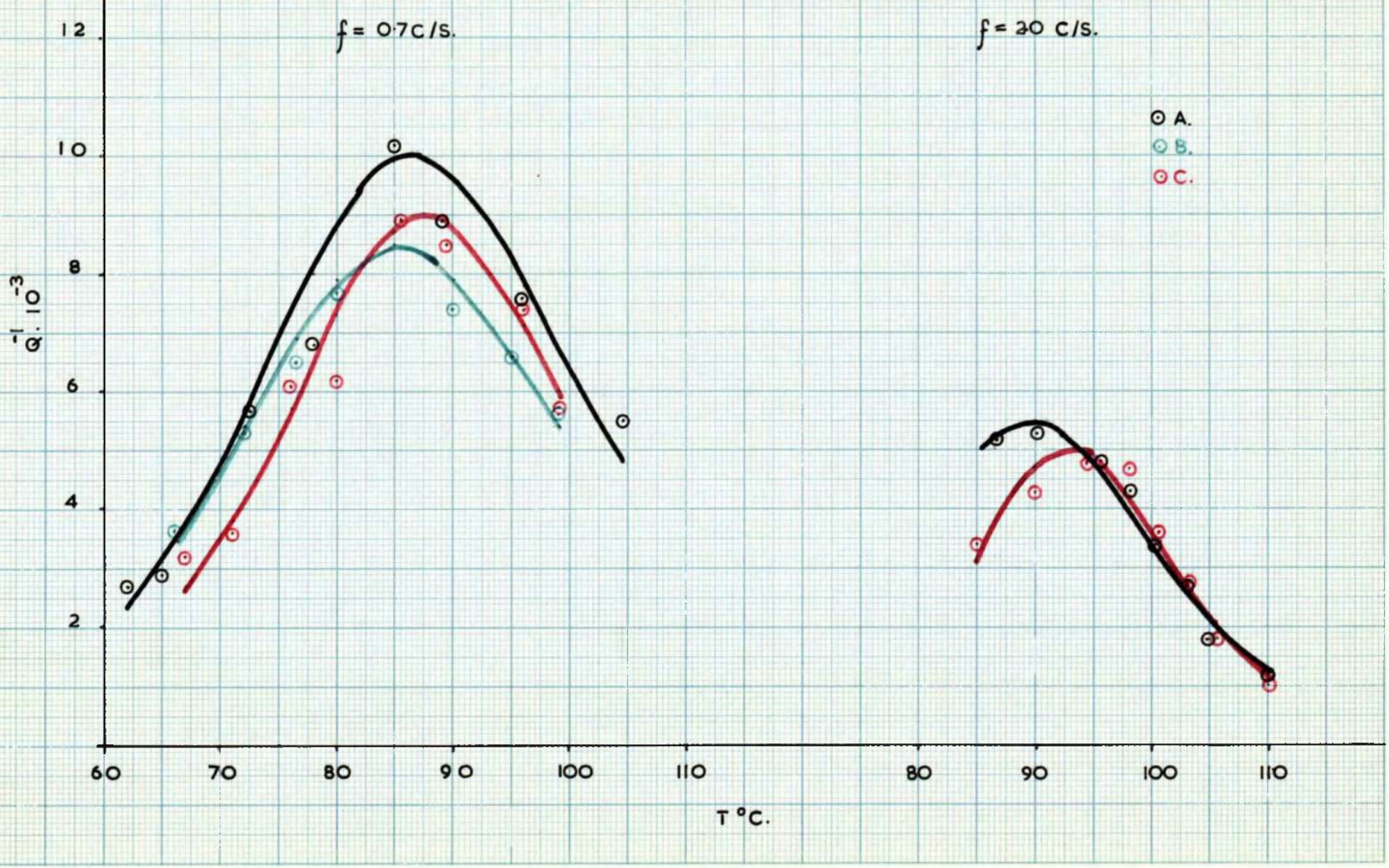

FIG. 22. ABNORMAL PEAK IN Fe-V ALLOYS.

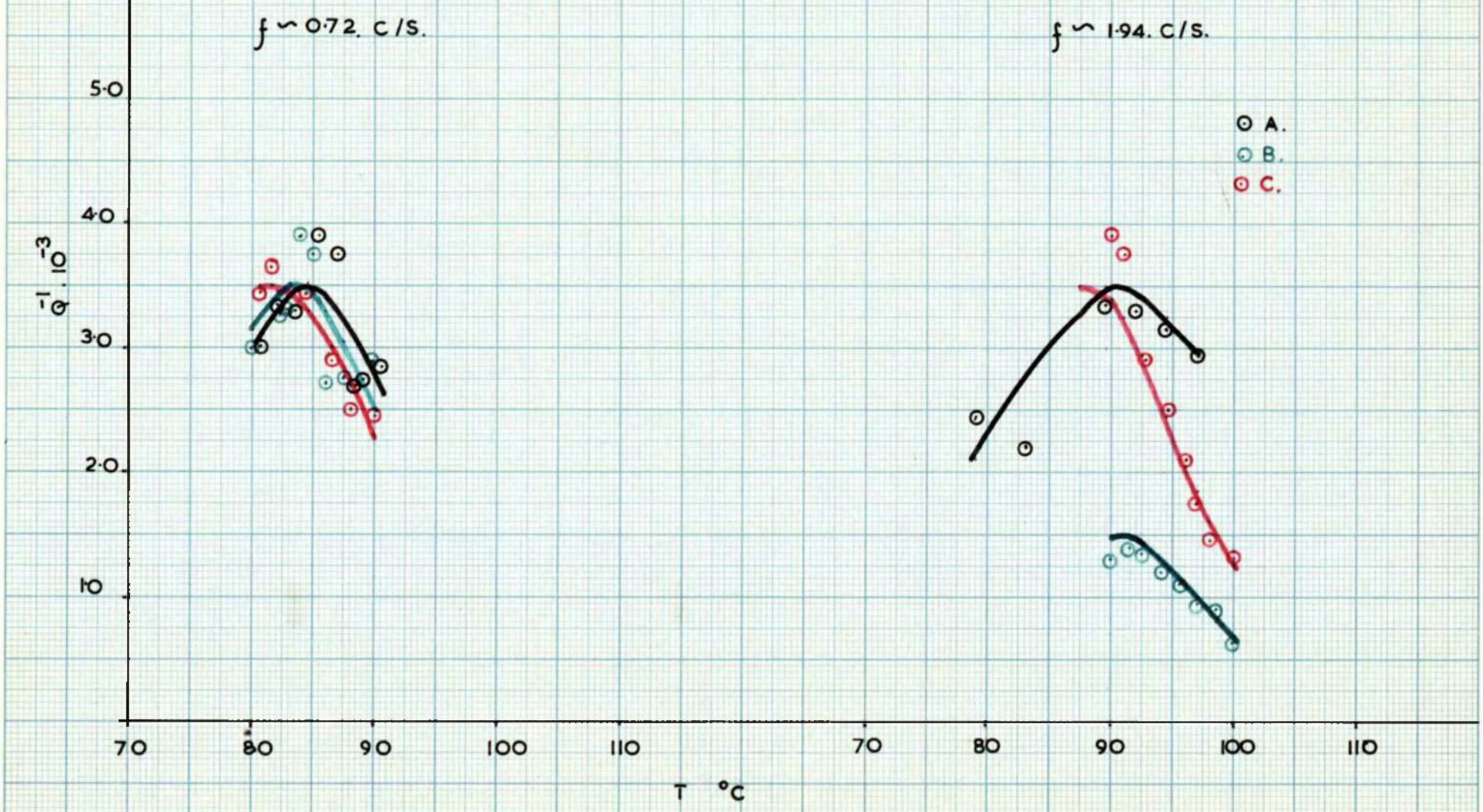

TABLE X. ABNORMAL PEAKS IN IRON - VANADIUM - NITROGEN ALLOYS.

Graph No.	% V	Time of Soak Hrs	Quenching Temp. °C	f	Abnormal Peak Computed Results Q^{-1} max	T peak °C	ΔH
21A	0·415	14	950	0·71	0·01	86·5	20,500
21A	0·415	16	950	2·0	0·0055	90·5	30,000
21B	0·62	14	950	0·71	0·0085	86	19,500
21C	0·69	14	950	0·71	0·009	87·5	22,500
21C	0·69	16	950	2·0	0·005	93	54,000
22A	0·415	16	955	1·94	0·0035	90·5	24,500
22A	0·415	1	955	0·76	0·0035	84·5	34,000
22B	0·62	16	955	1·96	0·0015	91	44,000
22B	0·62	1	955	0·71	0·0035	85·5	34,000
22C	0·69	16	955	1·96	0·0035	87·5	39,500
22C	0·69	1	955	0·72	0·0035	81·5	29,500

normal peak and at approximately 83°C for the abnormal peak. The damping was measured at intervals of 15 minutes initially and subsequently at longer intervals.

The general equation governing ageing, proposed by Wert[48], is of the form

$$\frac{\Delta C(t)}{Co} = 1 - \left[\exp - \left(\frac{t}{\tau}\right)^n\right] \qquad (11)$$

where $\Delta C(t)$ is the amount precipitated at time t, Co is the original concentration, t seconds is the time and τ and n are constants. $\frac{\Delta C(t)}{Co}$ is the fraction of solute precipitated and in terms of damping measurements may be represented by W where

$$W = \frac{Q^{-1}_{t=o} - Q^{-1}_{t=t}}{Q^{-1}_{t=o} - Q^{-1}_{t=\infty}}$$

$$\text{hence } W = 1 - \left[\exp - \left(\frac{t}{\tau}\right)^n\right]$$

$$\therefore \quad \text{Ln} \frac{1}{1-W} = \left(\frac{t}{\tau}\right)^n$$

$$\therefore \log \text{Ln} \frac{1}{1-W} = n \log t - n \log \tau \qquad (12)$$

This is the equation of a straight line. In the graphs, the left hand side of the equation is designated f(W). Thus a plot of f(W) vs. log t secs. results in a straight line of gradient n.

A computer programme 4 was designed to calculate the best fit of a straight line to the experimental points and compute the value of n, the gradient of the line. For the ageing of the high temperature peak, the experimental results

could be described by a single straight line. Ageing of the normal peak was best described by two straight lines and the programme was altered accordingly. Damping values at zero time were obtained by extrapolating a plot of Q^{-1}_{max} vs. time to zero time. This involved some uncertainty, however a range of $Q^{-1}_{t=0}$ values, straddling the value obtained by extrapolation, were used in the computation and the value giving the closest fit recorded. In the short term ageing experiments (abnormal peak), $Q^{-1}_{t=\infty}$ was generally taken as equal to the background damping value. In the longer term ageing experiments (normal peak) the last damping measurement was taken as being equal to $Q^{-1}_{t=\infty}$.

The results for the ageing of the abnormal peak are shown in Figure 23 and summarised in Table XI, whilst those obtained for the ageing of the normal peak are shown in Figures 24 and 25 and summarised in Tables XII and XIII. (In this series of experiments a single wire of each composition was used throughout).

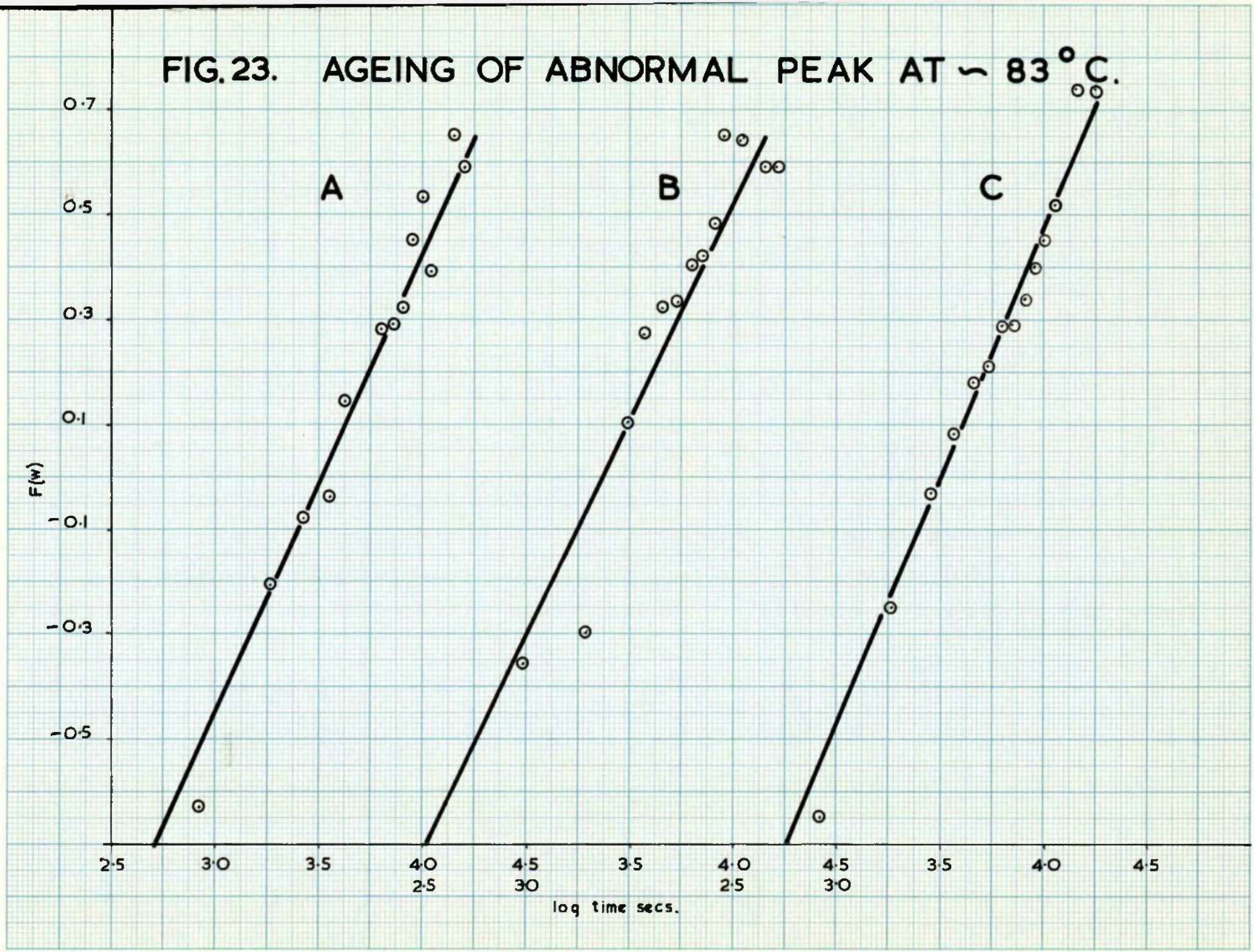
FIG. 23. AGEING OF ABNORMAL PEAK AT ~ 83 °C.
A
B
C
0·7
0·5
0·3
0·1
−0·1
−0·3
−0·5
F(W)
2·5
3·0
3·5
4·0
2·5
4·5
3·0
3·5
4·0
2·5
4·5
3·0
3·5
4·0
4·5
log time secs.

TABLE XI. AGEING OF THE HIGH TEMPERATURE PEAK

QUENCHED FROM 950°C

Graph No.	% V	% N	Ageing Temp. °C.	f	$Q_0^{-1} - Q_{\infty}^{-1}$	Gradient B
23A	0·415	-	85·9	0·76	0·0057	0·88
23B	0·62	0·21	85·1	0·74	0·0054	0·83
23C	0·69	0.18	85·7	0·75	0·0048	0·94

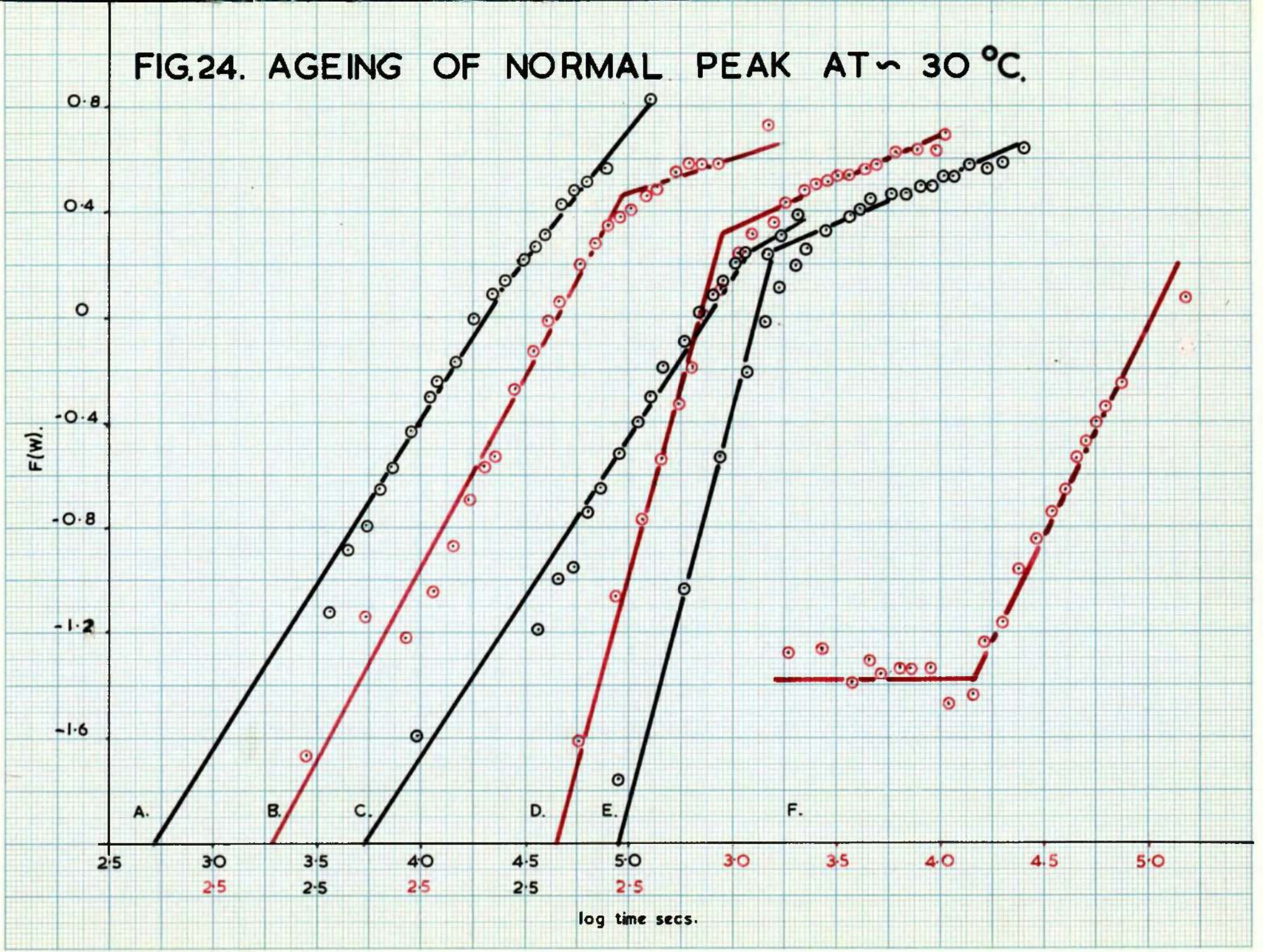
FIG.24. AGEING OF NORMAL PEAK AT ~ 30 °C.
0·8
0·4
0
-0·4
-0·8
-1·2
-1·6
F(W).
A.
B.
C.
D.
E.
F.
2·5
3·0
3·5
4·0
4·5
5·0
log time secs.

TABLE XII. AGEING OF THE NORMAL PEAK

QUENCHED FROM 590°C.

Graph No.	% V	% N	f	Ageing Temp. °C.	$\theta^{-1} - \theta_\infty^{-1}$	Gradient 1st R	Gradient 2nd R	A
24A	0·415	-	2·58	30·4	0·0247	1·27	0·96	70·6
24B	0·62	0·21	2·53	30·8	0·0252	1·46	0·25	89·5
24C	0·69	0·18	2·55	30·5	0·0222	1·21	0·48	80·0
24D	0·395	0·044	2·59	30·8	0·0371	2·27	0·55	82·2
24E	0·157	0·042	2·54	31·2	0·0316	2·46	0·35	72·1
24F	Pure Fe	0·031	2·4	31·2	0·0218	1·61	-	-

A is the percentage nitrogen precipitated at the change of gradient.

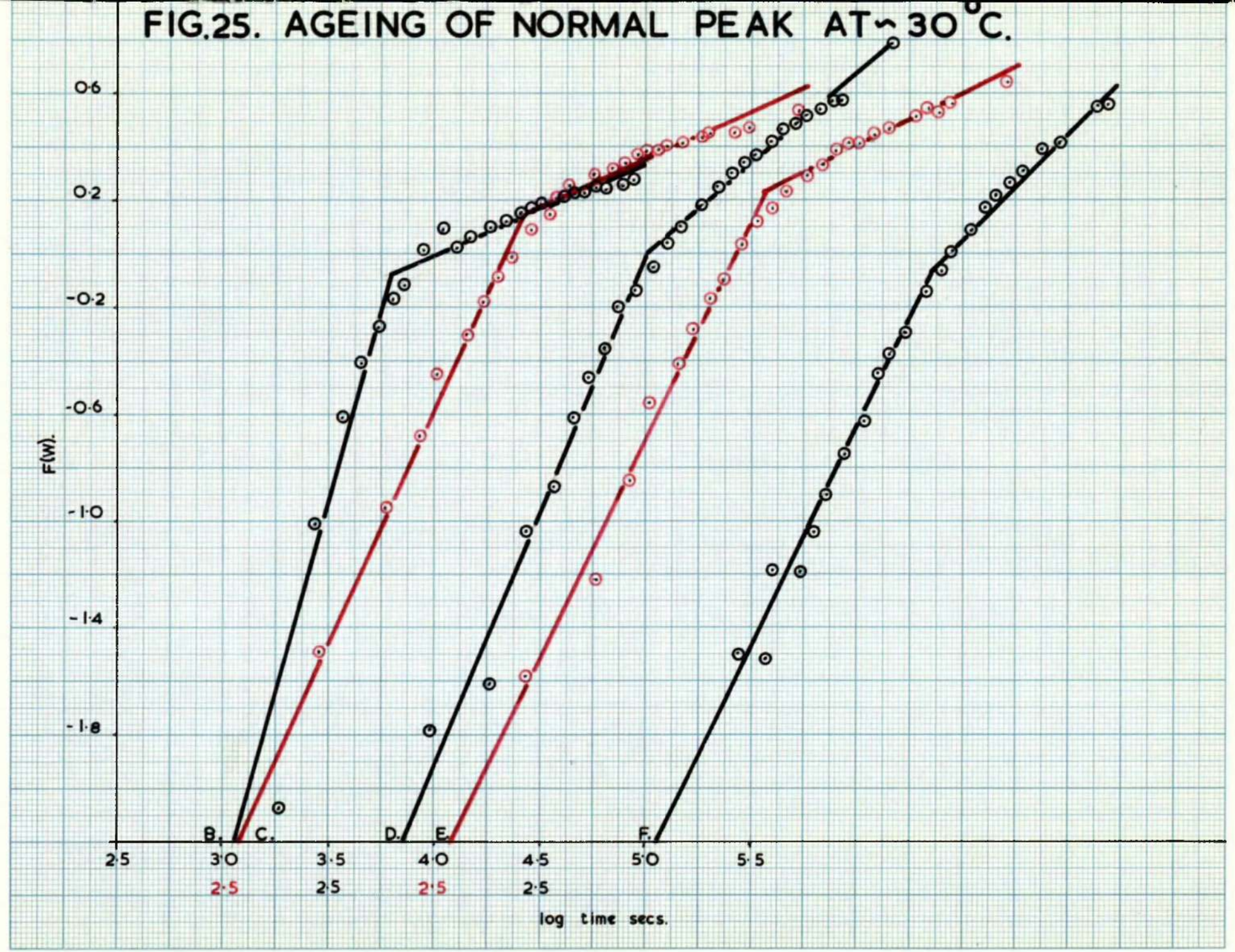
FIG.25. AGEING OF NORMAL PEAK AT ~ 30 °C.
0·6
0·2
-0·2
-0·6
-1·0
-1·4
-1·8
F(w).
B.
C.
D.
E.
F.
2·5
3·0
3·5
4·0
4·5
5·0
5·5
2·5
2·5
2·5
2·5
log time secs.

TABLE XIII. AGEING OF THE NORMAL PEAK

QUENCHED FROM 950°C

Graph No.	% V	% N	Ageing Temp. °C.	f	$Q\theta^{-1}$	$Q\theta^{-1}$	Gradient 1st n	Gradient 2nd n	A
25B	0·62	0·21	31·2	2·27	0·0250		2·9	0·54	49·0
25C	0·69	0·18	31·4	2·55	0·0227		1·75	0·35	62·1
25D	0·395	0·044	31·2	2·45	0·0265		1·86	0·68	59·5
25E	0·157	0·042	31·4	2·44	0·0297		1·62	0·40	73·0
25F	Pure Fe	0·051	31·2	2·59	0·0217		1·65	0·80	34·8

A is the percentage nitrogen precipitated at the change of gradient.

CHAPTER VI.

DISCUSSION OF RESULTS.

VI DISCUSSION OF RESULTS

1. Solubility of Nitrogen in α-iron

The solubilities obtained for nitrogen in α-iron in the early part of this work are shown graphically in Figure 6. The results may be expressed by the equation

$$\log N = \frac{-1500}{T} + 0.708$$ where N is

weight percent nitrogen. This also leads to a ΔH value of 6,850 cals/mole for the heat of solution of nitrogen in α-iron. The actual value of the solubility is of course dependent on the reliability of the value of the proportionality constant between damping and percentage nitrogen. No attempt has been made to determine the value of this factor in the present investigation; use was made of the value obtained by other investigators. The most reliable determinations of this factor have been those of Fast and Verrijp[25], (1.26), and Rawlings and Tambini,[24] (1.28). Since the present experimental conditions were very similar to those of Fast and Verrijp, i.e. the same specimen dimensions, grain size and frequencies were used, there was justification for employing their factor of 1.26. The present results are seen to lie between those of Rawlings and Tambini, and, Fast and Verrijp, agreeing with the former at low temperatures and tending towards the latter at high temperatures, yet the present values are higher than those of Fast and Verrijp at all temperatures. This is probably due

to the more efficient quench (water at 4°C was used) and, possibly, to the shorter time required to measure the damping after quenching, achieved in the present series of experiments. Nevertheless, the results obtained in this investigation appear to be low at high temperatures probably due to accidental precipitation before or during measurement. It is considered that the most reliable values are still those of Rawlings and Tambini.

Using similar experimental conditions the solubility of nitrogen in the presence of 0.15% vanadium was determined. The results of these experiments are shown in Figure 7. Initially, after nitriding the alloy for 8 hours in 8% NH_3 - H_2 mixtures, the solubilities obtained were substantially lower than the values for pure iron. This suggested that vanadium decreased the solubility of nitrogen in iron and, in order to verify this conclusion, several other nitriding treatments were used. At 400°C and 500°C treatments of 8 hours in 6% NH_3 - H_2 and 2 hours in pure ammonia both yielded solubility values which differed negligibly from the solubility of nitrogen in pure iron. This indicates that the results obtained using 8% NH_3 - H_2 for 8 hours are low at all temperatures, probably due to overnitriding. Treatment in 6% NH_3 - H_2 for 2 hours on the other hand appears to have been insufficient to saturate the wire at 400°C and 500°C. The results at 300°C obtained for all treatments, except 8 hours in 8% NH_3 - H_2, tend to be

high compared to the extrapolated $\alpha / \alpha + \gamma'$ solubility line. While this may be due to incomplete precipitation, a more likely explanation is that some Fe_4N precipitate has formed at this low temperature. The fact that wires containing vanadium appear to become overnitrided at lower ammonia potentials than pure iron is in accord with the very fast uptake of nitrogen by these wires. The conclusion to be drawn from these experiments is that, under suitable nitriding conditions, the alloy shows the same solubility for nitrogen as a pure iron wire. This, however, is not taken to indicate that vanadium in solid solution has no effect on nitrogen solubility. The interpretation placed upon the results is that the vanadium in solution has been precipitated almost completely as vanadium nitride with the result that the alloy behaves substantially as a pure iron wire, the measured solubility being that of nitrogen in equilibrium with Fe_4N and not VN. This interpretation is in agreement with thermodynamic data[71] which gives for $VN \rightarrow \underline{V} + \underline{N}$

$$K_B = [\% \underline{V}][f_N \% \underline{N}] = 2.46 \times 10^{-7} \text{ at } 590^{\circ}C.$$

Thus at temperatures used in the solubility experiments, the solubility of vanadium nitride is negligibly small.

2. Activation Energy for the Diffusion of Nitrogen in α-Iron.

The activation energy was computed using a programme, (Programme 1), based on

$$\frac{Q^{-1}_{max}}{Q^{-1}} = \cosh {}^{\Delta H}/_{R} \left({}^{1}/_{T_M} - {}^{1}/_{T}\right) \qquad (8)$$

to obtain the theoretical curve which best described the experimental points. In order to obtain an initial estimate of the likely range of the parameters Q^{-1}_{max} and T peak, a tentative curve was drawn through the experimental points by hand.

The values of activation energy obtained for the diffusion of nitrogen in pure iron, Table VI, are in reasonable agreement with published values. The mean value of 19,800 cals/mole is to be compared with 18,200 cals./mole[60] and 18,600 cals./mole[62], the accuracy usually quoted being $\pm$ 1 to 2 K cal.

It is interesting to compare the values of activation energy obtained by using equation (8) and those obtained by the "peak shift" method using equation (7).

$$\ln\left(\frac{W_2}{W_1}\right) = \Delta H/R\left(\frac{T_2 - T_1}{T_1 T_2}\right) \qquad (7)$$

As mentioned earlier, the accuracy of the activation energy obtained by using this equation depends solely on the accurate determination of the frequency and peak temperature. The former accuracy was fairly easily attained in the present work since the vibrations were recorded photographically. However, in order to minimise the error involved in determining the peak temperature, frequencies were chosen such that they caused the peaks to appear at temperatures at least 10 C^{o} apart. Applying this equation to the pure iron experiments performed at the highest and lowest frequencies, and using the T peak

values given by the computer, the value of 18,000 cals./mole is obtained, which is in excellent agreement with published values. From the position of peaks on the temperature axis at different frequencies, it is also possible to calculate the diffusion coefficient of nitrogen at the various peak temperatures and hence the diffusion equation. Since the activation energy and the position of the damping peak for a given frequency in the present work is in good agreement with reported values, it follows that the diffusion coefficients calculable from the author's results are also similar to those quoted in section 4 of the literature survey.

The activation energies obtained for the 0.157% V alloy appeared to be significantly lower than for pure iron. Various reasons might be suggested to account for this. From the above equation (8), it is seen that for a given peak temperature and any other temperature T, corresponding to a point Q^{-1} on the curve, Q^{-1}_{max}/Q^{-1} decreases with decreasing ΔH. Therefore, for any given process, a peak which is sharp and narrow will have a higher activation energy associated with it than a curve which is flat and broad. Thus the lower activation energies in the presence of vanadium indicate broadening of the peak and might suggest more than one relaxation process is operative. It would be expected, however, that this would also lead to a peak shift, compared to the pure iron nitrogen peak. No evidence of this was obtained, and no such

effect has been reported in the literature. Since it is known that vanadium increases the rate of precipitation of nitrogen, it is considered that ageing occurred during measurement, resulting in distortion of the peak shape. Thus the more accurately the internal friction curve is measured, the longer will be the time required, in all probability the overall curve will be more inaccurate and low ΔH values will be obtained. It appears, therefore, that the best results should be obtained by measuring a few points on either side of the peak as quickly as possible and this technique was adopted in subsequent experiments.

Applying the "peak shift" technique to the alloy results, again using computed T peak values, yields an activation energy of 18,000 cals./mole, identical to that obtained for pure iron. This is additional evidence for the interpretation given above of distortion of the peak shape. In view of the remarks made concerning the solubility of nitrogen in vanadium alloys, it is not surprising that the activation energy for the diffusion of nitrogen in these alloys also remains unaltered, since the specimen is essentially a pure iron wire containing a dispersion of vanadium nitride.

In order to obtain reliable values of activation energy, it seems desirable to use both equations (7) and (8). Thus for a single relaxation time curve of an alloy which is liable to age, it would appear that provided the peak temperature

is accurately known i.e. from a mathematical fit of the best theoretical curve describing the experimental results, the most reliable value of ΔH is obtained by the "peak shift" method. If, however, the peak temperature is estimated by eye from the experimental results, then it is questionable if the best results would be obtained using equation (7) unless the peaks were widely separated in temperature; a condition which cannot readily be achieved experimentally.

3. The Abnormal Peak in the Fe-V-N System.

The experiments performed during this investigation have shown that no abnormal peak could be produced by quenching alloys from temperatures lower than 900°C, nor was any abnormal peak found in wires with a vanadium content of less than approximately 0.3% V, irrespective of the heat treatment. Abnormal peaks were found in wires with a higher vanadium content quenched from higher temperatures.

The internal friction curves obtained in the range 20°C to 110°C for several vanadium alloys which had been quenched from 950°C are shown in Figures 11,12, and 13 and the results summarised in Table VII. Contrary to expectation, the computed peak temperature for the normal peak (except for 11A) was higher than expected for a frequency of 0.94 C/S and an activation energy of 18,000 cals./mole (the activation energy for the diffusion of nitrogen in iron). This was especially evident in results 11B and 11C, where the computed peak

temperature coincided almost exactly with the normal carbon peak. (According to Dijkstra[33] the carbon peak occurs at 36°C for $f \sim 1.0$ C/S). Undoubtedly the normal peaks were being influenced by the presence of carbon in solution.

The interference by carbon is reflected in the low values of ΔH obtained for all the alloys showing a peak shift except results 11B and 11C. In these two cases practically no nitrogen is in solution and the peak is due almost solely to carbon. The ΔH values obtained for these two experiments were 18,500 cals./mole and 25,000 cals./mole which are to be compared with 20,100 cals./mole, the value quoted by Wert[58] for the diffusion of carbon in iron.

In view of this unexpected carbon interference, it was desirable to resolve the experimental curves into component nitrogen and carbon peaks in order to gain an estimate of the amount of carbon in solution. A new computer programme, (Programme 3), was compiled which computed the two single relaxation time peaks of nitrogen (T peak = 22°C; ΔH = 18,000 cals./mole) and carbon (T peak = 35°C; ΔH = 20,500 cals./mole) whose sum best fitted the experimental curve. From the results shown in Table VII it can be seen that the carbon content can vary from zero to as much as 0.01% C.

As none of these wires showed any indication of a carbon peak when quenched from 590°C, it must be assumed that the carbon in solution has resulted from some reaction occurring at higher temperatures. The only reaction which can explain

the appearance of carbon in solution is decomposition of vanadium carbide, which has not been dissociated during the earlier purification treatment by dry hydrogen. In view of the fact that result 11A, where no soaking time has been allowed at 950°C, shows no interference from carbon it would appear that decomposition of vanadium carbide requires an appreciable time before equilibrium is reached.

It is evident from the results (Table VII) that there is also a large variation in the normal peak heights in the various alloys which cannot be ascribed simply to the slight variation in the quenching temperature. However, the rate of quenching is a possible variable, since the quenching operation involved removing the silica tube containing the wire manually from the furnace and plunging it into cold water. As each wire was quenched individually, it is likely that the quenching rates were not identical and this is thought to account for these variations. This view is substantiated by the results 13B and 13C. Both these results refer to the same wire and it would be expected that if considerable ageing occurred during the determination of both peaks in 13B then a higher peak would be obtained by determining only the high temperature peak which requires a much shorter time. In fact result 13C, in which this was done shows an abnormal peak height which is lower than that obtained in 13B and this can only be accounted for in terms of a less efficient quench in

the latter case compared to the former. These observations are in accord with the work of Fast and Meijering[70] who obtained a 12.5% increase in Q^{-1} max at 21°C by lowering the temperature of the water in the quenching bath from 14°C to 2°C. By combining the colder bath temperature with measurements of the peak height at 9°C, a 20% increase in Q^{-1} max was possible.

In the above experiments high temperature abnormal peaks were obtained only for alloys containing 0.415% V and 0.62% V. The abnormal peak temperature does not appear to be constant at a given frequency, suggesting that at least two distinctive mechanisms are operative. The experimentally determined curve is therefore a sum curve of these individual processes. The lack of appearance of an abnormal peak in the other alloys could be caused either by an insufficiently rapid quench or by the time of soak at 950°C not being sufficiently long to allow decomposition of the vanadium nitride or carbide to occur.

Since carbon had been shown to affect the normal peak, the possibility of the abnormal peak being broadened due to carbon was considered. In order to assess this effect, if any, it was desirable to establish whether an abnormal peak could be produced in an alloy containing carbon alone. Wert[69] has stated that no abnormal peak is produced by carbon in iron-vanadium alloys containing 0.5% V in the range -35°C to 200°C.

The results of the investigation on carburised iron wires are shown graphically in Figure 14 and summarised in Table VIII. Abnormal peaks were obtained in wires containing 0.62% V which had been carburised in toluene - hydrogen mixtures for 2.5 and 4 hours at 800°C. Thus it appeared that carbon and vanadium could interact in a similar way to nitrogen and vanadium although the existence of this peak has not been reported previously. It was noted that the normal carbon peak appeared to be broadened and displaced towards lower temperatures. Very low $\underline{\Delta H}$ values were obtained in most cases with a peak temperature approximately 6 C° lower than expected. This is taken to be evidence of an unstable condition associated with local high concentration of interstitial solute in presence of dissolved vanadium. A similar effect has been found by Paterson[80] in the Fe-Al-N system. Further evidence that this broadened normal carbon peak is metastable is shown by the fact that on homogenising these carburised wires at 950°C for 12 hours both the normal and abnormal carbon peaks disappeared. It seems likely that this is due to carbon combining with vanadium to form a precipitate of vanadium carbide, under conditions in which the equilibrium solubility of carbon was not measurable by internal friction.

The apparent contradiction that vanadium carbide showed insufficient dissociation at 950°C to give peaks in carburised wires, while apparently dissociated at the same

temperature to give carbon interference in nitrided wires, may be resolved by considering the thermodynamic data available for the solubility product of vanadium nitride and vanadium carbide.

At 950°C $VN \rightarrow \underline{V} + \underline{N}$ $\Delta G = 19{,}600$ cals./mole [71] (13)

Hence $K_A = [\% \underline{V}].[f_{N.} \underline{N} \%] = 3.16 \times 10^{-4}$ (14)

Also $VC \rightarrow V + C$ $\Delta G = 18{,}000$ cals./mole [72]

and $C \rightarrow \underline{C}$ $\Delta G = 18{,}500$ cals./mole [81]

$\therefore$ $VC \rightarrow V + \underline{C}$ $\Delta G = 36{,}500$ cals./mole

To find the free energy of solution of vanadium in iron, we note that

$VN \rightarrow V + \underline{N}$ $\Delta G = 30{,}300$ cals./mole [25][72]

Hence from (13) $V \rightarrow \underline{V}$ $\Delta G = -10{,}700$ cals./mole

$\therefore$ $VC \rightarrow \underline{V} + \underline{C}$ $\Delta G = 25{,}800$ cals./mole

and $K_B = [\% \underline{V}].[f_{c.} \underline{C} \%] = 2.51 \times 10^{-5}$ (15)

In the carburising experiments, the total carbon uptake by the wire was small due both to the relatively low temperature, 800°C, and to the low carburising potential. Thus on soaking at 950°C, practically all the vanadium was in solution. Taking this vanadium concentration in solution to be approximately 0.6% (Table VIII), equation (15) gives

$$\% \underline{C} = \frac{2.51 \times 10^{-5}}{0.60} = 4.19 \times 10^{-5}$$

This amount of carbon is below the level of detection of the internal friction apparatus and this explains why no carbon

peaks were obtained after homogenising the carburised wires. On the other hand, wires nitrided at 590°C contained practically no vanadium in solution, (as shown by the solubility and activation energy measurements on wires containing 0.157% V), and taking the nitrogen in solution to be approximately 0.025% N (Table VII), equation (14)

gives $$\% \underline{V} = \frac{1.16 \times 10^{-4}}{0.025} = 1.26 \times 10^{-2}$$

If this concentration of vanadium in solution is inserted in equation (15), it is seen that

$$\% \underline{C} = \frac{2.51 \times 10^{-5}}{1.26 \times 10^{-2}} = 1.99 \times 10^{-3}$$

and since this quantity of carbon is measureble, this explains why carbon interference was observed in nitrided wires quenched from 950°C. Although the heights of the carbon peaks shown in Table VII are higher than predicted by the thermodynamic calculation, such a calculation does show that measurable dissociation of vanadium carbide can occur, under certain conditions, in the presence of vanadium nitride. The disparity between the predicted value of peak height and the actual experimental peak height is not surprising in view of the possible uncertainty of the thermodynamic data.

Since carbon has been shown capable of interfering in the damping measurements and causing broadening every attempt was made to remove this residual carbon from the wires. Very prolonged dry hydrogen treatments were performed and no carbon

peak could be detected on quenching from 950°C. However, the next series of nitriding experiments performed using 1% and 6% NH_3 - H_2 mixtures at 850°C to 950°C still showed carbon interference. These results are shown graphically in Figures 15 to 20 and summarised in Table IX. Thus it is clear that the residual vanadium carbide cannot be decomposed by hydrogen treatment. The carbon contents were generally very small ranging from 0.0002% C to 0.004 % C approximately. Yet, because the amount of nitrogen in solution was also very small, the effect of carbon on the shape of the internal friction curve, and hence on the value of ΔH, was relatively large. Abnormal peaks were observed in wires quenched from above 900°C but these were very low peaks and little confidence can be placed in these results.

In view of the very small abnormal peaks obtained by nitriding at high temperature, it was decided to study the abnormal peak by soaking wires containing nitrogen and vanadium at high temperatures for long times. In order to minimise ageing effects, only the abnormal peaks were determined after quenching. These results are shown in Figures 21 and 22 and summarised in Table X.

Several conclusions may be drawn from the results shown in Table X.

1. The temperature of the abnormal peak is not invariant at a given frequency, strongly suggesting that the measured

abnormal peak is broadened and is the sum of at least two single time relaxation processes.

2. At constant frequency and vanadium content, the peak temperature tends to increase with increasing nitrogen content. This was also found by Fast and Meijering [20].

3. Since only a single wire representing each vanadium content was used, the results given in Table X refer to successive periods of soaking and the final values in the table apply to wires which have been held at 950°C for a total of 47 hours. It is interesting to note that the abnormal peak height decreases with the time of soaking at 950°C and that this is coupled with an increase in ΔH. For example, the initial peak height for 0.415% alloy (21A) was 0.01 with a ΔH of 20,500 cals./mole, while the final peak height after 47 hours soaking at 950°C was 0.0035 with a ΔH of 34,000 cals./mole (22A). Since the wires were sealed in thin silica tubes during soaking and since desorption of nitrogen requires the presence of hydrogen [25], this reduction in peak height is not explained by removal of nitrogen from the wire during treatment. Thus an irreversible process appears to be occurring during soaking and this is throught to be explainable in terms of changes in the size of vanadium nitride particles present. As the wires were initially nitrided at 590°C, and as vanadium diffusion at this temperature is extremely small, it is unlikely that a bulk precipitate of vanadium nitride was formed but rather an extremely fine

dispersion of vanadium nitride nuclei. It is tentatively suggested that this association between vanadium and nitrogen effectively prevents the vanadium from exerting any influence on nitrogen solubility and nitrogen diffusion but does not distort the iron lattice sufficiently to cause the formation of a different type of site capable of giving rise to a damping peak in the temperature range stidied. Thus at 590°C only the normal nitrogen peak is obtained. On soaking at 950°C both decomposition of vanadium nitride, to give a measurable solubility, and the gradual growth of vanadium nitride nuclei will occur. It is considered that the growth of the nuclei will first give rise to a coherent precipitate which will coarsen to produce a stable bulk precipitate.

This view is substantiated by the work of Fountain and Chipman[71] who found anomalous effects due to the particle size of vanadium nitride during their study of the solubility of vanadium nitride in iron. They reported a higher solubility product for vanadium and nitrogen in metastable equilibrium with an extremely fine dispersion of vanadium nitride particles ($\sim 10^{-7}$ cms. radius). For a given nitrogen content, their results indicate a vanadium solubility approximately twice that existing in the presence of a bulk precipitate. Their findings are in good agreement with the present results since initially a high vanadium solubility will lead to a higher abnormal peak height associated with Fe-V site jumps. As the

precipitate coarsens with time, the vanadium solubility will decrease and this will result in the observed decrease in abnormal peak.

It remains to consider the mechanisms contributing to the abnormal peak and the observed change in its shape (as shown by the average ΔH) with increasing soaking time. At the outset, it is clear that this abnormal peak cannot be explained by a similar mechanism to that proposed by Meijering [67] and Fast and Verrijp [68] to account for the broadening of the normal peak in Fe-Mn-N alloys which involved both Mn-Mn-N sites and Fe-Mn-N sites. The chemical affinity of vanadium for nitrogen is much greater than that of manganese for nitrogen, and, as has been shown earlier, the solubility of vanadium at 950°C is of the order of $\sim 10^{-2}$ wt.%. In these circumstances it is totally unrealistic to consider V-V pair formation, thus only Fe-V sites are considered to exist in the lattice.

Several possible mechanisms could contribute to the abnormal peak.

1. Nitrogen atom jumps associated with Fe-V sites.
2. Nitrogen atom jumps associated with distorted sites surrounding coherent vanadium nitride precipitates.
3. Jumps due to carbon in similar sites to those proposed for nitrogen.

In addition, as considered above, ageing can cause distortion of the peak giving a decrease in ΔH.

In view of the increasing ΔH values obtained, it is clear that the soaking time at 950°C markedly influences the mechanisms contributing to the abnormal peak. In order to obtain a clearer understanding of these mechanisms it is necessary to assess the effect of soaking time on each of the above four factors. It may be deduced from the thermodynamic calculation given earlier in this section that the equilibrium C/N ratio should be a constant and independent of the soaking time. Thus, while carbon could contribute to broadening, the relative effect should be constant and carbon therefore cannot be held responsible for the observed changes in T peak and ΔH. The effect of ageing should decrease with peak height but would be too small to produce the marked change in the character of the peak. The only conceivable change occurring within the wire, with increasing soaking time, is the growth of the vanadium nitride nuclei. Thus, the observed decrease in the abnormal peak height must be due to (1) a decrease in the number of distorted sites produced by a coherent precipitate and (2) a decrease in the number of Fe-V sites caused by the lower vanadium solubility in equilibrium with a bulk precipitate. The increase in ΔH obtained, corresponding to the decrease in Q^{-1} max, is due to the decreased contribution from nitrogen atoms in distorted sites so that, with longer soaking times, the abnormal peak approaches a single time relaxation peak i.e. a peak caused by nitrogen atom jumps solely in Fe-V interstices.

Since the observed abnormal peak height decreases with soaking time, it is clear that the mechanism occurring at the higher temperature is becoming less prominent and is due therefore to atom movements associated with a coherent vanadium nitride precipitate. The mechanism occurring at the lower temperature is due to nitrogen jumps associated with Fe-V sites. The results obtained for wires soaked for 46-47 hours at 950°C (the contribution from coherent precipitate sites being small), show that the activation energy for the diffusion of nitrogen in Fe-V sites is in the range 30,000 cals./mole to 40,000 cals./mole. A more exact analysis of the peak is not possible, since slight distortion due to carbon is probable.

The work of Fast and Meijering [70], who stated that the abnormal peak did not represent a single process, can also be explained in the light of the above theory. Since none of their experiments involved soaking a wire for more than approximately 20 hours, it is possible that the vanadium nitride precipitate was coherent throughout their experiments.

Using an activation energy of ΔH = 18,000 cals./mole for nitrogen and a peak temperature of 21.5°C for a frequency of 1 C/S, it was calculated that the mean time-of-stay of a nitrogen atom in the vicinity of a vanadium atom is approximately 300 times greater than in the vicinity of iron atoms only.

Attempts were made to calculate the solubility of vanadium nitride in iron using the height of the damping peaks

as a measure of nitrogen in solution. This value of nitrogen in solution was subtracted from the total nitrogen content of the wire as analysed, to give a measure of the nitrogen available to combine with the vanadium. Since the total vanadium analysis was known, it was possible to estimate the amount of vanadium in solution. Many such calculations using results obtained at temperatures in the range 850°C to 950°C indicated that no vanadium was present in solution (in agreement with the fact that the solubility of vanadium is extremely small, even at 950°C) whilst others yielded solubility products which were at least 10 times greater than those reported by Fountain and Chipman[71]. The vanadium analyses were performed on a cast basis and, due to the small sample which had to be used, the nitrogen analyses were also subject to uncertainty. In view of these uncertainties, it is not surprising that the values of solubility product obtained showed a large variation.

4. Ageing in Fe-V-N Alloys.

The ageing results are summarised in Tables XI, XII and XIII. It is noticed that in spite of the fact that the abnormal peak was aged at approximately 84°C compared to 30°C for the normal peak, the rate of ageing is much slower in the former case. This is in accord with the interpretation placed on the abnormal peak, since nitrogen atoms associated with iron-vanadium sites will not readily diffuse to existing precipitation sites. At the ageing temperature employed,

vanadium does not diffuse sufficiently fast to participate in ageing and para-precipitation occurs i.e. the precipitate inherits its alloy content from the matrix. Growth of these para-precipitates occurs by diffusion of nitrogen, with a corresponding decrease of the normal and to a lesser extent, of the abnormal peaks.

The results for ageing of the normal peak, when analysed in terms of Wert's equation[48], appear to indicate two stages characterised by different n values. The first of these is considered to be the most significant and applies up to approximately 80% of the total precipitation as reported by Wert. The only case in which an incubation period was observed before ageing commenced was in that of a pure iron wire quenched from 590°C. The n values derived for various wires show a considerable scatter. In general however, the rates of ageing in iron-vanadium alloys were higher than in pure iron. This may be explained by the large number of VN nuclei present in these alloys prior to quenching, which can act as sites for the precipitation of iron nitrides. As ageing was only studied at a single temperature, and after quenching from only two temperatures, the data obtained is insufficient for a detailed discussion of the factors affecting the ageing process.

CHAPTER VII.

CONCLUSIONS.

VII CONCLUSIONS

The significant features of the present work are as follows.

1. Data for the solubility and activation energy for diffusion of nitrogen in α-iron have been determined and shown to agree with previous work.

2. The solubility of vanadium in presence of nitrogen has been shown to be too small below about 900°C for any internal friction peak to be discerned by the present technique.

3. An abnormal peak in Fe-V-N alloys has been obtained by quenching from 950°C, as previously reported by Fast and Meijering[70]. Investigation of this has led to the conclusion that it is due to nitrogen atom jumps associated with Fe-V sites and also, except after prolonged soaking at 950°C, to jump processes associated with distorted interstices in the vicinity of vanadium nitride precipitates. After prolonged soaking, the peak approximates to a single relaxation time curve due to the former mechanism and the activation energy for this has been assessed at 30 to 40 K cals./mole.

4. A previously unreported abnormal peak has been shown to exist for Fe-V-C alloys under suitable conditions. The fact that this peak is only observable under equilibrium conditions when both C and V are relatively low leads to certain general conclusions regarding the detection of interaction peaks in iron alloys. It would appear that such "abnormal" peaks will

only be detectable by torsional pendulum when the solubility product for the solute and substitutional elements is not less than approximately 10^{-6} at the quenching temperature. Further, the concentration of either solute must not be less than 10^{-3} weight per cent. If the equilibrium interstitial solute concentration is less than this, then there is insufficient solute to give measurable internal friction. Conversely, if the substitutional solute concentration is less than 10^{-3}, there are insufficient "abnormal" sites in the lattice and again no interaction peak can be detected. These observations may explain, to some extent, the present unsatisfactory state of knowledge on interaction damping peaks. For example, although N and C generally give rise to similar internal friction characteristics, an abnormal peak had been reported for the Fe-V-N system but no comparable peak had been observed previously in the Fe-V-C system, possibly because the above concentration conditions were not fulfilled. Thus similar peaks may exist, due to C or N, in the Fe-Al and Fe-Ti systems since, if sufficiently high quenching temperatures are employed, it should be possible to satisfy the solubility conditions outlined above.

5. The computer programmes developed and utilised during the present work are considered to form a sound basis for the analysis of complex internal friction peaks.

CHAPTER VIII.

RESULTS.

FIGURE 6. THIS INVESTIGATION.

T °C	T °K	$\frac{1000}{T\ °K}$	a^{-1} mm	β H a^{-1} mm x 1·26	Mean β H and Deviation	log β H
350	623	1·61	0·0153	0·0193	0·0194 ± 0	- 1·712
			0·0154	0·0194		
400	673	1·49	0·0231	0·0291	0·0297 ± 0·00035	- 1·527
			0·0238	0·0291		
450	723	1·38	0·030	0·0416	0·0410 ± 0·0009	- 1·386
			0·0336	0·0424		
			0·0334	0·0383		
			0·0334	0·0371		
			0·0341	0·0430		
			0·0332	0·0404		
			0·0334	0·0458		
500	773	1·29	0·0430	0·0617	0·0571 ± 0·0009	- 1·243
			0·0449	0·0565		
			0·0434	0·0571		
			0·0422	0·0532		

OTHER INVESTIGATORS.

	T °C	T °K	$\frac{1000}{T\ °K}$	β H	log β H
Rawlings and Taylor	350	623	1·61	0·0197	- 1·705
	400	673	1·49	0·0280	- 1·553
	450	723	1·38	0·0459	- 1·339
	500	773	1·29	0·0695	- 1·158
Fast and Verwijp	350	623	1·61	0·0151	- 1·822
	400	673	1·49	0·0248	- 1·605
	450	723	1·38	0·0388	- 1·411
	500	773	1·29	0·0554	- 1·257

FIGURE 7.

t°C	T°K	$\frac{1000}{T}$	2 hrs. Pure NH_3		8 hrs. Pure NH_3		2 hrs. 6% NH_3		8 hrs. 6% NH_3	
			α^{-1} max	log $\frac{1}{\alpha}$ H	α^{-1} max	log $\frac{1}{\alpha}$ H	α^{-1} max	log $\frac{1}{\alpha}$ H	α^{-1} max	log $\frac{1}{\alpha}$ H
300	573	1·75	0·0134	- 1·778	0·00948	- 2·024	0·0119	- 1·884	0·0115	- 1·939
400	673	1·38	0·0233	- 1·551	0·0245	- 1·611	0·0212	- 1·674	0·0247	- 1·606
500	773	1·29	0·0434	- 1·373	0·0377	- 1·401	0·0319	- 1·559	0·0444	- 1·371

FIGURE 8.

	T°C	α^{-1} exp.	Deviation	α^{-1} theoretical
A	21	0·0292	0·0007	0·0285
	23	0·0305	−0·00136	0·0319
	25	0·0338	0·00115	0·0327
	27	0·0334	−0·00018	0·0336
	28	0·0320	0·00008	0·0319
	31	0·0270	0·00031	0·0273
	33	0·0263	0·00018	0·0262
	35	0·0232	0·00027	0·0229
	37	0·0171	0·00075	0·0175
C	18	0·0350	0·00049	0·0345
	20	0·0342	−0·00011	0·0343
	21	0·0346	0·00012	0·0345
	22	0·0343	−0·00010	0·0345
	23	0·0341	−0·00002	0·0343
	24	0·0339	−0·00010	0·0340
	26	0·0336	0·00060	0·0330
B	22	0·0341	0·0004	0·0337
	26	0·0358	−0·00007	0·0365
	28	0·0361	0·00002	0·0359
	31	0·0352	0·00055	0·0346
	32·5	0·0336	0·00014	0·0335
	34	0·0334	0·00124	0·0322
	36	0·0304	0·00002	0·0304
	39	0·00727	−0·00077	0·00804
D	29	0·0346	0·00020	0·0344
	30	0·0347	−0·00008	0·0348
	31	0·0347	−0·00033	0·0350
	35·5	0·0336	0·0000	0·0336
	36·5	0·0332	0·00028	0·0329
	37·5	0·0317	−0·00046	0·0322
	38·5	0·0313	−0·00006	0·0314
	39·5	0·0300	0·00035	0·0305
	42	0·00771	0·00013	0·00758

FIGURE 9.

	T°C	σ^{-2} exp.	Deviation	σ^{-2} theoretical		T°C	σ^{-2} exp.	Deviation	σ^{-2} theoretical
2	18	0.0120	0.00039	0.0108	9	18	0.0105	-0.00005	0.0105
	19	0.0106	-0.00096	0.0112		19	0.0108	0.00035	0.0105
						20	0.0106	0.00018	0.0105
	21	0.0117	0.00017	0.0115		21	0.0101	-0.00027	0.0105
	22	0.0116	0.00007	0.0115		22	0.0103	-0.00007	0.0104
	23	0.0116	0.00018	0.0114		23	0.0100	0.00001	0.0100
	24	0.0113	0.00018	0.0111					
	25	0.0107	-0.00013	0.0108	8	17	0.0129	-0.00011	0.0130
						18	0.0132	-0.00037	0.0136
6	16	0.0119	-0.00043	0.0123		19	0.0140	-0.00005	0.0145
	17	0.0121	-0.0008	0.0129		20	0.0140	-0.00021	0.0142
	18	0.0137	0.00032	0.0134		21	0.0146	0.00015	0.0144
	19	0.0131	0.00018	0.0130		22	0.0131	-0.00037	0.0135
	20	0.0132	0.00004	0.0128		23	0.0132	-0.00006	0.0134
	21	0.0130	0.00017	0.0114		24	0.0143	0.00002	0.0143
	22	0.0125	-0.00002	0.0125		25	0.0138	-0.00014	0.0139
	23	0.0126	0.00015	0.0111		26	0.0136	0.00006	0.0135
	24	0.0102	-0.00017	0.0119		27	0.0129	-0.00020	0.0131
	25	0.0114	0.00006	0.0101					
	26	0.0102	0.00033	0.0139					

FIGURE 10. COMPARISON CURVES $\Delta H = 18{,}900$ cals/mole.

	$T^{\circ}C$	a^{-1} exp.	Deviation	a^{-1} theoretical		$T^{\circ}C$	a^{-1} exp.	Deviation	a^{-1} theoretical
I	29	0.0146	0.00006	0.0141	II	17	0.0129	0.00033	0.0126
	30	0.0147	0.00007	0.0144		18	0.0132	-0.00006	0.0133
	31	0.0147	0.00007	0.0146		19	0.0140	0.00023	0.0138
	35.5	0.0156	0.00008	0.0155		20	0.0140	-0.00013	0.0141
	36.5	0.0152	0.00022	0.0150		21	0.0146	0.00017	0.0144
	37.5	0.0117	-0.00028	0.0124		22	0.0148	-0.00037	0.0145
	38.5	0.0113	-0.00042	0.0117		23	0.0142	-0.00022	0.0144
	39.5	0.0109	-0.00014	0.0110		24	0.0143	0.00010	0.0142
	42	0.00971	-0.00021	0.00992		25	0.0138	0.00009	0.0138
						26	0.0136	0.00034	0.0133
						27	0.0129	0.00032	0.0127

FIGURE 11.

	t°C	ϵ^{-1} exp.	Deviation	ϵ^{-1} theoretical		t°C	ϵ^{-1} exp.	Deviation	ϵ^{-1} theoretical
A	18	0.0163	-0.00154	0.0178	B	19	0.00282	0.0005	0.00232
	19	0.0187	0.00052	0.0182		20.5	0.00213	0.00036	0.00177
	19.5	0.0204	0.00183	0.0186		21	0.00179	-0.00007	0.00186
	22	0.0189	-0.00009	0.0190		21.5	0.00154	-0.00042	0.00196
	23.5	0.0167	-0.00195	0.0187		22	0.00190	-0.00016	0.00206
	35	0.0104	0.00052	0.00988		23	0.00219	-0.00008	0.00227
	45	0.00894	-0.00218	0.00912		46.5	0.00308	0.00031	0.00277
	56	0.00274	0.00009	0.00165		56.5	0.00094	-0.00038	0.00132
	66	0.00150	0.00043	0.00075		67.5	0.0000		
	76	0.00124	0.00089	0.00035		75	0.0000		
	81.5	0.00045				86	0.0000		
	84	0.00032				87.5	0.0000		
	85.5	0.00022				89.5	0.0000		
	87.5	0.00008				92	0.0000		
	90	0.00030				93.5	0.0000		
	94	0.00022				96.5	0.0000		
	97	0.00008				99	0.0000		
	102	0.00069				105	0.0000		
	106	0.00099				110	0.0000		
C	18.5	0.00069	-0.00043	0.00020					
	20	0.00081	-0.00031	0.00112					
	21	0.00108	-0.00011	0.00119					
	23	0.00136	-0.00021	0.00157					
	25	0.00198	-0.00008	0.00206					
	30.5	0.00320	0.00057	0.00263					
	34.5	0.00459	-0.00031	0.00490					

FIGURE 11 continued

	T°C	θ^{-1} exp.	Deviation	θ^{-1} theoretical
C	57.5	0.00503	0.00032	0.00471
	61	0.00336	-0.00071	0.00407
	65	0.00291	0.00047	0.00303
	69	0.0000		
	73	0.0000		
	77.5	0.0000		
	85	0.0000		
	89	0.0000		
	93	0.0000		
	97.5	0.0000		
	101.5	0.0000		
	105	0.0000		
	109.5	0.0000		

FIGURE 12.

	$t^{\circ}C$	α^{-1} exp.	α^{-1} nitrogen	α^{-1} carbon	Deviation	α^{-1} [illegible] theoretical
A	18.5	0.0226	0.0215	0.00135	-0.00027	0.0228
	20	0.0227	0.0225	0.00150	-0.00148	0.0252
	22	0.0262	0.0230	0.00230	0.00120	0.0250
	23.5	0.0259	0.0227	0.00234	0.00034	0.0251
	25.5	0.0263	0.0216	0.00283	0.00138	0.0264
	30	0.0186	0.0171	0.00398	-0.00345	0.0221
	35	0.0169	0.0117	0.00460	0.00059	0.0163
	45	0.00850	0.00483	0.00286	0.00072	0.00779
	56.5	0.00269	0.00154	0.00108	-0.00087	0.00286
	65	0.00078				
	75	0.00085				
	84.5	0.0000				
	89	0.0000				
	93	0.0000				
	99	0.0000				
	102	0.0000				
	105	0.0000				
	109	0.0000				
B	19	0.0262	0.0220	0.00308	0.00007	0.0240
	20	0.0254	0.0215	0.00345	-0.00058	0.0250
	21	0.0254	0.0219	0.00306	-0.00034	0.0258
	23	0.0262	0.0219	0.00278	-0.00046	0.0267
	25	0.0275	0.0220	0.00302	0.00069	0.0268
	27.5	0.0258	0.0189	0.00322	-0.00056	0.0262
	30	0.0232	0.0163	0.00356	0.00021	0.0249
	34.5	0.0216	0.0117	0.00409	0.00005	0.0216
	46.5	0.0154	0.00484	0.00546	0.00082	0.00958
	57	0.00470	0.00169	0.00210	0.00091	0.00379
	65	0.00160	0.00058	0.00101	-0.00029	0.00189
	76	0.00140				
	83	0.0000				
	88	0.0000				
	92	0.0000				
	95.5	0.0000				
	98.5	0.0000				
	101.5	0.0000				
	106.5	0.0000				
	109	0.0000				

FIGURE 13.

	$T^{\circ}C$	a^{-1} exp.	a^{-1} nitrogen	a^{-1} carbon	Deviation	a^{-1} theoretical
A	16	0.0189	0.0165	0.00066	0.00122	0.0172
	17	0.0195	0.0175	0.00074	0.00127	0.0182
	18.5	0.0197	0.0187	0.00080	0.00131	0.0196
	19.5	0.0214	0.0193	0.00099	0.00148	0.0203
	20.5	0.0204	0.0198	0.00111	-0.00046	0.0209
	21	0.0210	0.0199	0.00117	-0.00006	0.0211
	22	0.0211	0.0200	0.00130	-0.00020	0.0213
	25	0.0217	0.0198	0.00196	-0.00134	0.0208
	26.5	0.0200	0.0180	0.00202	-0.00006	0.0201
	29	0.0170	0.0158	0.00264	-0.00186	0.0183
	33	0.0150	0.0110	0.00293	0.00112	0.0139
	36.5	0.0113	0.00898	0.00296	-0.00060	0.0119
	46	0.0055	0.00393	0.00172	-0.00015	0.00565
	54	0.0032	0.00198	0.00054	0.00038	0.00252
	64	0.0014	0.00027	0.00033	0.00079	0.00106
	76	0.0018			0.00003	0.00177
	85	0.0030			0.00004	0.00296
	89	0.0025			-0.00015	0.00265
	96	0.0018			0.00004	0.00156
	101	0.0011			0.00011	0.00099
	105	0.0004			-0.00027	0.00067
	111	0.0002			-0.00034	0.00054
B	20.5	0.0101	0.00859	0.00188	0.00022	0.00988
	22	0.00980	0.00870	0.00151	-0.00048	0.0102
	23.5	0.00970	0.00868	0.00177	-0.00066	0.0104
	25	0.00970	0.00830	0.00205	-0.00065	0.0104
	27.5	0.00930	0.00749	0.00254	-0.00073	0.0100
	30	0.00900	0.00696	0.00301	-0.00057	0.00947

FIGURE 19 continued

	T°C	a^{-1} exp.	a^{-1} nitrogen	a^{-1} carbon	Deviation	a^{-1} theoretical
3	38	0.00770	0.00364	0.00332	0.00096	0.00074
	50	0.00380	0.00181	0.00141	0.00118	0.00262
	59	0.00250	0.00057	0.00062	0.00132	0.00118
	72	0.00380			0.00090	0.00290
	81	0.00210			-0.00005	0.00215
	88	0.00720			-0.00029	0.00749
	94	0.00660			0.00042	0.00618
	99	0.00430			-0.00012	0.00442
6	76	0.00320			0.00066	0.00254
	81.5	0.00434			0.00048	0.00386
	85	0.00460			-0.00056	0.00516
	88	0.00530			-0.00072	0.00602
	93	0.00630			-0.00023	0.00653
	96	0.00570			-0.00048	0.00618
	99	0.00500			-0.00057	0.00557
	103	0.00430			-0.00008	0.00438
	107	0.00340			0.00005	0.00336
	110	0.00250			-0.00018	0.00268

TABLE 24.

	t^0C	α^{-1} exp.	Deviation	α^{-1} theoretical		t^0C	α^{-1} exp.	Deviation	α^{-1} theoretical
A	19	0.00177	0.00003	0.00174	B	20	0.00439	-0.00011	0.00450
	28	0.00204	-0.00006	0.00210		31.5	0.00460	-0.00008	0.00468
	34	0.00197	-0.00004	0.00201		38	0.00507	-0.00032	0.00539
	37	0.00188	-0.00001	0.00189		41	0.00515	-0.00044	0.00559
	39	0.00197	0.00019	0.00178		44.5	0.00534	-0.00017	0.00551
	41	0.00175	0.00008	0.00167		49	0.00520	0.00016	0.00504
	43	0.00171	0.00015	0.00156		51	0.00500	0.00017	0.00483
	46	0.00148	-0.00002	0.00150		61	0.00503	0.00002	0.00501
	53.5	0.00096	-0.00006	0.0010		73	0.00545	-0.00058	0.00604
	64	0.00082				81	0.00484	0.00051	0.00433
	75	0.0000				86	0.00496	0.00028	0.00468
	80.5	0.00045				90	0.00470	0.00020	0.00450
	85.5	0.00037				95	0.00456	0.00015	0.00441
	88.5	0.00046				98.5	0.00481	0.00053	0.00428
	91.5	0.00069				102	0.00490	0.00059	0.00431
	95	0.00051							
	99	0.00057			B	31	0.00306	-0.00001	0.00307
						33.5	0.00314	0.00004	0.00310
C	21	0.00201	-0.00005	0.00206		36	0.0038	0.00076	0.00304
	31	0.00248	-0.00027	0.00275		41	0.00358	-0.00083	0.00275
	39	0.00286	-0.00007	0.00293		45	0.00352	0.00012	0.00340
	41	0.00197	0.00027	0.00170		51	0.00331	-0.00001	0.00332
	43.5	0.00158	-0.00011	0.00169		61	0.00468	-0.0005	0.00478
	45.5	0.00125	-0.00029	0.00154		71	0.00533	-0.00075	0.00608
	54.5	0.00083				81.5	0.00650	0.00020	0.00630
	64	0.0000				86	0.00632	-0.00028	0.00660
	81	0.00051				88.5	0.00604	-0.00035	0.00639
	85	0.00037				91	0.00547	-0.00074	0.00621
	90	0.00039				93	0.00523	-0.00081	0.00604
	93.5	0.00078				96.5	0.00573	0.00003	0.00570
	100	0.00027				98	0.00575	0.00033	0.00542
						103	0.00544	0.00048	0.00496

FIGURE 15.

	T°C	Ω^{-1} exp.	Ω^{-1} nitrogen	Ω^{-1} carbon	Deviation	Ω^{-1} sum theoretical
A	16	0.0095	0.0086	0.0006	0.0013	0.0092
	18	0.0103	0.0097	0.0008	0.0005	0.0100
	20	0.0110	0.0098	0.0010	0.0017	0.0108
	22	0.0112	0.0095	0.0012	0.0003	0.0111
	23.5	0.0106	0.0093	0.0032	-0.0020	0.0124
	26	0.0105	0.0094	0.0026	-0.0008	0.0113
	28	0.0093	0.0093	0.0073	-0.0036	0.0066
	30	0.0071	0.0095	0.0085	0.0009	0.0080
	40	0.0032	0.0051	0.0033	0.0006	0.0039
	60	0.0042	0.0008	0.0033	0.0008	0.0077
	75	0.0078				
	80.5	0.0097				
	84.5	0.0085				
	87	0.0042				
	92	0.0072				
	95	0.0042				
	98	0.0026				

FIGURE 25 continued

	T°C	$\alpha^{-1}_{exp.}$	$\alpha^{-1}_{nitrogen}$	α^{-1}_{carbon}	Deviation	$\alpha^{-1}_{sum\ theoretical}$
B	19	0.0101	0.00897	0.00112	0.00018	0.00968
	20	0.0101	0.00901	0.00126	0.00004	0.0101
	22.5	0.0110	0.00899	0.00168	0.00056	0.0106
	23	0.0105	0.00895	0.00274	-0.00019	0.0107
	25.5	0.0108	0.00893	0.00222	-0.00046	0.0107
	30	0.00956	0.00668	0.00311	-0.00023	0.00979
	41	0.00568	0.00474	0.00097	-0.00003	0.00571
	50	0.00303	0.00185	0.00145	0.00032	0.00271
	60.5	0.00192	0.00098	0.00095	0.00015	0.00207
	72	0.00135				
	82	0.00121				
	85	0.00115				
	89	0.00105				
	92.5	0.00085				
	96	0.00057				

FIGURE 16.

	$t^{\circ}C$	a^{-2} exp.	Deviation	a^{-2} theoretical		$t^{\circ}C$	a^{-2} exp.	Deviation	a^{-2} theoretical
A	21	0.00405	0.00012	0.00413	B	21	0.00378	-0.00009	0.00387
	21.5	0.00414	0.00003	0.00411		22	0.00386	-0.00004	0.00390
	22	0.00405	-0.00002	0.00407		22.5	0.00404	0.00015	0.00389
	23	0.00431	-0.00006	0.00437		24	0.00409	0.00029	0.00380
	25	0.00436	-0.00001	0.00437		27	0.00317	-0.00017	0.00334
	26.5	0.00428	0.00007	0.00421		30	0.00289	0.00017	0.00272
	30	0.00370	0.0002	0.00350		40.5	0.000366	-0.00006	0.00103
	39	0.00133	-0.00021	0.00154		49	0.00045		
	46.5	0.00026				60	0.00022		
	68.5	0.00052				69	0.0000		
	80	0.00063				80.5	0.0000		
	84.5	0.00072				84	0.00020		
	87.5	0.00048				87	0.00008		
	92	0.00070				90	0.0002		
	96	0.00064				93.5	0.0000		
						96.5	0.0000		
						99	0.0000		

FIGURE 17.

	T°C	Q^{-1} exp.	Q^{-1} nitrogen	Q^{-1} carbon	Deviation	Q^{-1} Theoretical
A	17	0.00385	0.00306	0.00822	-0.00003	0.00388
	19	0.00339	0.00333	0.00827	-0.00022	0.00361
	21	0.00387	0.00348	0.00334	0.00005	0.00382
	23	0.00373	0.00363	0.00367	-0.00006	0.00369
	25	0.00389	0.00334	0.00351	0.00004	0.00385
	26.5	0.00383	0.00351	0.00370	-0.00018	0.00389
	29.5	0.00386	0.00381	0.00376	0.00006	0.008
	36.5	0.00382	0.00351	0.00357	-0.00006	0.00388
	41	0.00385			-0.00006	0.000318
	70	0.00383			-0.00002	0.00389
	79.5	0.00374			-0.00006	0.00380
	83	0.00380			-0.00009	0.00373
	87	0.00335			-0.00002	0.00337
	89.5	0.00345			0.00002	0.00349
	94	0.00350			0.00002	0.00317
	97.5	0.00388			0.00010	0.00398
B	22	0.00330	0.00275	0.00354	0.00009	0.00329
	23	0.00306	0.00274	0.00360	-0.00007	0.00333
	24	0.00365	0.00309	0.00366	0.00030	0.00335
	25.5	0.00338	0.00298	0.00376	0.00006	0.00334
	28	0.00294	0.00351	0.00313	-0.00009	0.00303
	37	0.0026				
	46	0.00313				
	57	0.000378			0.00016	0.000738
	71	0.00322			-0.0002	0.00318
	80.5	0.00386			0.00017	0.00369
	84	0.00372			0.00002	0.00369
	87.5	0.00372			0.00009	0.00362
	91.5	0.00349			-0.00005	0.00350
	95	0.00350			0.00009	0.00355
	99.5	0.00322			-0.00014	0.00336

FIGURE 18.

	t°C	$a^{-1}_{exp.}$	$a^{-1}_{nitrogen}$	a^{-1}_{carbon}	Deviation	a^{-1} sum theoretical
A	18	0.00470			-0.00007	0.00477
	21	0.00507			0.00001	0.00506
	23	0.00507			0.00001	0.00506
	24.5	0.00493			0.00005	0.00488
	29.5	0.00368			0.00009	0.00359
	33.5	0.00254			0.00019	0.00235
	49	0.00083				
	59	0.0000				
	71.5	0.0000				
	81	0.00011				
	86	0.00004				
	87.5	0.00008				
	92	0.00020				
	95	0.00011				
	100	0.0000				
B	19	0.00521	0.00448	0.00027	0.00007	
	21	0.00489	0.00372	0.00091	-0.00016	
	23.5	0.00345	0.00268	0.00084	0.00033	
	24.5	0.00421	0.00336	0.00078	0.00006	
	27	0.00355	0.00307	0.00060	-0.00013	
	29	0.00312	0.00233	0.00070	-0.00013	
	33.5	0.00201	0.00210	0.00060	-0.00027	
	48	0.00121	0.00095	0.00042	0.00004	
	60.5	0.00139				
	71.5	0.00220				
	81.5	0.00215				
	85.5	0.00199				
	89	0.00232				
	91.5	0.00223				
	97	0.00251				

FIGURE 19.

	γ^0	α^{-1} exp.	α^{-1} nitrogen	α^{-1} carbon	Deviation	α^{-1} gas theoretical
A	18	0.00127	0.00108	0.00006	0.00021	0.00106
	19	0.00130	0.00110	0.00007	0.00013	0.00117
	21	0.00105	0.00118	0.00009	-0.00010	0.00123
	23	0.00127	0.00134	0.00011	0.00002	0.00145
	24.5	0.00118	0.00111	0.00013	-0.00006	0.00124
	30	0.00103	0.00085	0.00020	-0.00002	0.00105
	40	0.00067	0.00038	0.00020	0.00009	0.00058
	49	0.00032				
	59	0.00020				
	69	0.00020				
	80	0.00027				
	83.5	0.00045				
	87	0.00034				
	90.5	0.00002				
	93.5	0.00045				
B	20	0.00165	0.00147	0.00013	0.00005	0.00160
	22	0.00150	0.00150	0.00016	0.00014	0.00166
	24	0.00160	0.00147	0.00020	0.00001	0.00167
	25.5	0.00136	0.00142	0.00023	-0.00006	0.00159
	28.5	0.00149	0.00122	0.00029	-0.00003	0.00152
	31.5	0.00100	0.00097	0.00035	0.00003	0.00098
	40	0.00060	0.00045	0.00018	0.00017	0.00063
	50	0.00035				
	70.5	0.00066				
	80	0.00035				
	83	0.00032				
	87	0.00039				
	90.5	0.0000				
	94	0.0000				
	98	0.0000				

FIGURE 20.

	T°C	$\alpha^{-1}_{exp.}$	$\alpha^{-1}_{nitrogen}$	α^{-1}_{carbon}	Deviation	$\alpha^{-1}_{theoretical}$
A	18	0.00121	0.00098	0.00015	0.00008	0.00113
	20	0.00149	0.00105	0.00019	0.00026	0.00123
	22	0.00130	0.00107	0.00023	0.0000	0.00130
	24	0.00100	0.00105	0.00029	-0.00025	0.00133
	26	0.00149	0.00099	0.00036	0.00016	0.00133
	28	0.00100	0.00074	0.00049	-0.00023	0.00123
	30.5	0.00108	0.00038	0.00045	0.00029	0.00079
	50	0.00063	0.00015	0.00022	0.00027	0.00036
	60	0.00067			0.00016	0.00051
	70	0.00072			-0.00022	0.00094
	81	0.00148			0.00012	0.00130
	84	0.00131			-0.00036	0.00129
	88	0.00136			0.00016	0.00120
	90	0.00103			-0.00011	0.00114
	94.5	0.00094			-0.00002	0.00096
B	19	0.00091	0.00086	0.00014	-0.00009	0.00100
	21.5	0.00127	0.00090	0.00019	0.00019	0.00108
	24	0.00118	0.00088	0.00024	0.00006	0.00112
	25.5	0.00088	0.00084	0.00028	-0.00024	0.00112
	28.5	0.00108	0.00073	0.00035	-0.00001	0.00109
	30	0.00094	0.00056	0.00043	0.00016	0.00078
	40.5	0.00051	0.00034	0.00021	0.00016	0.00055
	50	0.00038			-0.00001	0.00039
	70.5	0.00148			-0.00003	0.00151
	82	0.00151			0.00023	0.00128
	86	0.00124			-0.00034	0.00158
	89	0.00162			0.00015	0.00147
	92	0.00127			-0.00007	0.00134
	95	0.00118			-0.00003	0.00121
	98	0.00108			0.0000	0.00108

FIGURE 21. LOW FREQUENCY.

	T°C	Q^{-1} exp.	Deviation	Q^{-1} theoretical		T°C	Q^{-1} exp.	Deviation	Q^{-1} theoretical
A	62	0.00869	0.00029	0.00840	B	66	0.00760	0.0008	0.0075
	65	0.00887	-0.00027	0.00914		72	0.00927	-0.0008	0.00937
	72.5	0.00970	0.0000	0.00970		76.5	0.00869	-0.00021	0.00890
	78	0.00683	-0.00117	0.00800		80	0.00777	-0.00023	0.00790
	85	0.0108	0.00086	0.00994		90	0.00782	-0.00018	0.00793
	89	0.00893	-0.00080	0.00921		95	0.00681	0.00002	0.00679
	96	0.00796	-0.00022	0.00776		99	0.00760	0.00022	0.00738
	104.5	0.00954	0.00076	0.00878					
C	67	0.00318	0.00053	0.00265					
	71	0.00358	-0.00022	0.00380					
	76	0.00508	0.00040	0.00468					
	80	0.00621	-0.00118	0.00739					
	85.5	0.00807	0.00001	0.00806					
	89.5	0.00691	-0.00095	0.00886					
	96	0.00735	0.00028	0.00707					
	99	0.00969	-0.00027	0.00996					

HIGH FREQUENCY.

	T°C	Q^{-1} exp.	Deviation	Q^{-1} theoretical		T°C	Q^{-1} exp.	Deviation	Q^{-1} theoretical
A	86.5	0.00528	0.00032	0.00496	C	85	0.00540	0.00027	0.00513
	90	0.00509	-0.00009	0.00518		90	0.00532	-0.00029	0.00561
	95.5	0.00483	0.00010	0.00473		96.5	0.00484	-0.00007	0.00491
	98	0.00432	0.00032	0.00400		98	0.00473	0.00048	0.00425
	100	0.00360	-0.00028	0.00388		100.5	0.00360	0.00020	0.00340
	103	0.00378	0.00011	0.00367		103	0.00357	-0.00009	0.00366
	105	0.00376	-0.00039	0.00415		105.5	0.00376	-0.00058	0.00434
	110	0.00320	-0.00031	0.00351		110	0.00328	-0.00029	0.00357

FIGURE 22. LOW FREQUENCY.

	T°C	Q^{-1} exp.	Deviation	Q^{-1} theoretical		T°C	Q^{-1} exp.	Deviation	Q^{-1} theoretical
A	80.5	0.00302	-0.00002	0.00304	B	80	0.00302	-0.00012	0.00314
	82	0.00336	0.00005	0.00331		82	0.00336	-0.00007	0.00343
	83.5	0.00368	-0.00019	0.00387		83	0.00328	-0.00021	0.00349
	85.5	0.00389	0.00042	0.00347		84	0.00389	0.00040	0.00349
	87	0.00373	0.00041	0.00332		85	0.00373	0.00030	0.00343
	88.5	0.00370	-0.00036	0.00306		86	0.00370	- 0.00032	0.00332
	89	0.00273	-0.00023	0.00296		87.5	0.00273	-0.00033	0.00306
	90.5	0.00285	0.00021	0.00264		90	0.00285	0.00033	0.00252
C	80.5	0.00346	-0.00002	0.00348					
	82.5	0.00365	0.00015	0.00350					
	84.5	0.00346	0.00037	0.00309					
	86.5	0.00288	-0.00010	0.00298					
	88	0.00250	-0.00020	0.00270					
	90	0.00246	0.00016	0.00230					

HIGH FREQUENCY

	T°C	Q^{-1} exp.	Deviation	Q^{-1} theoretical		T°C	Q^{-1} exp.	Deviation	Q^{-1} theoretical
A	78	0.00340	0.00036	0.00308	B	90	0.00131	-0.00017	0.00148
	83	0.00221	-0.00056	0.00277		91.5	0.00141	-0.00008	0.00149
	89.5	0.00237	-0.00011	0.00248		92.5	0.00135	-0.00010	0.00145
	92	0.00230	-0.00016	0.00246		94	0.00119	-0.00034	0.00153
	94.5	0.00217	-0.00010	0.00227		96	0.00116	0.00006	0.00110
	97	0.00197	0.00002	0.00195		97	0.000959	-0.00002	0.000979
						98.5	0.000875	0.00007	0.000805
C	90	0.00309	0.00048	0.00261		100	0.000625	-0.00003	0.000655
	91	0.00276	0.00050	0.00226					
	92.5	0.00207	-0.00008	0.00215					
	94.5	0.00190	0.00006	0.00184					
	96	0.00210	0.00004	0.00206					
	97	0.00176	-0.00007	0.00183					
	98	0.00145	-0.00017	0.00162					
	100	0.00120	0.00005	0.00114					

FIGURE 23.

	a_0^{-1}	a_∞^{-1}	Time mins.	log t	$a_0^{-1} - a_t^{-1}$	W	f (W)
A	0.00625	0.000850	14	2.92	0.00112	0.208	-0.633
			30	3.26	0.00250	0.462	-0.208
			45	3.43	0.00305	0.564	-0.0804
			60	3.56	0.00322	0.595	-0.0434
			75	3.65	0.00407	0.754	0.143
			105	3.80	0.00460	0.848	0.275
			120	3.86	0.00464	0.860	0.293
			136	3.91	0.00474	0.878	0.323
			151	3.96	0.00507	0.938	0.445
			166	4.00	0.00522	0.966	0.529
			181	4.04	0.00494	0.915	0.392
			240	4.16	0.00534	0.988	0.649
			271	4.21	0.00529	0.980	0.594
B	0.00595	0.000850	16	2.98	0.00182	0.355	-0.358
			32	3.28	0.00199	0.389	-0.299
			51	3.49	0.00368	0.719	0.104
			60	3.56	0.00432	0.844	0.269
			76	3.66	0.00449	0.877	0.321
			90	3.73	0.00454	0.886	0.336
			105	3.80	0.00471	0.920	0.403
			120	3.86	0.00475	0.928	0.420
			137	3.92	0.00487	0.952	0.482
			150	3.95	0.00506	0.989	0.647
			180	4.03	0.00505	0.987	0.636
			240	4.16	0.00502	0.980	0.590
			270	4.21	0.00502	0.980	0.590

FIGURE 23 continued.

	a_0^{-1}	a_∞^{-1}	Time mins.	log t	$a_0^{-1} - a_t^{-1}$	W	f (W)
6	0.00520	0.000785	14	2.92	0.000[illegible]	0.211	-0.648
			30	3.26	0.00195	0.[illegible]	-0.249
			46	3.44	0.00273	0.609	-0.0171
			62	3.56	0.00313	0.700	0.0799
			75	3.65	0.00330	0.702	0.183
			91	3.74	0.00360	0.[illegible]4	0.212
			105	3.80	0.00383	0.856	0.287
			121	3.86	0.00383	0.856	0.287
			135	3.91	0.00389	0.[illegible]8	0.345
			150	3.95	0.00421	0.918	0.402
			165	4.00	0.00421	0.[illegible]8	0.451
			195	4.07	0.00432	0.968	0.584
			240	4.36	0.00446	0.996	0.736
			320	4.86	0.00446	0.996	0.736

FIGURE 24.

	a_0^{-1}	a_∞^{-1}	Time mins.	log t	$a_0^{-1} - a_t^{-1}$	W	$f(W)$
A	0.0258	0.00258	60	3.56	0.00872	0.0732	-1.118
			75	3.65	0.00827	0.122	-0.886
			91	3.74	0.00550	0.149	-0.798
			105	3.80	0.00968	0.199	-0.693
			120	3.86	0.00603	0.257	-0.574
			136	3.95	0.00738	0.313	-0.486
			179	4.03	0.00922	0.398	-0.362
			209	4.10	0.0104	0.446	-0.259
			240	4.16	0.0116	0.493	-0.167
			299	4.25	0.0148	0.628	-0.0040
			321	4.31	0.0166	0.706	0.0274
			420	4.30	0.0176	0.751	0.143
			509	4.49	0.0180	0.808	0.218
			572	4.54	0.0198	0.844	0.269
			660	4.60	0.0205	0.874	0.317
			708	4.67	0.0219	0.932	0.388
			901	4.73	0.0223	0.950	0.478
			1,020	4.79	0.0226	0.961	0.512
			1,260	4.88	0.0229	0.976	0.571
			2,100	5.10	0.0235	0.999	0.853
B	0.0265	0.00288	15	2.95	0.00252	0.0234	-1.660
			29	3.24	0.00870	0.0703	-1.139
			45	3.43	0.00842	0.0586	-1.221
			60	3.56	0.00822	0.0771	-1.048
			74	3.65	0.00564	0.126	-0.871
			89	3.73	0.00643	0.183	-0.694
			105	3.80	0.00578	0.239	-0.565
			118	3.85	0.00585	0.258	-0.505
			153	3.96	0.0100	0.434	-0.278

FIGURE 24 continued.

	a_0^{-1}	a_∞^{-1}	Time mins	log t	$a_0^{-1} - a_t^{-1}$	W	f (W)
B			180	4.09	0.0128	0.587	-0.185
			210	4.10	0.0151	0.692	-0.0117
			239	4.16	0.0165	0.683	0.0599
			300	4.26	0.0192	0.792	0.196
			355	4.33	0.0206	0.849	0.276
			420	4.40	0.0217	0.895	0.352
			480	4.46	0.0228	0.911	0.384
			540	4.51	0.0234	0.925	0.414
			630	4.58	0.0238	0.943	0.467
			715	4.63	0.0251	0.954	0.490
			870	4.78	0.0255	0.971	0.549
			1,005	4.78	0.0257	0.980	0.591
			1,140	4.84	0.0257	0.978	0.580
			1,380	4.92	0.0257	0.979	0.585
			2,445	5.17	0.0261	0.995	0.789
C	0.0235	0.00823	16	2.98	0.000580	0.0858	-1.592
			60	3.96	0.00132	0.0817	-1.194
			77	3.47	0.00207	0.0968	-0.995
			90	3.73	0.00285	0.105	-0.954
			105	3.80	0.00364	0.130	-0.737
			120	3.86	0.00438	0.802	-0.697
			149	3.95	0.00561	0.868	-0.516
			181	4.04	0.00700	0.387	-0.401
			210	4.10	0.00843	0.394	-0.300
			240	4.16	0.0101	0.473	-0.294
			300	4.26	0.0119	0.599	-0.0074
			360	4.34	0.0138	0.686	0.0157
			420	4.40	0.0152	0.709	0.0316
			480	4.46	0.0160	0.747	0.139

FIGURE 24 continued

	c_0^{-1}	c_{∞}^{-1}	Time min.	log t	$c_0^{-1} - c_t^{-1}$	W	r (W)
C			540	4.51	0.0171	0.800	0.906
			600	4.56	0.0179	0.827	0.945
			720	4.67	0.0175	0.817	0.930
			900	4.73	0.0186	0.869	0.918
			1,080	4.81	0.0194	0.910	0.921
D	0.0398	0.00814	15	2.95	0.0003	0.008	-0.119
			30	3.26	0.0009	0.0292	-1.608
			45	3.43	0.00389	0.0833	-1.060
			60	3.56	0.00525	0.159	-0.766
			75	3.68	0.00833	0.258	-0.558
			91	3.74	0.0139	0.374	-0.389
			105	3.80	0.0176	0.474	-0.298
			119	3.89	0.0214	0.605	-0.0084
			150	3.95	0.0269	0.726	0.112
			180	4.03	0.0305	0.822	0.237
			210	4.10	0.0321	0.867	0.305
			240	4.16	0.0335	0.903	0.367
			300	4.26	0.0346	0.933	0.433
			375	4.35	0.0353	0.952	0.483
			422	4.40	0.0355	0.959	0.504
			483	4.46	0.0356	0.962	0.530
			510	4.51	0.0358	0.966	0.529
			600	4.56	0.0358	0.967	0.533
			720	4.64	0.0362	0.975	0.566
			840	4.70	0.0363	0.978	0.582
			1,020	4.79	0.0365	0.985	0.621
			1,260	4.88	0.0365	0.986	0.627
			1,560	4.97	0.0368	0.986	0.629
			1,860	5.05	0.0368	0.993	0.697

FIGURE 59 continued

	a_0^{-1}	a_∞^{-1}	Time mins.	log t	$a_0^{-1} - a_t^{-1}$	W	f(W)
N	0.0346	0.00257	15	2.95	0.00055	0.0178	-1.757
			30	3.26	0.00088	0.0304	-1.634
			45	3.43	0.00211	0.255	-0.532
			60	3.56	0.0146	0.460	-0.211
			75	3.65	0.0196	0.615	-0.0895
			90	3.73	0.0229	0.721	0.106
			105	3.80	0.0252	0.792	0.197
			120	3.86	0.0268	0.840	0.263
			150	3.95	0.0282	0.871	0.319
			179	4.07	0.0290	0.911	0.395
			210	4.10	0.0295	0.927	0.417
			240	4.16	0.0299	0.939	0.446
			300	4.26	0.0301	0.946	0.465
			360	4.33	0.0302	0.950	0.475
			420	4.40	0.0304	0.956	0.495
			480	4.46	0.0305	0.957	0.497
			540	4.51	0.0306	0.960	0.533
			600	4.56	0.0308	0.966	0.588
			720	4.64	0.0311	0.977	0.596
			900	4.73	0.0310	0.975	0.568
			1,080	4.81	0.0312	0.980	0.593
			1,320	4.90	0.0314	0.987	0.638
P	0.0347	0.00235	30	3.26	0.00125	0.0314	-1.478
			45	3.43	0.00118	0.0287	-1.863
			60	3.58	0.00090	0.0202	-1.957
			75	3.65	0.00110	0.0292	-1.895
			90	3.73	0.00097	0.0254	-1.956
			105	3.80	0.00103	0.0260	-1.939
			120	3.86	0.00101	0.0251	-1.939

FIGURE 24 continued

a^{-1}_0	a^{-1}_∞	Time min.	log t	$a^{-1}_0 - a^{-1}_t$	W	r (W)
P		150	5.05	0.00203	0.0460	-1.339
		190	4.03	0.00275	0.0395	-1.404
		240	4.16	0.00351	0.0362	-1.441
		270	4.31	0.00426	0.0363	-1.354
		330	4.50	0.00549	0.0666	-1.161
		390	4.57	0.00634	0.105	-0.958
		480	4.96	0.00902	0.155	-0.838
		570	4.53	0.00970	0.166	-0.743
		660	4.69	0.00430	0.196	-0.661
		750	4.65	0.00564	0.232	-0.537
		840	4.70	0.00605	0.289	-0.468
		930	4.75	0.00720	0.386	-0.404
		1,050	4.80	0.00815	0.365	-0.349
		1,230	4.87	0.00965	0.458	-0.298
		2,550	5.19	0.0155	0.693	0.0727

FIGURE 25.

	a^{-1}_0	a^{-1}_∞	Time mins.	log t	$a^{-1}_0 - a^{-1}_t$	V	f (V)
B	0.0826	0.00838	15	2.95	0.00810	0.0069	-2.319
			30	3.26	0.000190	0.0093	-2.072
			45	3.43	0.00180	0.0287	-1.812
			60	3.56	0.00180	0.427	-0.632
			75	3.65	0.00698	0.520	-0.316
			90	3.73	0.00858	0.433	-0.373
			105	3.80	0.00994	0.490	-0.278
			120	3.86	0.0109	0.536	-0.215
			150	3.95	0.0129	0.617	0.0055
			180	4.03	0.0145	0.704	0.0845
			210	4.10	0.0158	0.699	0.0191
			240	4.16	0.0138	0.688	0.0595
			300	4.26	0.0146	0.717	0.101
			360	4.34	0.0149	0.735	0.134
			420	4.40	0.0154	0.758	0.153
			480	4.46	0.0157	0.773	0.171
			540	4.51	0.0158	0.780	0.180
			600	4.60	0.0162	0.800	0.207
			720	4.65	0.0164	0.810	0.220
			840	4.70	0.0165	0.814	0.226
			960	4.76	0.0167	0.824	0.240
			1,080	4.81	0.0168	0.827	0.244
			1,200	4.88	0.0168	0.834	0.254
			1,440	4.94	0.0171	0.845	0.270
C	0.0846	0.00159	15	2.95	0.000590	0.0256	-1.592
			30	3.26	0.000817	0.107	-0.916
			45	3.43	0.00158	0.190	-0.676
			60	3.56	0.00285	0.298	-0.392
			75	3.65	0.00314	0.327	-0.296

FIGURE 25 continued

	a_0^{-1}	a_∞^{-1}	Time mins.	log t	$a_0^{-1} - a_t^{-1}$	W	r (W)
C			90	3.73	0.0112	0.487	-0.176
			105	3.80	0.0129	0.559	-0.0865
			120	3.86	0.0143	0.621	-0.0119
			150	3.95	0.0163	0.710	0.0927
			181	4.04	0.0175	0.760	0.154
			210	4.10	0.0184	0.798	0.204
			240	4.16	0.0191	0.828	0.246
			300	4.26	0.0197	0.856	0.287
			360	4.34	0.0202	0.877	0.321
			420	4.40	0.0204	0.888	0.340
			480	4.45	0.0208	0.906	0.373
			540	4.51	0.0209	0.910	0.381
			600	4.56	0.0210	0.912	0.386
			690	4.62	0.0211	0.917	0.397
			810	4.69	0.0213	0.925	0.413
			960	4.76	0.0215	0.932	0.430
			1,040	4.80	0.0216	0.940	0.450
			1,350	4.91	0.0216	0.939	0.447
			1,590	4.98	0.0218	0.946	0.466
			2,775	5.22	0.0222	0.966	0.530
D	0.0284	0.00213	16	2.98	0.000440	0.0167	-1.780
			30	3.26	0.000650	0.0247	-1.609
			45	3.43	0.00228	0.0868	-1.041
			60	3.56	0.00331	0.126	-0.871
			75	3.65	0.00569	0.217	-0.613
			90	3.73	0.00775	0.295	-0.457
			104	3.80	0.00927	0.353	-0.362
			120	3.86	0.0123	0.466	-0.202
			150	3.95	0.0135	0.513	-0.143

FIGURE 25 continued

	a_0^{-1}	a_∞^{-1}	Time mins.	log t	$a_0^{-1} - a_t^{-1}$	W	r (W)
D			180	4.04	0.0156	0.598	-0.0496
			210	4.10	0.0173	0.659	0.0318
			240	4.16	0.0187	0.713	0.0965
			300	4.26	0.0206	0.786	0.188
			360	4.34	0.0218	0.828	0.248
			420	4.40	0.0227	0.865	0.301
			480	4.46	0.0234	0.890	0.343
			540	4.51	0.0238	0.905	0.371
			600	4.58	0.0244	0.927	0.419
			720	4.69	0.0248	0.943	0.456
			840	4.78	0.0250	0.953	0.479
			960	4.86	0.0253	0.963	0.519
			1,140	4.98	0.0255	0.969	0.548
			1,260	5.08	0.0256	0.976	0.571
			1,440	5.23	0.0256	0.975	0.571
			2,430	5.46	0.0262	0.998	0.701
E	0.0385	0.00878	14	2.92	0.000790	0.0866	-1.578
			30	3.46	0.00377	0.0896	-1.215
			45	3.79	0.00593	0.138	-0.897
			60	3.96	0.00718	0.262	-0.598
			75	3.65	0.00854	0.322	-0.483
			90	3.93	0.0088	0.350	-0.379
			105	3.80	0.0105	0.390	-0.278
			120	3.86	0.0109	0.552	-0.0947
			150	3.95	0.0134	0.633	0.0859
			180	4.03	0.0227	0.731	0.118
			210	4.10	0.0230	0.774	0.378
			240	4.16	0.0248	0.813	0.225
			300	4.26	0.0256	0.851	0.294

FIGURE 25 continued

	a_0^{-1}	a_∞^{-1}	Time mins.	log t	$a_0^{-1} - a_t^{-1}$	W	f (W)
E			360	4.54	0.0858	0.834	0.333
			420	4.70	0.0870	0.511	0.303
			482	4.86	0.0873	0.521	0.305
			540	4.91	0.0875	0.525	0.310
			630	4.98	0.0870	0.537	0.321
			720	5.04	0.0880	0.545	0.332
			875	4.77	0.0885	0.560	0.348
			1,120	4.83	0.0888	0.569	0.358
			1,850	4.89	0.0887	0.567	0.356
			1,500	4.95	0.0889	0.573	0.359
			2,700	5.11	0.0893	0.588	0.615
F	0.0134	0.00870	45	3.43	0.000610	0.0317	-1.492
			60	3.56	0.000650	0.0289	-1.537
			67	3.60	0.00154	0.0217	-1.194
			90	3.73	0.00156	0.0606	-1.188
			105	3.80	0.00189	0.0870	-1.041
			120	3.86	0.00298	0.119	-0.897
			150	3.95	0.00394	0.163	-0.749
			183	4.04	0.00450	0.207	-0.633
			210	4.10	0.00594	0.301	-0.466
			240	4.16	0.00796	0.398	-0.349
			285	4.23	0.00862	0.397	-0.296
			360	4.34	0.0112	0.514	-0.302
			420	4.40	0.0125	0.573	-0.0679
			480	4.46	0.0139	0.639	0.0180
			570	4.53	0.0153	0.704	0.0895
			660	4.60	0.0163	0.774	0.173
			780	4.67	0.0176	0.813	0.254
			900	4.73	0.0183	0.843	0.307

FIGURE 25 continued

	a_0^{-1}	a_∞^{-1}	Time mins	log t	$a_0^{-1} - a_t^{-1}$	W	f (W)
F			1,020	4.79	0.0189	0.971	0.511
			1,200	4.86	0.0198	0.984	0.590
			1,440	4.96	0.0202	0.988	0.629
			2,220	5.24	0.0211	0.970	0.505
			2,580	5.19	0.0211	0.974	0.562

CHAPTER IX.

APPENDIX

IX APPENDIX

COMPUTER PROGRAMMES

Programme 1.

This programme was designed to select from a range of activation energies, peak temperatures and peak heights, the best curve fitting the experimental points. This was performed using the autocode system in a Sirius computer. The basic equation used for computation was $\frac{Q^{-1}max}{Q^{-1}} = \cosh \frac{\Delta H}{R}(1/T - \frac{1}{T_M})$

```
 JV1                    instruction for using autocode
  V200 = TAPE 1         read experimental run no.
  V70  = TAPE 3         read increments of ΔH, T peak, Q^-1
  V1   = TAPE 6         read limits of ΔH, °K, Q^-1 max
  V73  = V3
  V74  = V5
  V10  = TAPE*          read experimental values of °K and Q^-1
  N1   = NO
  V60  = 100
10)V55 = 100
 7)V7  = 100
 4)V8  = 0
  NO   = 0
 1)V51 = V3 - V (11+ NO)
  V51  = V1 x V51
  V52  = V51 /1.987
  V51  = V51 /V3
  V51  = V51 /V(11 + NO)
  V52  = EXP V51
  V53  = 1/V52
```

```
   V51  =  V52 + V53
   V51  =  V51/2
   V51  =  V5/V51
   V51  =  V(10 + NO) - V51
   V51  =  V51 x V51
   V8   =  V8 + V51
   NO   =  NO + 2
   →1, N1 ≠ NO
   →2, V7 ≥ V8
   →3
2) V7   =  V8
   V9   =  V5
   →3
3) V5   =  V5 + V72
   →4, V6 ≥ V5
   V5   =  V74
   →5, V55 > V7
   →6
5) V55  =  V7
   V56  =  V3
   V57  =  V9
   →6
6) V3   =  V3 + V71
   →7, V4 ≥ V3
   V3   =  V73
PRINT V200, 3062
PRINT V55,  3008
PRINT V1,   4100
PRINT V56,  4062
PRINT V57,  4005
```

Using lowest ΔH, T peak, Q^{-1}_{max} deviations of experimental points from theoretical calculated for all experimental results. Deviation stored.

Using lowest ΔH, T peak, deviation calculated for all values of Q^{-1}_{max} and minimum deviation and best Q^{-1}_{max} stored.

Using lowest ΔH, deviation calculated for all values of T peak & Q^{-1}_{max}. Minimum deviation and the best combination of T peak and Q^{-1}_{max} stored.

---

experimental run number
minimum deviation
lowest ΔH
best T peak
best Q^{-1}_{max}

```
 →8, V60 > V55
 →9
8) V60  =   V5
   V61  =   V1
   V62  =   V56
   V63  =   V57
 →9
9) V1   =   V1 + V70
→10, V2 ≥ V1
TEXT
   H    T    Q
PRINT V61, 3100
PRINT V62, 4062
PRINT V63, 4005
PRINT V61, 4008
TEXT
RESIDUAL   Q    T
NO   =   0
1) V51  =  V62 - V (11 + NO)
   V51  =  V61 x V51
   V51  =  V51 /1.987
   V51  =  V51 /V62
   V51  =  V51 /V (11 + NO)
   V52  =  EXP V51
   V53  =  1/V52
   V51  =  V52 + V53
   V51  =  V51/2
   V51  =  V63/V51
   V51  =  V (10 + NO) - V51
PRINT V51, 3005
PRINT V (11 + NO), 4062
    NO  =  NO + 2
  →11, NO ≠  N
  ( →0)
```

Calculation repeated for all values of ΔH. Minimum deviation, best H, T peak, Q^{-1}max stored.

best ΔH

best T peak

best Q^{-1}max

Using the best values of ΔH, T peak, Q^{-1}max deviation of theoretical values from experimental values calculated for each experimental temperature.

Programme 2

This programme is similar to the previous one, and is designed to fit the best theoretical curve of known ΔH T peak to the experimental values.

```
JV1
V200  =  TAPE 1          read experimental run no.
V1    =  TAPE 4          read ΔH, T peak, Q^-1 max lower -
                           Q^-1 max upper x 0.0002.
V10   =  TAPE*           read experimental values.
PRINT V200, 3062
V5    =  100
4)V6  =  0
N1    =  0
1)V51 =  V2 - V (11 + N1)
  V51 =  V1 x V51        Using ΔH, T peak and lowest Q^-1 max
  V51 =  V51 /1.987      values deviation from theoretical
  V51 =  V51 /V2         values for each experimental value
  V51 =  V51/V (11 + N1) calculated for all experimental
  V52 =  EXP V51         results.  Deviations stored.
  V53 =  1/V52
  V51 =  V52 + V53
  V51 =  V51/2
  V51 =  V3/V51
  V51 =  V(10 + N1) - V51
  V51 =  V51 x V51
  V6  =  V6 + V51
  N1  =  N1 + 2
 →1, N1 ≠ N0
 →2, V5 > V6
 →3                      Calculation repeated for all values
2) V5 =  V6              of Q^-1 max.  Minimum deviation and
   V7 =  V3              best Q^-1 max stored.
```

```
  →3
3) V3 =  V3 + 0.0002
  →4, V4 ≥ V3
PRINT V7, 3005                    best Q^-1 max
PRINT V5, 4008                    deviation
N2    =  0
5)V51 =  V2 - V (11 + N2)
  V51 =  V1 x V51                 Using the best Q^-1 max deviation
  V51 =  V51 /1.987               of theoretical values from
  V51 =  V51 /V2                  experimental values calculated
  V51 =  V51/V (11 + N2)          for each experimental temperature.
  V52 =  EXP V51
  V53 =  1/V52
  V51 =  V52 + V53
  V51 =  V51/2
  V51 =  V7/V51
  V51 =  V (10 + N2) - V51
PRINT V51, 3005                   deviation
PRINT V (11 + N2), 4061           experimental temperature
  N2  =  N2 + 2
 →5, N2 ≠ N0
(→0)
```

Programme 3.

This programme was designed to resolve a broadened normal peak into the constituent carbon and nitrogen peaks whose sum best fitted the experimental results.

```
J V1
  V18 =  TAPE                    read the experimental number.
  V1  =  TAPE 10                 read ΔH(N), T peak(N), Ω^-1max(N),
  V100=  TAPE *                  ΔH(C), T peak(C), Ω^-1max(C)/
  N1  =  N0                      Ω^-1max(N) (minimum value),
  V21 =  100                     Ω^-1max(N) (minimum), Ω^-1max(C)/
  N0  =  0                       Ω^-1max(N) (maximum value),
  V20 =  0                       δΩ^-1max(N), δΩ^-1max(C)/Ω^-1max(N).
1) V0 =  V2 - V(101 + N0)
   V0 =  V1 x V0                 Using T peak(N) and ΔH(N)
   V0 =  V0/1.987                calculated cosh ΔH/R(T peak-T exp.)
   V0 =  V0/V2                                       T peak.T exp.
   V0 =  V0/V(101 + N0)          for all the experimental values
   V12=  EXP V0                  and stored the results.
   V13=  1/V12
   V0 =  V12 + V13
   V0 =  V0/2
   V (200 + N0) = V0
   N0 =  N0 + 2
   →1, N1 ≠ N0
   N0 =  0
2) V0 =  V5 - V (101 + N0)       Using T peak(C), ΔH(C) calculated
   V0 =  V4 x V0                 cosh ΔH/R (T peak - T exp)  for
   V0 =  V0/1.987                          Tm.  T exp.
   V0 =  V0/V5                   all the experimental values and
                                 stored the results.
```

```
   V0  =  V0/V (101 + N0)
   V12 =  EXP V0
   V13 =  1/V12
   V0  =  V12 + V13
   V0  =  V0/2
   V (201 + N0) = V0
   N0  =  N0 + 2
   →2, N1 ≠ N0
   V19 =  V6
7) N0  =  0
3) V0  =  V3/V (200 + N0)
   V12 =  V3 x V19
   V12 =  V12/V (201 + N0)
    V0 =  V0 + V12
    V0 =  V(100 + N0) - V0
    V (300 + N0) = V0
    V0 =  V0 x V0
   V20 =  V20 + V0
    N0 =  N0 + 2
  →3, N1 ≠ N0
 →4, V20 > V21
   V21 =  V20
    N0 =  0
5) V(301 + N0) = V(300 + N0)
    N0 =  N0 + 2
  →5, N1 ≠ N0
   V16 =  V3
   V17 =  V19
4) V20 =  0
   V19 = V19 +  V10
  →6, V19 > V8
  →7
```

Calculated the theoretical $\Omega^{-1}_{(N)}$ and $\Omega^{-1}_{(C)}$ for each experimental temperature, subtracted these from the experimental values and stored the sum of the square of the deviations.

Calculated deviations for all values of $\Omega^{-1}max_{(C)}/\Omega^{-1}max_{(N)}$

```
6)  V19  =  V6                    Repeated calculation with a
    V 3  =  V3 - V9               different value of Q^-1max(N)
  →7, V3 ≥ V7
TEXT
RUN                 Q1            Q1/Q2 RESIDUAL
PRINT V18, 3002                   run number
PRINT V16, 4005                   Q^-1max(N)
PRINT V17, 4002                   Ratio Q^-1max (C)/Q^-1max(N)
PRINT V21, 4008                   Sum of square of deviations
TEXT
NITROGEN PEAK
     N0  =  0
9)   V0  =  V16/V (200 + N0)
PRINT V0, 3005                    Q^-1values for nitrogen peak
     N0  =  N0 + 2
 →9, N1 ≠ N0
TEXT
CARBON PEAK
     N0  =  0
10)  V0  =  V17 x V16
     V0  =  V0/V (201 + N0)
PRINT V0, 3005                    Q^-1values for carbon peak
     N0  =  N0 + 2
→10, N1 ≠ N0
     N0  =  0
TEXT
DEVIATION
8)PRINT V(301 + N0),3005          Deviations
     N0  =  N0 + 2
 →8, N1 ≠ N0
( →0)
```

Programme 4

This programme was designed to calculate the gradient of the two straight lines best fitting the experimental results obtained in precipitation studies. The equation used was

$$\ln \ln \frac{1}{1-W} = \ln b + n \ln t \quad \text{where}$$

$$W = \frac{\Omega_o^{-1} - \Omega_t^{-1}}{\Omega_o^{-1} - \Omega_\infty^{-1}}$$

The best fit was found by the least squares method and the gradient was calculated from

$$n = \frac{\sum x \sum y - \frac{\sum x \sum y}{N}}{\sum x^2 - \frac{(\sum x)^2}{N}}$$

JV1

V61 =	TAPE 3	read Ω_o^{-1} , Ω_∞^{-1} , experimental run number.
N2 =	TAPE 3	2 x no. pts. on first line, 2 x no. pts. on second line, no. of pts. to be tried.
V1 =	TAPE*	read experimental values of Ω^{-1} and t in secs.
N1 =	N0	no. of experimental results.

N0 = 1
PRINT V63, 3062
1)V64= V61 - V62
V70 = V61 - VN0
V70 = V70/V64
V70 = 1 - V70
V70 = 1/V70
V70 = LOG V70

```
   VNO  =   LOG V70
V(1 +NO)=   LOG V(1 + NO)
   NO   =   NO + 2
  →1, N1 > NO
```

The appropriate functions i.e. $\ln \ln \frac{1}{1-W}$ and ln t calculated for all experimental values and stored.

```
5) V76 =   0
   V75 =   0
   V74 =   0
   V77 =   0
   V85 =   0
   V87 =   0
    NO =   1
6) V72 =   VNO x V (1+NO)
   V73 =   V(1 + NO) x  V(1 + NO)
   V74 =   V74 + V (1 + NO)
   V75 =   V75 + VNO
   V76 =   V76 + V72
   V77 =   V77 + V73
    NO =   NO + 2
  →6, N2 > NO
   V81 =   V74 x V75
   V86 =   N2
   V81 =   V81/V86
   V81 =   V81 x 2
   V81 =   V76 - V81
   V82 =   V74 x V74
   V82 =   V82/V86
   V82 =   V82 x 2
   V82 =   V77 - V82
   V81 =   V81/V82
   V82 =   V86/2
   V83 =   V74/v82
   V82 =   V75/V82
   V83 =   V81 x V83
   V83 =   V82 - V83
```

$\Sigma xy \cdot \Sigma x^2$ calculated for points on first line only.

Gradient calculated for first line only.

```
   N0  =  1
2) V84 = V81 x V (1 + N0)
   V84 = V84 x V83
   V84 = V84 - VN0
   V84 = V84 x V84
   V85 = V85 + V84
    N0 = N0 + 2
  → 2, N2 > N0
PRINT  V81, 3023
PRINT  V85, 4046
   V74 = 0
   V75 = 0
   V76 = 0
   V77 = 0
3) V72 = VN0 x V (1 + N0)
   V73 = V (1 + N0) x V (1 + N0)
   V74 = V74 + V (1 + N0)
   V75 = V75 + VN0
   V76 = V76 + V72
   V77 = V77 + V73
    N0 = N0 + 2
  → 3, N1 > N0
   V81 = V74 x V75
   V86 = N3
   V81 = V81/V86
   V81 = V81 x 2
   V81 = V76 - V81
   V82 = V74 x V74
   V82 = V82/V86
   V82 = V82 x 2
   V82 = V77 - V82
   V81 = V81/V82
   V82 = V86/2
   V83 = V74/V82
```

Gradient of first line

Deviation calculated for first line

$\sum xy$ & $\sum x^2$ calculated for points on only second line

```
 V82  =  V75/V82
 V83  =  V81 x V83
 V83  =  V82 - V83          Calculated gradient for second line.
  N0  =  N2 + 1
4)V84 =  V81 x V (1 + N0)
 V84  =  V84 + V83
 V84  =  V84 - VN0
 V84  =  V84 x V84
 V87  =  V87 + V84
  N0  =  N0 + 2
 →4, N1 > N0                Calculated deviation for second line.
 V88  =  V85 + V87          Added sum of deviations of both lines
PRINT V81, 3023             Gradient of second line
PRINT V87, 4046             Deviation for second line
PRINT V88, 4046             Sum of the deviations
  N2 =  N2 + 2
  N3 =  N3 - 2              No. of pts. on first line increased
  N4 =  N4 - 1              by one, number of points on second
 →5, N4 ≠ 0                 line decreased by one, calculation
 (→ 0)                      repeated.
```

METHOD OF NITROGEN ANALYSIS

The method is essentially one issued by British Chemical Standards along with Standard no. 230. It is attributed to W. C. Neivell, Iron and Steel Institute, May 1945.

The sample is dissolved in 5ml. H_2SO_4 and 20 ml. water. When dissolved, approximately 5 ml. of 30% H_2O_2 is added and the solution evaporated to fuming. It is then cooled, diluted and transferred to a 250 ml. graduated flask. 40 ml. of 20% W/V NaOH is added while keeping the solution cool. The bulk is made up to 250 ml., well shaken and the precipitate allowed to settle. It is then filtered, the first filling of the paper being rejected. 50 ml. of the filtrate is transferred to a 50 ml. Nessler cylinder, 1 ml. of 5% solution of Gum Arabic added followed by 1 ml. of standard Nessler reagent and the solution well mixed. A blank of all reagents, treated in the same manner as the sample, is put in another 50 ml. cylinder and the depth of colour compared in a Nesslerizer with that of standard ammonia discs. Three discs were used covering the range 10 to 100 p.p.m. NH_3.

The nitrogen content of the sample is

$$\text{Nitrogen} = \frac{\text{Disc reading} \times 0.82\ (NH_3\text{-}N_2) \times 100 \times \frac{250}{50}}{\text{Wt. of sample} \times 10^6} \text{ per cent.}$$

The weight of sample is chosen to give a depth of colour within the range of the discs. The nitrogen contents of the samples analysed, range from under 0.03% to over 0.4%. Generally a

sample weight of 0.1 to 0.2 gms. was used, but if the resulting colour was outwith the range 20 - 70 p.p.m., the test was repeated with a more suitable weight.

Along with each batch of tests, say 3 samples and a blank, a 1 gm. sample of B.C.S. 265 was run through. This is a low carbon steel standardised for nitrogen (0.020%). This was done as an overall check on manipulation. All the reagents used were of ANALAR quality. De-ionised water was used throughout. No colour was seen in any of the blank estimations. The rejection of the first 50 ml. or so of the filtrate effectively disposed of the ammonia of the filter paper. This was found preferable to acid washing. The best gum arabic obtainable contained some ammonia. To eliminate this, the solubin of the gum was treated with a cation exchange resin and finally passed through a column of the resin.

With a sample of 3.5 gms. the B.S. limits are as follows.

Up to 0.02% N	$\pm$ 0.001 %
With 0.1 % N	$\pm$ 0.005 %
With 0.2 % N	$\pm$ 0.01 %

Due to the small sample weights used in the present investigation, the limits of reproducibility are probably about four times greater than the B.S. limits.

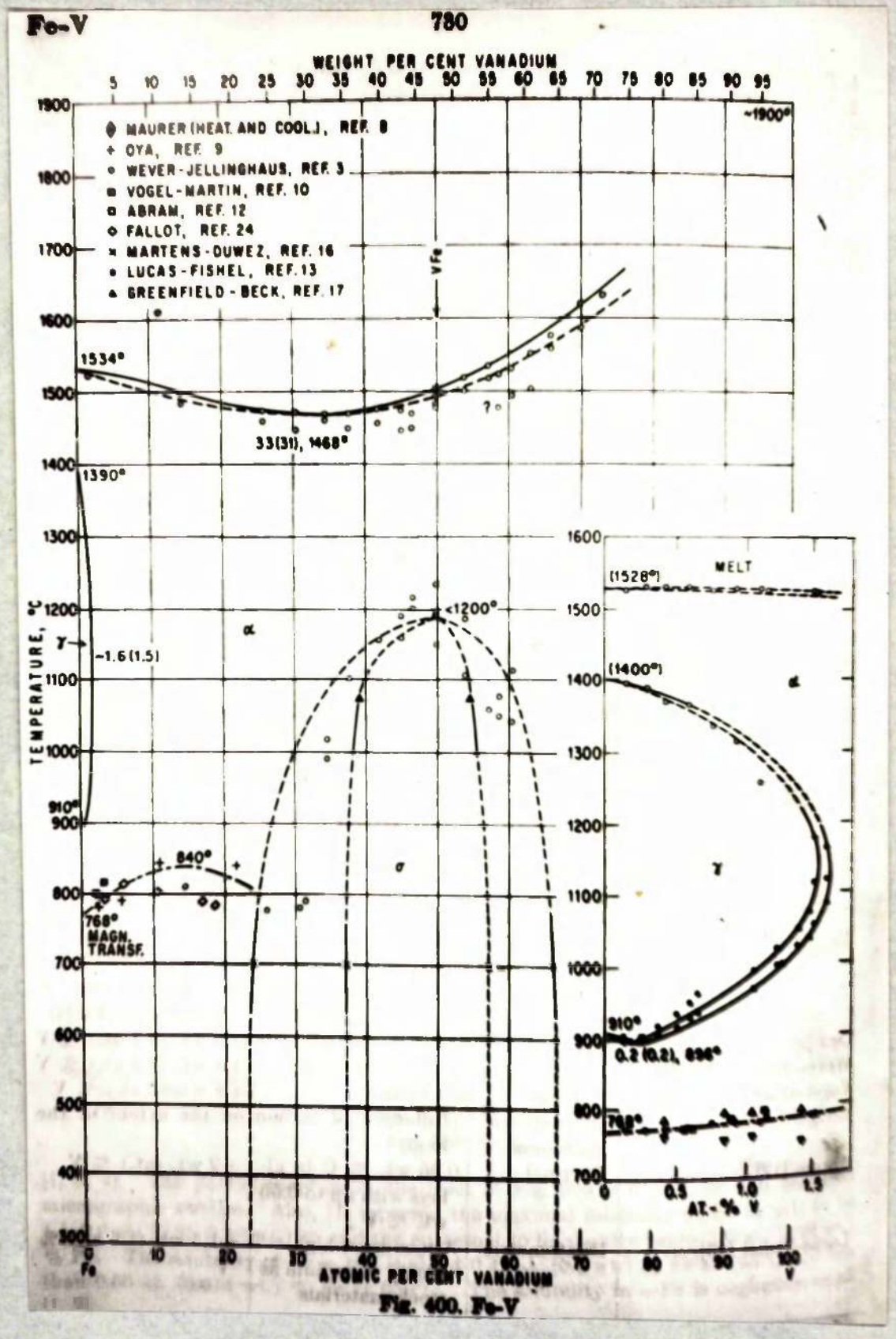

Figure 26 The Iron-Vanadium System [82]

CHAPTER X.

REFERENCES

X. REFERENCES.

1. S. EPSTEIN, H.J. CUTLER, J.W. FRAME. Journal of Metals 1950, 2, 830.

2. C. ZENER. Elasticity and Anelasticity of Metals. The University of Chicago Press. 1948.

3. L.J. DIJKSTRA. Philips Research Reports. 1947, 2, 357.

4. J.L. SNOEK. Physica. 1941, 8, 711.

5. N.J. PETCH. J.I.S.I. 1949, 147, 231.

6. D.A. LEAK, W.R. THOMAS, G.M. LEAK. Acta Metallurgica. 1955, 3, 501.

7. A.S. NORWICK. Internal Friction in Metals. Progress in Metal Physics. (Edited by B. Chalmers). Volume 4 1953. London (Pergamon Press).

8. K.M. ENTWHISTLE. The Damping Capacity of Metals. The Physical Examination of Metals. (Edited by B. Chalmers and A.G. Quarrell). 1960 London. (Edward Arnold Ltd.).

9. G.M. LEAK. Application of Internal Friction Measurements to the Study of Gases in Metals. The Determination of Gases in Metals. Iron and Steel Report. 1960.

10. T.S. Kê. Physical Review. 1948, 74, 9.

11. T.S. Kê. ibid. 1948, 74, 914.

12. T.S. Kê. ibid. 1948, 74, 16.

13. R.W. POWERS. Acta Metallurgica. 1955, 3, 135.

14. R.W. POWERS, M. DOYLE. ibid. 1956, 4, 233.

15. C. ANG. ibid. 1953, 1, 123

16. R.W. POWERS, ibid. 1954, 2, 604.

17. R.W. POWERS, M. DOYLE. ibid. 1958, 6, 643.

18. R.W. POWERS, M. DOYLE. Trans. A.I.M.E. 1957, 9, 1285.

19. C. ANG, C. WERT. ibid. 1953, 5, 1032.

20. C. WOODRUFF. Physical Review. 1903, 16, 325.

21. J.L. SNOEK. Physica. 1939, 6, 591.

22. D. POLDER. Philips Research Reports. 1945, 1, 5.

23. J. SMIT, H.G. VAN BEUREN. ibid. 1954, 9, 460.

24. R. RAWLINGS, D. TAMBINI. J.I.S.I. 1956, 184, 302.

25. J.D. FAST, M.B. VERRIJP. ibid. 1955, 180, 337.

26. G. LAGERBERG, A. JOSEFSSON. Acta Metallurgica. 1955, 3, 236.

27. R. RAWLINGS. ibid. 1956, 4, 213.

28. G. LAGERBERG, E.G. WOLFF. ibid. 1958, 6, 136.

29. H. ASTROM, G. BORELIUS. ibid. 1954, 2, 547.

30. J.D. FAST, M.B. VERRIJP. ibid. 1955, 3, 203.

31. R. RAWLINGS, D. TAMBINI. ibid. 1955, 3, 212.

32. M. HANSEN. Constitution of Binary Alloys. McGraw-Hill Book Co. New York. 1958, 671.

33. L.J. DIJKSTRA. Trans. A.I.M.E. 1949, 185, 252.

34. K.H. JACK. Proceedings of the Royal Society of London. 1951, 208, 216.

35. K.H. JACK. Acta Crystallographica. 1950, 3, 392.

36. A. FRY. Stahl u Eisen. 1923, 43, 1271.

37. O. EISENHUT, E. KAUPP, Z. Elektrochem. 1930, 36, 392.

38. D. SEFERIAN. "Etude de la formation des nitrures de fer par fusion et dus systeme fer-azote." 1935. Paris.

39. W. KOSTER. Arch. Eisenhuttenw. 1929, 3, 637.

40. G. BORELIUS, S. BERGLUND, O. AVSAN. Arkiv. Fysik. 1950, 2, 551.

41. V.G. PARANJPE, M. COHEN, M.B. BEVER, C.F. FLOE. Journal of Metals. 1950, 2, 261.

42. T.S. Kê. Physical Review. 1947, 71, 533.

43. L. CHANG, M. GENSAMER. Acta Metallurgica. 1953, 1, 483.

44. E. T. TURKDOGAN, N. S. CORNEY. J.I.S.I. 1955, 180, 344.

45. C. WERT. Journal of Metals. 1950, 2, 1242.

46. C. WERT. Thermodynamics in Physical Metallurgy. A.S.M. Publication. 1950, 178.

47. M. VOLMER. Kinetik der Phasenbildung, Dresden. 1939.

48. C. WERT. Journal of Applied Physics. 1949, 20, 943.

49. C. WERT, C. ZENER. ibid. 1950, 21, 5.

50. C. ZENER. ibid. 1949, 20, 950.

51. A. TSOU, J. HUTTING, J. HENTER. J.I.S.I. 1952, 172, 163.

52. W. PITSCH, K. LÜCKE. Arch. Eisenhuttenw. 1956, 27, 45.

53. F. S. HAM. J. Phys. Chem. Solids. 1958, 6, 335.

54. C. WERT. Acta Metallurgica. 1954, 2, 362.

55. R. H. DOREMUS. Trans. A.I.M.E. 1960, 218, 569.

56. P. CHOLLET, C. CRUSSARD. Compte Rendus. 1962, 255, July issue.

57. J. D. FAST. Metaux, Corrosion, Industries. 1961, 36, 383 and 431.

58. C. WERT. Physical Review. 1950, 79, 601.

59. J. K. STANLEY. Trans. A.I.M.E. 1949, 185, 752.

60. C. WERT. Journal of Applied Physics. 1950, 21, 1196.

61. C. WERT, C. ZENER. Physical Review. 1949, 76, 1169.

62. J. D. FAST, M. B. VERRIJP. J.I.S.I. 1954, 176, 24.

63. P. BUSBY, D. HART, C. WELLS. Journal of Metals. 1956, 8, 686.

64. T. S. Kê. Trans A.I.M.E. 1948, 176, 448.

65. J. D. FAST, L. J. DIJKSTRA. Philips Technical Review. 1951-52, 13, 172.

66. L. J. DIJKSTRA, R. J. SLADEK. Journal of Metals. 1952, 5, 164.

67. J. L. MEIJERING. Metaux, Corrosion, Industries. 1961, 36,107

68. J. D. FAST, M. B. VERRIJP. Ibid. 1961, 36, 112.

69. C. WERT. Journal of Metals. 1952, 4, 602.

70. J. D. FAST, J. L. MEIJERING. Philips Research Reports. 1953, 8, 1.

71. R. W. FOUNTAIN, J. CHIPMAN. Trans A.I.M.E. 1958, 212, 787.

72. J. F. ELLIOT, M. GLEISER. Thermochemistry for Steelmaking. Pergamon Press. London. 1960.

73. J. PEARSON, U. ENDE. J.I.S.I. 1953, 175, 52.

74. E. T. TURKDOGAN, S. IGNATOWICZ, J. PEARSON. J.I.S.I. 1955, 181, 227.

75. L. G. KOROLEV, A. V. MOROZOV. Izvest. Vuz. Chern. Met. 1962, 9, 39.

76. O. KUBASCHEWSKI, E. LL. EVANS. Metallurgical Thermochemistry. Butterworth Springer Ltd., London. 1951.

77. Basic Open Hearth Steelmaking. A.I.M.E. Publication. New York. 1944, 488.

78. C. S. BARRET. Structure of Metals. McGraw-Hill Publishing Co. Ltd., New York. 1952, 87.

79. E. LEHRER. Z. Elektrochem. 1930, 36, 383.

80. L. J. PATERSON. Ph.D. Thesis. University of Glasgow. 1964.

81. L. S. DARKEN, L. S. GURRY. Physical Chemistry of Metals. McGraw - Hill Book Co., New York. 1953, 405.

82. M. HANSEN. Constitution of Binary Alloys. McGraw - Hill Book Co., New York. 1958, 730.

CHAPTER XI.

ACKNOWLEDGEMENTS

XI ACKNOWLEDGEMENTS

I welcome this opportunity of expressing my gratitude to all who assisted me in this investigation.

To Dr. Rankin Kennedy whose unfailing help and encouragement have proved inestimable.

To Professor E. C. Ellwood for his keen interest in this research and for generously making available the facilities of the Department of Metallurgy, Royal College of Science and Technology.

To B.I.S.R.A. for donating the high purity iron used.

To Messrs. Via-Vac Ltd., Wishaw, for placing their vacuum casting equipment at my disposal, and in particular to Mr. J. Brown for the highly appreciated part he played in this respect.

To Mr. J. Kyle, Chief Chemist, Wm. Beardmore & Co. Ltd., for kindly analysing the casts.

To Mr. R. Hamilton of Messrs. Colvilles Ltd., and Mr. J. Arnott for their willingness in performing the nitrogen analyses.

To the Department of Scientific and Industrial Research without whose financial support this investigation would not have been possible.